THE HONG KONG
POLYTECHNIC UNIVERSITY
香港理工大學
Pao Yue-kong Library
包玉剛圖書館

Copyright Undertaking

This thesis is protected by copyright, with all rights reserved.

By reading and using the thesis, the reader understands and agrees to the following terms:

1. The reader will abide by the rules and legal ordinances governing copyright regarding the use of the thesis.
2. The reader will use the thesis for the purpose of research or private study only and not for distribution or further reproduction or any other purpose.
3. The reader agrees to indemnify and hold the University harmless from and against any loss, damage, cost, liability or expenses arising from copyright infringement or unauthorized usage.

IMPORTANT

If you have reasons to believe that any materials in this thesis are deemed not suitable to be distributed in this form, or a copyright owner having difficulty with the material being included in our database, please contact lbsys@polyu.edu.hk providing details. The Library will look into your claim and consider taking remedial action upon receipt of the written requests.

Pao Yue-kong Library, The Hong Kong Polytechnic University, Hung Hom, Kowloon, Hong Kong

http://www.lib.polyu.edu.hk

This thesis in electronic version is provided to the Library by the author. In the case where its contents is different from the printed version, the printed version shall prevail.

The Hong Kong Polytechnic University

Department of Building Services Engineering

Simulation and Experimental Investigation on Optimum Applications of the Shading-type BIPV and BIPVT Systems on Vertical Building Facades

Sun Liangliang

A thesis submitted in partial fulfillment of the requirements

for the Degree of Doctor of Philosophy

June 2011

CERTIFICATE OF ORIGINALITY

I hereby declare that this thesis is my own work and that, to the best of my knowledge and belief, it reproduces no material previously published or written, nor material that has been accepted for the award of any other degree or diploma, except where due acknowledgement has been made in the text.

_____ (Signed)

Sun Liangliang (Name of student)

Department of Building Services Engineering

The Hong Kong Polytechnic University

Hong Kong SAR, China

June 2011

ABSTRACT

Abstract of thesis entitled:

Simulation and Experimental Investigation on Optimum Applications of the Shading-type BIPV and BIPVT Systems on Vertical Building Facades

Submitted by: Sun Liangliang

For the degree of: Doctor of Philosophy

at The Hong Kong Polytechnic University in June 2011.

Among the various types of renewable technology, solar photovoltaic has the potential for large scale applications in the future due to its clean nature and decreasing cost in recent years. Building Integrated Photovoltaic (BIPV) and Building Integrated Photovoltaic Thermal (BIPVT) are both common applications of photovoltaic technology. In recent years, BIPV and BIPVT technology applications have been developed rapidly because of its unique characteristic, i.e. to combine clean power production with other functional features on building facade and hot water production.

Although a number of reports have been published for the BIPV and BIPVT applications, there are still problems to be solved, especially for their application in high-rise buildings. In Hong Kong, most of the buildings are high-rise buildings. Most people live in small to medium flats. There is not enough roof area for locating photovoltaic (PV) modules for solar energy application on the roofs of the buildings. If the PV module can be used on vertical façades of such high-rise buildings, the less

roof are problem can be solved for solar energy applications. This thesis aims to investigate how to use solar photovoltaic effectively on vertical facades of high-rise buildings.

Firstly, the energy performance of the shading-type BIPV claddings on vertical buildings' facade is analyzed by using a dynamic heat transfer method. A 2D numerical model was developed to explore the impacts of building orientations, inclinations and wall utilization fractions on the energy performance of the shading-type BIPV claddings in terms of annual power output of PV modules and cooling load reduction of windows and concrete walls. When the area of PV modules is considered, the maximum electricity saving of the shading-type BIPV claddings could be 239.5kWh/m^2, which is twice of the maximum electricity generation of the PV modules alone. It is indicated that the shading-type BIPV claddings can significantly increase the total energy benefits relative to PV modules. It is thus a good choice to apply the shading-type BIPV system in buildings like in Hong Kong.

Secondly, in order to further improve the energy performance of the BIPV system, a quasi 3D dynamic simulation model was developed to evaluate the energy performance of the BIPVT hot water system under natural circulation. A test rig was set up and calibrated for this study. An experimental study was carried out in the solar simulation lab of the Department of the Building Services Engineering and the predicted results were then compared with experimental data to evaluate the numerical simulation accuracy. The experimental measurements taken in the full scale indoor test facility are in good agreement with the predicted results. In addition, the influence of the configuration parameters of the BIPVT module has been

analyzed. The simulation results show that the configuration parameters of the BIPVT module should be optimized to maximize its energy performance. The fact is that a little change of the configuration parameters of the BIPVT module can significantly increase the energy performance of the PV module, especially the thermal efficiency of the BIPVT module.

At last, a building-integrated photovoltaic-thermal (BIPVT) energy system designed for a flat of two residents is proposed for generating electricity and producing hot water from vertical facade of high-rise residential buildings in Hong Kong. The annual hourly energy performance simulation of the system was conducted on the basis of dynamic heat transfer analysis and the typical meteorological year (TMY) weather data of Hong Kong. The simulation results obtained from a case study indicate that the proposed BIPVT hot water system can effectively increase the total energy benefits compared with a photovoltaic (PV) system integrated on vertical building facades. When the BIPVT modules are connected in series, the electrical energy efficiency, thermal energy efficiency and combined energy efficiency of the BIPVT system are, respectively, 10.0%, 34.9% and 44.9%. Such a system can offer 82.3% of the annual hot water supply to the flat in a year. The proposed system is found to be suitable for vertical facade of high-rise residential buildings in Hong Kong so that the problem of limited roof area in a high-rise building can be solved for solar energy application in a density urban area like Hong Kong.

Keywords: Building Integrated Photovoltaic (BIPV); Vertical facades; Building Integrated Photovoltaic Thermal (BIPVT) hot water system; Natural circulation; Numerical prediction; Experimental investigation.

PUBLICATIONS LIST

Journal papers:

1. Sun LL and Yang HX. Impacts of the Shading-Type Building-Integrated Photovoltaic Claddings on Electricity Generation and Cooling Load Component through Shaded Windows. Energy and Buildings 2010; 42(4): 455-460.
2. Sun LL, Lu L and Yang HX. Optimum Design of Shading-Type Building-Integrated Photovoltaic Claddings with Different Surface Azimuth Angles. Applied Energy, in Press.
3. Sun LL and Yang HX. Parameter Evaluation and Optimum Design of Building-Integrated Photovoltaic-Thermal Modules. Submitted to Applied Energy.
4. Sun LL and Yang HX. Performance Evaluation of a BIPVT hot water system with natural circulation for Hong Kong Residence. Submitted to Energy and Buildings.

Conference papers:

1. Yang HX, Lou CZ and Sun LL. Building-Integrated Photovoltaic for Maximum Power Generation. 2nd Electronics System-Integration Technology Conference (ESTC-2008), London, England, September 2008.
2. Sun LL and Yang HX. Optimum Design of Building Integrated Photovoltaic Arrays as Shading Devices. 4th International Green Energy Conference (IGEC-2008), Beijing, China, October 2008.

3. Sun LL, Lou CZ, An DW and Yang HX. Study on Building-Integrated Photovoltaic Technologies and Applications in Hong Kong. ISES Solar World Congress 2009 (SWC-2009), Pretoria, South Africa, October 2009.
4. Sun LL, Lu L and Yang HX. Optimum Design of Shading-Type Building-Integrated Photovoltaic Claddings with Different Surface Azimuth Angles. 2nd International Conference on Applied Energy (ICAE-2010), Singapore, April 2010.
5. Sun LL and Yang HX. Dynamic Performance of Shading-Type Building-Integrated Photovoltaic claddings in Hong Kong. 5th International Green Energy Conference (IGEC-2010), Waterloo, Canada, June 2010.
6. Sun LL and Yang HX. Parameter Evaluation and Optimum Design of Building-Integrated Photovoltaic-Thermal Modules. 1st International Conference on Sustainable Urbanization (ICSU-2010), Hong Kong, China, December 2010.

Chapters of Book:

1. Yang HX and Zhou W，Application and technology of Solar Integrated Building, China Architecture & Building Press.

   (1) Chapter 4: Development, Economic and Environmental of Building Integrated Photovoltaic Technology;

   (2) Chapter 7: Solar cooling and Storage Technology of Air Conditioning System.

2. Yang HX, Project of Building Integrated Photovoltaic system (in Press).

   (1) Section 1.4: Optimum inclination and orientation of BIPV modules；

(2) Section 2.2: Roof-attached Photovoltaic system of Li Shaoji Building in Hong Kong Polytechnic University；

(3) Section 2.4: Roof-integrated Photovoltaic system of Kadoorie Farm；

(4) Section 2.6: Roof-attached Photovoltaic system of Taipa Market in Macau；

(5) Section 3.9: Photovoltaic system of Functional Building in Ri Xin New Technology Photovoltaic Industry Park.

ACKNOWLEDGEMENTS

I would like to offer my sincere gratitude to my chief-supervisor, Prof. Yang Hongxing for his expert guidance, continuous encouragement and constant support during my three years of post graduate study for my PhD. His expertise in renewable energy research and his wisdom opened my eyes and decreased my ignorance. I cherish the opportunity of studying under him during this period.

Thanks are also due to Dr. Lu Lin of the Department of Building Services Engineering for her academic guidance and kind assistance.

Thanks are also due to my colleagues in the Renewable Energy Research Group and technicians in the Building Services Department, for their assistance in laboratory work.

Finally, I wish to dedicate this thesis to my parents and to thank them for their love, patience and support.

TABLE OF CONTENTS

CERTIFICATE OF ORIGINALITY I

ABSTRACT II

PUBLICATIONS LIST V

ACKNOWLEDGEMENTS VIII

TABLE OF CONTENTS IX

LIST OF FIGURES XV

LIST OF TABLES XIX

NOMENCLATURE XX

CHAPTER 1 INTRODUCTION 1

1.1 Building Integrated Photovoltaic (BIPV) 1

1.1.1 Advantages and disadvantages of the BIPV system 2

1.1.2 Integrating approach of the BIPV system 4

1.2 Building Integrated Photovoltaic Thermal (BIPVT) 9

1.2.1 Types of the PVT module 9

1.2.2 Advantages and disadvantages of the BIPVT system 10

1.3 Potential of the BIPV application in Hong Kong 10

1.4 Objectives of this research project 12

CHAPTER 2: LITERATURE REVIEW 14

2.1 Introduction 14

2.2 Energy performance of the BIPV facade 14

2.3 The projects of the shading-type BIPV claddings 16

2.4 Performance of the BIPVT system 20

2.5 Parameter evaluation of the PVT system 23

2.6 Experimental investigation of the BIPVT system 25

2.7 Summary 26

CHAPTER 3: MODEL OF SHADING-TYPE BIPV CLADDINGS 27

3.1 Introduction 27

3.2 The solar radiation on a tilt surface 27

3.2.1 Beam radiation on a tilt surface 28

3.2.2 Diffuse solar radiation on a tilt surface 30

3.2.3 Ground reflected solar radiation on a tilt surface 32

3.2.4 Total solar radiation on a tilt surface 33

3.2.5 Beam and diffuse solar radiation on a horizontal surface 33

3.3 Thermal and electrical models of the PV module 34

3.3.1 Dynamic heat transfer model of PV module 34

3.3.2 Electrical model of PV module 37

3.4 Thermal model of the window 37

3.4.1 Dynamic heat transfer model of window 37

3.4.2 Calculation of F_u 39

3.5 Thermal model of concrete wall 41

3.6 Calculation of convective heat transfer coefficient 42

3.7 Optical model of the glazing 43

3.8 Cooling load calculation of window and concrete wall 45

3.9 Calculation of combined electrical energy 46

3.10 Numerical resolution 46

3.11 Summary 47

CHAPTER 4: ENERGY PERFORMANCE OF SHADING-TYPE BIPV CLADDINGS 48

4.1 Introduction 48

4.2 System description 48

4.3 Simulation results and discussions 50

4.3.1 Electrical power of PV modules 50

4.3.2 Cooling load reduction of windows and concrete walls 53

4.3.3 Combined electrical energy 58

4.4 Summary 62

CHAPTER 5: MODELING OF THE BIPTV HOT WATER SYSTEM WITH NATURAL CIRCULATION 64

5.1 Introduction 64

5.2 Dynamic heat transfer model of the BIPVT system 67

5.2.1 The covering glass 67

5.2.2 The PV module 69

5.2.3 The thermal absorber 70

5.2.4 The water tubes 71

5.2.5 The connecting pipe 72

5.2.6 The thermal storage tank 73

5.3 Flow rate determination 73

5.4 Combined electrical power and thermal energy 74

5.5 Summary 75

CHAPTER 6: EXPERIMENTAL INVESTIGATION OF THE PVT HOT WATER SYSTEM WITH NATURAL CIRCULATION 76

6.1 Introduction 76

6.2 Experimental set-up 76

6.2.1 The PVT module 78

6.2.2 The Solar simulator 80

6.2.3 The GL800 data logger 81

6.2.4 The I-V curve tracer MP-170 84

6.3 Thermal property of the PVT hot water system 86

6.3.1 Stability of the solar radiation 86

6.3.2 Thermal contact 86

6.3.3 Thermal insulation 87

6.4 Energy performance of the PVT hot water system 90

6.4.1 Electrical energy efficiency 90

6.4.2 Thermal efficiency 93

6.5 Effect of varied parameters 94

6.5.1 Different solar radiation levels 94

6.5.2 Different vertical distances of barycenters 96

6.6 Simulation validation 99

6.7 Summary 101

CHAPTER 7: PARAMETER ESTIMATION OF PVT HOT WATER SYSTEM 102

7.1 Introduction 102

7.2 Effect of parameters 103

7.2.1 Thickness of covering glass (l_{cg}) 103

7.2.2 Thickness of air gap (l_a) 104

7.2.3 Thickness and conductivity of silicon gel (l_{si} & λ_{si}) 106

7.2.4 Thickness and material of thermal absorber (l_c & M_c) 106

7.2.5 Internal diameter and spacing between water tubes (d_i & w) 108

7.2.6 Thickness of thermal insulation material (l_{in}) 110

7.2.7 Volume of thermal storage tank (V_w) 111

7.2.8 Vertical distance of barycentres (ΔH) 112

7.3 Comparison of initial design and optimum design 114

7.4 Summary 116

CHAPTER 8: APPLICATION OF THE SHADING TYPE BIPVT HOT WATER SYSTEM IN RESIDENTIAL BUILDINGS 117

8.1 Introduction 117

8.2 Simulation results and discussions 119

8.2.1 Yearly energy performance 120

8.2.2 Monthly energy performance 123

8.2.3 Hourly energy performance 129

8.3 Summary 131

CHAPTER 9: CONCLUSIONS AND RECOMMENDATIONS FOR FUTURE WORK 133

9.1 Summary of research results 133

9.2 Recommendations for future work 135

REFERENCES 136

LIST OF FIGURES

Figure 1.1 the PV roof in EMSD 4

Figure 1.2 the PV roof in Penny Bay 5

Figure 1.3 the PV skylight in EMSD 6

Figure 1.4 the Sun-shading system in Science Park 7

Figure 1.5 the PV facade of One Peking 7

Figure 1.6 A semi-transparent BIPV facade system 8

Figure 2.1 South facade of SBIC East Building 17

Figure 2.2 City Hall from the south 18

Figure 2.3 PV systems of SIECT building 19

Figure 2.4 Sun-shading system of ECN building 20

Figure 3.1 Structure of a PV module 35

Figure 3.2 Schematic of shaded window 39

Figure 3.4 The orthogonal coordinates 40

Figure 4.1 The schematic of the shading-type BIPV claddings 49

Figure 4.2 Annual electricity generation per unit PV area 51

Figure 4.3 Annual power output of PV modules (R=20%) 52

Figure 4.4 Annual power output of south-facing PV modules 52

Figure 4.5 Annual cooling load per unit window area 53

Figure 4.6 Annual cooling load per unit concrete wall area 54

Figure 4.7 Cooling load reduction per unit window area (R=20%) 55

Figure 4.8 Cooling load reduction ratio of windows (R=20%) 55

Figure 4.9 Cooling load reduction ratio of south windows 56

Figure 4.10 Cooling load reduction per unit concrete wall area 57

Figure 4.11 Cooling load reduction ratio of concrete walls 57

Figure 4.12 Annual electricity saving per unit PV area (*R*=20%) 59

Figure 4.13 Annual electricity saving per unit PV area (*R*=40%) 59

Figure 4.14 Annual electricity saving per unit PV area (*R*=60%) 60

Figure 4.15 Annual electricity saving per unit PV area (*R*=80%) 60

Figure 4.16 Annual electricity saving per unit PV area (*R*=100%) 61

Figure 5.1 Schematic diagram of the BIPVT hot water system 65

Figure 5.2 The schematic of BIPVT modules installation 66

Figure 5.3 Front view and cross section of the BIPVT module 67

Figure 6.1 Photo of the test rig in the Solar Simulation Lab 77

Figure 6.2 Schematic of the PVT hot water system 78

Figure 6.3 Photo of the test rig in the Solar Simulation Lab 79

Figure 6.4 Photo of the solar simulator in the Solar Simulation Lab 81

Figure 6.5 Photo of the GL800 data logger 82

Figure 6.6 Photo of the MP-170 84

Figure 6.7 Solar radiations on a tilt surface 86

Figure 6.8 Temperatures of PV module, thermal absorber and water tube 87

Figure 6.9 Temperature of thermal absorber, ambient air and the back surface of metal frame 88

Figure 6.10 Measurement data of water temperature 89

Figure 6.11 Temperatures of water in the thermal storage tank 90

Figure 6.12 Maximum power of BIPVT module 91

Figure 6.13 Electrical efficiency of BIPVT module 92

Figure 6.14 Flow rate of water 92

Figure 6.15 Thermal efficiencies of the PVT module and the PVT hot water system 93
Figure 6.16 Electrical efficiency of the PVT module 94
Figure 6.17 Flow rate of water 95
Figure 6.18 Thermal efficiency of the PVT module 95
Figure 6.19 Thermal efficiency of the PVT hot water system 96
Figure 6.20 Electrical efficiency of PVT module 97
Figure 6.21 Flow rate of water 97
Figure 6.22 Thermal efficiency of the PVT module 98
Figure 6.23 Thermal efficiency of the PVT hot water system 98
Figure 6.24 Minutely variation of PV power output-simulation and experiment 100
Figure 6.25 Minutely variation of water temperature-simulation and experiment 100
Figure 7.1 Variation ratios with respect to cover glass thickness 103
Figure 7.2 Variation ratios with respect to air gap thickness 104
Figure 7.3 Variation ratios with respect to silicon gel thickness 105
Figure 7.4 Variation ratios with respect to silicon gel conductivity 105
Figure 7.5 Variation ratios with respect to thermal absorber thickness 107
Figure 7.6 Variation ratios with respect to thermal absorber material 107
Figure 7.7 Variation ratios with respect to water tube internal diameter 108
Figure 7.8 Variation ratios with respect to water tube spacing 109
Figure 7.9 Variation ratios with respect to thermal insulation thickness 110
Figure 7.10 Variation ratios with respect to thermal storage tank volume 111
Figure 7.11 Hourly temperature of water in tank 112

Figure 7.12 Variation ratios with respect to height 113

Figure 7.13 Hourly profile of electrical efficiency 113

Figure 7.14 Hourly profiles of thermal efficiency and combined energy efficiency 115

Figure 8.1 Schematic diagram of the BIPVT hot water system 118

Figure 8.2 Arrangement of BIPVT modules 118

Figure 8.3 Front view of the BIPVT module 119

Figure 8.4 Annual power output of BIPVT modules 121

Figure 8.5 Annual heat gain of water 122

Figure 8.6 Annual combined electrical energy of the BIPV hot water system 122

Figure 8.7 Monthly power output of BIPVT modules 124

Figure 8.8 Monthly heat gain of water 124

Figure 8.9 Monthly combined electrical energy of the BIPVT hot water system 125

Figure 8.10 Monthly variations of electrical efficiency 126

Figure 8.11 Monthly variations of thermal efficiency 126

Figure 8.12 Monthly variations of combined electrical efficiency 127

Figure 8.13 Monthly solar fraction of hot water supply 127

Figure 8.14 Number of days (T_w>45℃) 128

Figure 8.15 Hourly variation of temperature 129

Figure 8.16 Hourly variation of electrical efficiency 130

Figure 8.17 Hourly variation of thermal efficiency 130

Figure 8.18 Hourly variation of combined energy efficiency 131

LIST OF TABLES

Table 1.1 Equivalent horizontal area of buildings 10

Table 1.2 Potential power generation of the BIPV system in Hong Kong 11

Table 3.1 The Perez model coefficients for solar radiation calculation 30

Table 4.1 Length of overhangs 49

Table 4.2 Optimum tilt angles for different orientations and wall utilization fractions 61

Table 6.1 Basic parameters of the PVT module 80

Table 6.2 Specifications of the GL800 data logger 83

Table 6.3 Specifications of the MP-170 I-V curve tracer 86

Table 7.1 Parameter comparison between initial design and optimum design 113

NOMENCLATURE

Symbols	Description
A_w	Area of wall (m^2)
A_p	Area of PV module (m^2)
A_g	Area of window (m^2)
A_u	Area of unshaded window (m^2)
A_s	Area of shaded window (m^2)
A_j	Area of internal envelope (m^2)
C_p	Specific heat capacity of PV module (J/(kg·K))
C_{sc}	Specific heat capacity of silicon cell (J/(kg·K))
C_{EVA}	Specific heat capacity of EVA sheet (J/(kg·K))
C_{TPT}	Specific heat capacity of TPT back sheet (J/(kg·K))
C_g	Specific heat capacity of window (J/(kg·K))
C_w	Specific heat capacity of wall (J/(kg·K))
C_{cg}	Specific heat capacity of covering glass (J/(kg·K))
COP	Coefficient of performance (-)
d_o	External diameter of water tube (mm)
d_i	Internal diameter of water tube (mm)
d_{cp}	Internal diameter of connecting pipe (mm)

E_{comb} Combined electrical power (W)

E_p Electrical power of PV module (W)

E_{g+w} Electrical power due to cooling load reduction of window and wall (W)

F_u Unshaded ratio (-)

F_{o-s} View factor between overhang and sky (-)

g Gravitational acceleration (m/s^2)

G_{bh} Horizontal beam solar radiation (W/m^2)

G_{dh} Horizontal diffuse solar radiation (W/m^2)

G_{th} Tolat horizontal solar radiation (W/m^2)

G_{bn} Dirct beam solar radiation (W/m^2)

G_{bt} Beam solar radiation on a tilt surface (W/m^2)

G_{dt} Diffuse solar radiation on a tilt surface (W/m^2)

G_{grt} Ground reflected solar radiation on a tilt surface (W/m^2)

G_{tt} Total solar radiation on a tilt surface (W/m^2)

G_p Total solar radiation absorbed by PV module (W/m^2)

G_g Total solar radiation absorbed by window (W/m^2)

G_w Total solar radiation absorbed by wall (W/m^2)

G_{bv} Beam solar radiation on a vertical surface (W/m^2)

G_{dv} Diffuse solar radiation on a vertical surface (W/m^2)

G_{grv} Ground reflected solar radiation on a vertical surface (W/m^2)

G_{cg} Total solar radiation absorbed by covering glass (W/m^2)

H_g Height of window (m)

H_w Height of wall (m)

H_t Buoyant head (kg/m^2)

H_f Friction loss (kg/m^2)

h_o Outside convective heat transfer coefficient ($W/(m^2 \cdot K)$)

$h_{p\text{-}s}$ Radiant heat transfer coefficient between PV module and sky ($W/(m^2 \cdot K)$)

$h_{p\text{-}w}$ Radiant heat transfer coefficient between PV module and wall ($W/(m^2 \cdot K)$)

$h_{g\text{-}s}$ Radiant heat transfer coefficient between window and sky ($W/(m^2 \cdot K)$)

$h_{g\text{-}j}$ Radiant heat transfer coefficient between window and internal envelope ($W/(m^2 \cdot K)$)

$h_{w\text{-}j}$ Radiant heat transfer coefficient between wall and internal envelope ($W/(m^2 \cdot K)$)

$h_{i,g}$ Convective heat transfer coefficient of the window inside surface ($W/(m^2 \cdot K)$)

$h_{i,w}$ Convective heat transfer coefficient of the wall inside surface ($W/(m^2 \cdot K)$)

$h_{g\text{-}s}$ Radiant heat transfer coefficient between covering glass and sky ($W/(m^2 \cdot K)$)

$h_{r,\, p\text{-}cg}$ Radiant heat transfer coefficient between PV module and covering glass ($W/(m^2 \cdot K)$)

$h_{c,p\text{-}cg}$	Convective heat transfer coefficient between PV module and covering glass (W/(m^2·K))
h_f	Convective heat transfer coefficient between water and water tube (W/(m^2·K))
K_g	Extinction coefficient of window (1/m)
k	Thermal diffusivity (m^2/s)
L_o	Length of overhang (m)
L_{swp}	Length of supply water pipe (m)
L_{rwp}	Length of return water pipe (m)
l_p	Thickness of PV module (mm)
l_{fg}	Thickness of front glass (mm)
l_{sc}	Thickness of silicon cell (mm)
l_{EVA}	Thickness of EVA sheet (mm)
l_g	Thickness of window (mm)
l_w	Thickness of wall (mm)
l_{TPT}	Thickness of TPT back sheet (mm)
l_{cg}	Thickness of covering glass (mm)
l_a	Thickness of air gap (mm)
N	Number of water tubes (-)
Nu	Nusselt number (-)
Pr	Prandtl number (-)

Q_w Cooling load of wall (W)

$Q_{g,c}$ Cooling load of window due to convective heat gain (W)

$Q_{g,d}$ Cooling load of window due to diffuse solar heat gain (W)

$Q_{g,b}$ Cooling load of window due to beam solar heat gain (W)

$q_{g,d}$ Diffuse solar heat gain of window (W)

$q_{g,b}$ Beam solar heat gain of window (W)

R Wall utilization fraction (%)

R_b Geometric factor (-)

Re Reynolds number (-)

R_{si} Thermal conductive resistance of silicon gel ($(m^2 \cdot K)/ W$)

R_{in} Thermal conductive resistance of thermal insulation ($(m^2 \cdot K)/ W$)

R_B Thermal conductive resistance of bond ($(m^2 \cdot K)/ W$)

T_p Temperature of PV module (K)

T_o Temperature of outdoor air (K)

T_s Temperature of sky (K)

T_w Temperature of wall (K)

T_g Temperature of window (K)

T_j Temperature of internal envelope (K)

T_{cg} Temperature of covering glass (K)

T_c Temperature of thermal absorber (K)

T_f Temperature of water in water tube (K)

T_{wt} Temperature of water in water tank (K)

T_{swp} Temperature of water in supply water pipe (K)

T_{rwp} Temperature of water in return water pipe (K)

t Time (s)

X_{wp} View factor between wall and PV module (-)

X_{gj} View factor between window and internal envelope (-)

X_{wj} View factor between wall and internal envelope (-)

x, y Coordinates (-)

Greek symbols

θ Incidence angle (deg)

δ Solar declination (deg)

φ Latitude angle (deg)

β Tilt angle (deg)

ω Hour angle (deg)

γ Surface azimuth angle (deg)

ζ Reflectance (-)

α Absorptance (-)

η Energy efficiency of PV module (%)

ρ	Density (kg/m^3)
λ	Thermal conductivity (W/(m·K))
ε	Emittance (-)
τ	Transmittance (-)
v	Kinematic viscosity (m^2/s)

Subscripts

a	Air gap
b	Beam
c	Thermal absorber
cg	Covering glass
cp	Connecting pipe
d	Diffuse
e	Electric heater
f	Water in water tube
fg	Front glass
g	Glass pane
gr	Ground reflectance
hw	Hot water
o	Outdoor

i	Indoor
p	Photovoltaic module
s	Sky
swp	Supply water pipe
rwp	Return water pipe

CHAPTER 1 INTRODUCTION

1.1 Building Integrated Photovoltaic (BIPV)

Nowadays, energy supply is essential for mankind. Most of the activities in the current industrial age require the supply of electrical power. The two most prevailing kinds of primary energy resources are oil and coal. According to a recent world energy statistics, in 2010, oil and coal constitute more than 60.2% of the world's energy supply among various energy sources. However, the combustion of the oil and coal brings in harmful environmental problems, such as climate change, air pollution and acid rain. In addition to environmental threats, the limited reserves of ordinary energy sources in the world have also been widely concerned. It is anticipated that, at current consumption rates, the supply of coal will last for around 200 years and oil for approximately 40 years. The shortage of fossil fuels will happen in the foreseeable future. Owing to the negative effects and the finite supply of fossil fuels, the development of new sources of energy that is sustainable and environmental friendly, such as renewable energy, is necessary.

Among the various types of renewable energy, solar photovoltaic is one of the popular and well-developed options. Photovoltaic (PV) technology has received serious concern since the 1970s. Building Integrated Photovoltaic (BIPV) is a common application of photovoltaic technology in urban areas. Early projects integrated PV into residential houses. In the late 1970s and early 1980s, much effort has been paid on PV integration in commercial developments (Strong et al. 1996). As scientists and politicians have continued to look at alternative energy and energy

conservation as solution of pollution and global climate change, BIPV applications have developed rapidly worldwide in the past two decades. A number of BIPV systems have been installed in many countries over the period (Strong et al., 1996; Pearsall et al., 1996; Schoen et al., 2001; Bhargava et al., 2001; Yoo et al., 2002; Yang et al., 2005, Aristizabal et al., 2008 and Yoon et al., 2011). In recent years, the BIPV technology has developed quickly around the world because it combines the energy production with other functional features on building envelopes. PV modules integrated into the building envelops can reduce the overall cost by forming part of the external envelopes and replacing traditional building elements. PV roofs, PV curtain wall and PV overhangs and are typical applications of the BIPV systems to achieve a energy efficient and aesthetically pleasing outlook in buildings.

1.1.1 Advantages and disadvantages of the BIPV system

Until now, BIPV modules have been compromise between energy and aesthetics, as despite being efficient energy providers, the modules were not always pleasing to the eye. However, BIPV modules have become more and more colorful and attractive. Using BIPV modules can create a visually arresting building. The integration of BIPV modules into buildings is so flexible that the architects can design a building using their imagination and make the building impressive and environment-friendly. It strikingly improves the image of a building and increases the resale value.

BIPV systems can either be connected to the utility grid or designed as stand-alone systems. Buildings integrated with BIPV modules can eliminate the demands of the traditional energy generator and reduce the emission of green house gases. And the

owner of the building can make savings through lower electricity bills due to peak shaving.

There are also many advantages including:

(1) BIPV modules can replace traditional building materials (e.g. spandrel glass) and building processes.

(2) BIPV modules can be integration into saw-tooth designs and awnings on a building façade. These modules can be used in entrances, terraces or simply as awnings to shade the rooms inside.

(3) Using semi-transparent BIPV modules as skylight systems in entrance halls, atria or courtyards. It is an efficient use of solar energy and an exciting design of buildings.

(4) BIPV modules protect against the weather, giving shade from the sun as well as protection from wind and rain.

On the other hand, there are also some disadvantages of BIPV systems such as high cost and architectonic integration. Once the challenges of cost and aesthetics are overcome, maintenance is the single largest issue for BIPV systems because it may be costly to repair once installed. Automating failure detection and ease of maintenance procedures are of paramount importance to building owners and operators. An added effort and investment in terms of planning and maintenance may also be required. In addition, BIPV brings together two historically separated trades – construction and electrical. Overcoming the friction that arises from such convergence is critical to promoting the application of BIPV technology at a healthy pace.

1.1.2 Integrating approach of the BIPV system

BIPV systems have been well-developed all over the world among the other types of PV applications. This is because the BIPV systems require no additional land and they can provide electricity near the point of use. In the past decade, a number of new buildings have been integrated with BIPV systems as an alternative power source. The following section will give a brief overview on the type of the BIPV system that is commonly found in current applications.

Figure 1.1 the PV roof in the office building of Electrical and Mechanical Services Depart (EMSD)

All parts of the surfaces of the building are suitable for installing photovoltaic arrays, provided that the surface can receive adequate amount of solar radiation. The installation methods of the photovoltaic arrays can be categorized into three main types according to their approaches of integration, namely, roof-mounted systems, sunshades systems and façade systems. The typical projects of each type of the

systems are described in the following three paragraphs. These BIPV systems are located in Hong Kong.

Figure 1.2 the PV roof in the office building of fire station in Penny Bay

(a) Roof-mounted systems

PV modules in this kind of system are installed on the roof of the buildings. The PV modules can be either installed as an independent array on the rooftop (as shown in Figure 1.1) or combined with the roof structural system (as shown in Figure 1.2). The slope and orientation of the independent module array can be selected so that the most solar radiation can be captured. This arrangement can avoid a substantial amount of heat gain due to sunshine on the building roof. However, water proofing issues have to be considered. For PV modules that are integrated to the roof structure, typical application can be found on the top of an atrium. As shown in Figure 1.3 semi-transparent PV modules are used together with clear glazing in this case for providing daylight to the indoors. Not surprisingly, the roof-mounted BIPV system is the most prevalent one among the other types of integration because it receives more solar energy for low-latitude areas and PV modules installed on the roof are less

likely to be shaded by other obstacles. Also, this system will bring less impact to the appearance of the building.

Figure 1.3 the PV skylight in the office building of Electrical and Mechanical Services Depart (EMSD)

(b) Sun-shading systems

PV modules can be installed as awnings outside the windows to shade direct sunlight. As a result, the system can provide energy benefits not only though the electricity generation by the PV modules but also through the reduction of solar heat gain to the building. The inclination of the PV modules can also be designed to maximize energy production. However, compromise should be made with the aesthetic consideration because the PV modules can be easily seen from the outside of the building. The sun-shading systems also incur higher installation cost among the others because of addition structural requirement. Figure 1.4 shows a photo of a sun-shading system in the office building of Science Park.

Figure 1.4 the Sun-shading system in the office building of Science Park

(c) Façade systems

In these kinds of systems, PV modules act as a part of the outer skin of the building. The PV modules used in the systems can be either opaque or semi-transparent. Therefore, these kinds of systems can be further divided into two sub-categories; they are PV cladding and semi-transparent PV glazing, as shown in Figures 1.5 and 1.6.

Figure 1.5 A semi-transparent BIPV facade

Figure 1.6 the PV facade of the building of One Peking

Mounting a series of opaque PV modules on building façade can form a PV cladding. The modules are usually mounted on cladding rails in order to provide a ventilation gap between the building structure and the PV modules. The gap has the beneficial effect of reducing the temperature of the modules, thus increasing power converting efficiency. In the case of a semi-transparent PV module, opaque solar cells are encapsulated in middle of two glass sheets to form a "glass-solar cells-glass" structure. This kind of PV module can be used in window systems to admit daylight as well as produce electricity. Further, the PV modules can be incorporated into double-glazed curtain wall systems by using the modules as the outer pane of the system. The area of the space between the solar cells can be selected by balancing the daylight requirement and the electricity yield. This kind of integration is highly cost effective because the PV modules can replace the traditional glass on the building façades to reduce the installation cost. It is necessary to mention that a kind

of “see-through” thin film solar cell has been invented as semi-transparent BIPV module. The structure of the solar cell is the same as the ordinary thin film solar cells but with microscopic holes to make the cell semi-transparent.

1.2 Building Integrated Photovoltaic Thermal (BIPVT)

1.2.1 Types of the PVT module

Photovoltaic thermal modules vary in design for different applications, ranging from PVT domestic hot water systems to ventilated PV facades and actively cooled PV concentrators. The markets for both solar thermal and PV are growing rapidly and have reached a very substantial size. PVT modules have broad range of application, that is, it is not only suitable for domestic hot water heating (water type PVT modules), but also for commercial buildings (air type PVT modules to preheat ventilation air during winter and to provide the driving force for natural ventilation during summer). Hence, the market for PVT modules might even be larger than the market for solar thermal collectors. The thermal demand can be covered by choosing the appropriate PVT system.

There exist various forms of PVT modules. According to the types of solar cell, there are the monocrystalline silicon PVT module, the polycrtystalline silicon PVT module and the amorphous silicon PVT module. Depending on the types of heat removal fluid, PVT modules can be classified as the liquid-type PVT module (water-type PVT module) and the air-type PVT module. If a PVT module has a glass cover to reduce the thermal losses, it is named as the glazed PVT module. If such a cover is not present, the PVT module is referred to as the unglazed PVT module.

1.2.2 Advantages and disadvantages of the BIPVT system

Hybrid photovoltaic thermal system in the other hand is the continuity of the PV system and solar thermal system, combining two systems into one system. The system can be segregated into two parts: the PV technology which is derived from solar cell technology and converts solar energy into electricity and thermal solar technology which is derived from thermal collectors and converts solar energy into heat. The BIPVT system has many advantages such as:

(1) It works on noiseless environment;

(2) It does not produce any toxic waste or radioactive material;

(3) It is a highly credible system with life span expectation between 20 and 30 years;

(4) It is a system of low maintenance.

1.3 Potential of the BIPV application in Hong Kong

The effectiveness of deployment of BIPV depends on technical and administrative factors. Before any administrative issues are considered, technical feasibility is a pre-requisite of BIPV applications and has to be evaluated in advance. From the perspective of technical aspect, except the solar radiation, the availability of area for mounting PV modules is also the crucial factors to be considered.

The available electricity will be much smaller for actual situation due to the constraints of land use. Thus, a term “equivalent horizontal area” was introduced to estimate the potential energy yielded from BIPV technology by the Electrical and Mechanical Services Department, HKSAR. Fung (2006) estimated the equivalent horizontal area for different types of buildings, as listed in Table 1.1. It indicates that

about 36.9% of the total area of buildings in Hong Kong are suitable to install PV modules.

Table 1.1 Equivalent horizontal area of buildings

Building type	Area (km^2)	Asssumed ratio of equivalent horizontal area	Equivalent horizontal area (km^2)
Residential	45	0.3	13.5
Public rental housing	14	0.3	4.2
Commercial	2	0.5	1
Industrial	11	0.5	5.5
Government, institution and community facilities	21	0.2	4.2
Temporary housing areas	1	0	0
Vacant development land	27	0.6	16.2
Total	121	n/a	44.6

For the high-rise building, PV modules are usually integrated vertically into its facades rather than placed horizontally because there is not enough roof area. So it is more practical to estimate the energy output from the vertical facades. Fung (2006) also evaluated the potential energy yielded for roof and vertical facade in Hong Kong, as listed in Table 1.2.

Table 1.2 Potential power generation of the BIPV system in Hong Kong

Building type	Potential power generation (GWh/y)	
	Roof	Vertical facade
Residential	1914	5451
Public rental housing	596	1696
Commercial	142	404
Industrial	780	2220
Government, institution and community facilities	596	1696
Temporary housing areas	0	0
Vacant development land	2297	6540
Total	6325	18007

Table 1.2 shows the yearly potential power generation is 6325GWh of the roof and 18007GWh of the vertical facade. It indicates that potential power generation of the vertical facade is much lager than that of the roof. According to Hong Kong Energy End-use Data (2010), the total electricity consumption of the year 2008 is about 40929GWh. This is equivalent to about 44% of the electricity consumption in 2008.

1.4 Objectives of this research project

Both integrating PV modules into buildings and combining PV modules with collectors are increasing trends for application of PV modules in buildings. Comparing with a simple PV system, the BIPV system and the BIPVT system can produce more energy benefits in addition to the electricity generation. The payback time of such systems is much lower than that of the simple PV system. Therefore, it

is necessary to study the energy performance of the BIPV system and the BIPVT system.

The objectives of the research are as follows:

1) To develop a mathematical model to explore the energy performance of the shading-type BIPV claddings. The impacts of the inclination and orientation are analyzed on the basis of the above model.
2) To develop a mathematical model to explore the energy performance of the BIPVT hot water system with natural circulation. Several main configuration parameters of such system are evaluated and optimized.
3) To obtain experimental information on a real test-rig of the PVT hot water system under controlled conditions to gain insight into the complex behavior of the PVT hot water system with natural circulation. The measurements shall serve for model verification purposes.

CHAPTER 2: LITERATURE REVIEW

2.1 Introduction

This chapter provides an overview of the integration types of the BIPV system in different building parts such as flat roofs and vertical facades, as well as glazed roof and sunshade devices. Although the shading-type BIPV system is not playing the leading role in the BIPV market, a number of shading-type BIPV projects have been completed in the past decade. This chapter introduces some significant projects in detail. In addition, a literature review of the BIPVT system is also presented in this chapter. The literature review focuses on the energy performance estimation, configuration parameters evaluation and optimization, and experimental investigation of the BIPVT system.

2.2 Energy performance of the BIPV facade

As the BIPV technology is becoming more and more popular, a great number of applications can be found around the world. BIPV modules are usually integrated into the external envelope of a building. In order to reduce the module's temperature and improves the electrical performance of the PV modules, an air gap can be designed behind the module to allow natural ventilation between the modules and the building walls (Brinkworth et al., 1997). Therefore, more consideration is needed in evaluating the heat transfer through the PV façade. A considerable number of studies on the heat transfer and energy performance of the PV façade have been carried out. Brinkworth et al. (1997) validated that PV module temperature and heat gain into the

building can be significantly reduced by a ventilated air gap behind the PV modules. Similar studies on the heat transfer characteristics of ventilated PV facade have also been conducted by various specialists (Moshfegh et al., 1998; Brinkworth et al., 2000; Yang et al., 2000; Infield et al., 2004).

Another comprehensive study on the thermal characteristics of a PV façade was carried out by Jones et al. (2001). They developed a model for determining the temperature of PV modules by resolving the differential equations. Convective and radiative heat transfer between the PV module and the ambient as well as the solar irradiance input to the module was considered in the model. The authors also included the PV modules' electrical power output in the equation. The model was a non-steady state equation of the module's temperature and was solved numerically by Euler method. Other than the heat transfer characteristics, the optimum area of PV module on a solar façade has also been investigated. According to Vartiainen (2000), a solar façade was defined as a façade which was composed of clear or diffusive glazing, semi-transparent PV glazing and opaque area covered by PV modules. He has developed a detailed daylight simulation program to estimate the daylight availability of different solar façade arrangements. For varied solar façade patterns, he predicted the electricity benefits of the solar façade by taking into account the electrical power output from the PV modules and the electrical energy saving due to daylight utilization. However, Vartiainen's study mainly focused on the daylight simulation, but the analysis on the electrical performance of PV modules was relatively simple, and only the optimum window area was reported.

In addition, many theoretical and experimental studies have been conducted to maximize the energy benefits of BIPV systems, in terms of the power output of PV modules and the cooling load reduction of buildings. Yoo et al. (2002 and 2010) examined a south-facing shading-type BIPV system and suggested that the shading-type BIPV claddings should be applied for both generating electricity and providing shading for the building. Chow et al. (2007 and 2009) have evaluated and tested a southwest-facing BIPVT wall located in Hong Kong. In comparison with the conventional wall, the range of the BIPVT wall internal surface temperature is smaller and the space cooling load can be lowered by 50% in the hottest summer. Wang et al. (2006) indicated that a BIPV roof with ventilated air gap has high PV energy efficiency and low cooling load in hot summer. James et al. (2009) investigated a semitransparent PV atrium and found that it has a great amount of multiple advantages such as electricity generation, solar shading, attractive look and environmental statements. Zogou et al. (2011) has examined south-facing double PV facades of an office building on basis of energy simulation using the TRANSYS. The existence of double PV facades can considerably reduce the cooling energy consumption of buildings if alternative night cooling strategy is allowed.

2.3 The projects of the shading-type BIPV claddings

There have been many successful sun shading-type BIPV projects developed around the world, as follows:

(1) The SBIC East Building (as shown in Figure 2.1) is located in Shibuya, where a nearly developed city center is being expanded. It was designed by Jiro Ohno, Nihon Sekkei and has a total of 29.7kWp BIPV installed. It

consists of eight stairs and two basements. Its total floor area is 7663m^2. In the original plan PV arrays were not included at all. However, when a solution was needed for reducing the air-conditioning load, BIPV became a viable option by placing the PV modules as semi-transparent vertical louvers, and thus using them as shading elements. In addition to the vertical PV louvers, standard type PV arrays on the roof, integrated PV in the rooftop pergola and screen furling were combined to achieve a total PV capacity of 29.7kWp.

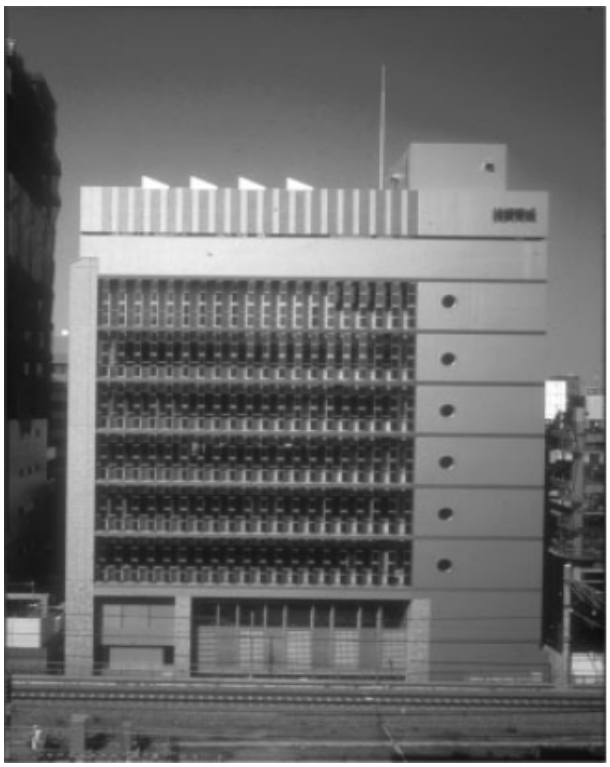

Figure 2.1 South facade of SBIC East Building in Shibuya

(2) As shown in Figure 2.2, the building of the City Hall was designed to have horizontal PV louvers on the south side and on the roof, vertical PV louvers on the north side and PV void panels on the east and west sides. By using PV modules as elements on each side of the building, no additional shading measures are needed, whereas the PV modules also secure natural ventilation. The total installed PV capacity is 195kWp and energy saving has been

achieved by applying the modules as louvers, which reduces the air-conditioning load. In order to cope with the strong sea breeze and the giant typhoons hitting Okinawa every year, the PV modules have been reinforced by tempered glass at both sides. The huge shaded space below the PV eaves has become a recreation and relaxation place for the citizens of Itoman City. It is called Amahaji which stands for a symbol of an environmentally friendly building.

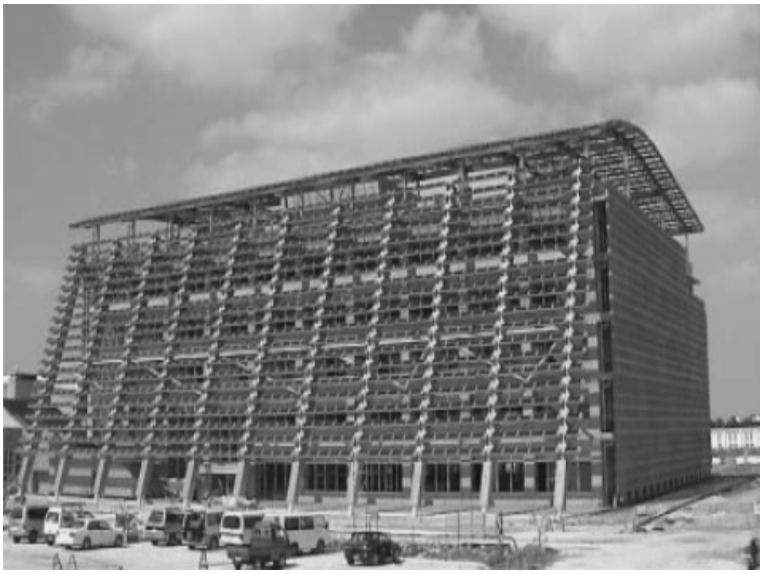

Figure 2.2 City Hall from the south

(3) A building-integrated photovoltaic system (BIPV) has been operated over 1 year in the Samsung Institute of Engineering & Construction Technology (SIECT) in Korea. The PV cells are mounted on the south facade and on the roof of the SIECT in the Giheung area. The PV modules are utilized as external shading devices of the building. In the summer the PV modules can help to reduce cooling loads. While in the heating season, solar energy is allowed to enter the building. Because of the design compromises non-optimal tilt angles and occasional shading of the PV modules make the efficiency of

PV system lower than the peak rating of the cells. The yearly average efficiency of the sunshade solar panel is 9.2% (average over 28.6℃ surface temperature), with a minimum of 3.6% (average over 27.9℃ surface temperature) in June and a maximum of 20.2% (average over 19.5℃ surface temperature) in December. It is recommended that a solar cell panel as a shading device on a south facade should be applied in such a way that it is not shaded by the above panel. For example, the angle of the sun-shading panel should be planned to be flexible, changing at least according to the season. Alternatively, a more economical option would be the installation of solar cell panels on every second story.

Figure 2.3 PV system of SIECT building

(4) The ECN's building is equipped with sunshade devices made of PV modules. The PV modules of the awning and of the lamellas are grouped into 13 vertical sections, with one inverter per section. One PV system consists of 7 lamella strings and 2 awning strings, each string having 6 modules. The lamellas have a tilt angle of 38° and the awning has a tilt angle of 18°. The facade is almost

south oriented. Due to the differences in the orientation of the awning strings and the lamella strings the irradiations and module temperatures are different. Since the voltages are forced to be equal due to the parallel connection of the strings the various strings cannot he operated in their own MPP (maximum power point). This mismatch causes a loss in the overall performance.

Figure 2.4 Sun-shading system of ECN building

2.4 Performance of the BIPVT system

In recent years, more and more studies are focused on the application of the BIPVT system since it can obtain much more energy benefits than the single PV system. This is in favor of the development of the PV technology. Chow et al. (2003) have analyzed the water-type PVT module with single glazing in a dynamic condition. The tube underneath flat plate with metallic bond collector was used. They observed that the photovoltaic conversion efficiency at the reduced temperature is increased by 2% at mass flow rate of 0.01 kg/s for 10000 W/(m^2·K) plate to bond heat transfer coefficient. An additional thermal efficiency of 60% was also observed. For water heating under natural mode of operation, Huang et al. (2001) have studied experimentally the unglazed integrated photovoltaic and thermal solar system

(IPVTS). They observed that the primary energy saving efficiency of the IPVTS exceeds 0.60 which is higher than that for a conventional solar water heater or pure PV system. Kalogirou (2001) has studied the monthly performance of an unglazed hybrid PVT system under forced mode of operation for climatic condition of Southern Cyprus and observed an increase of the mean annual efficiency of the PV solar system from 2.8% to 7.7% with thermal efficiency of 49%, respectively. Similar study has also been carried out by Zondag et al. (2002). They have referred to hybrid PVT as a combi-panel that converts solar energy into both electrical and thermal energy. The electrical and thermal efficiency of the combi-panel were reported as 6.7% and 33%, respectively. Sandnes et al. (2002) have observed the behavior of a combined photovoltaic thermal (PVT) collector which was constructed by pasting single-crystal silicon cells onto a black plastic solar heat absorber (unglazed PVT system). They recommended that the combined PV/T concept must be used for low temperature thermal application for increasing the electrical efficiency of the PV system, e.g., for space heating of a building. Zakharchenko et al. (2004) have also studied unglazed hybrid PV thermal (PVT) system with a suitable thermal contact between the panel and the collector. They have proved that the areas of a PV panel and collector in a PVT system need not be equal for higher overall efficiency. To operate PV module at low temperature, PV module should cover the low temperature part of the collector (at cold water inlet portion). Further, an unglazed hybrid photovoltaic thermal panel with booster diffuse reflector was integrated with the horizontal roof of a building by Tripanagnostopoulos et al. (2002).

Similar to the air-type BIPVT modules, water-type BIPVT modules are used for heating water for various domestic and industrial applications. The domestic water heater generally uses flat plate collectors in parallel connection and run automatically with thermo-siphon principle where as the industrial water heater consists of a number of flat plate collectors in series and the thermo-siphon action does not work in this case. Hence, it uses a photovoltaic driven water pump to maintain a flow of water inside the water collector. He et al. (2006) defined the performance of a PVT module by a combination of efficiencies, thermal efficiency and electrical efficiency. They are, respectively, the ratio of the useful thermal gain and electrical gain of the system to the incident solar irradiation on the collector's aperture within a given period. The sum of the two gives the total efficiency that is commonly used to assess the overall performance. They also reported a daily thermal efficiency of around 40% of the system. Several researchers (Garg et al., 1999; Othman et al., 2005; Radziemska, 2003) have also defined a combined photovoltaic thermal efficiency as the same as He et al. (2006) by adding the thermal and electrical efficiencies of the PVT system. Chow et al. (2007) have done an experimental study of a facade-integrated photovoltaic/thermal water-heating system and found the thermal efficiency as 38.9% and the corresponding electrical efficiency as 8.56% during the late summer of Hong Kong. They compared both forced mode as well as natural mode of water circulation and found that the latter is more preferable and suggested that the system can serve as a water preheating system. Ji et al. (2003) have done a theoretical study on PV/T water collector by comparing the annual performance of a thin film cell and monocrystalline silicon cell modules and reported that they give 58.9% and 70.3% overall thermal efficiency, respectively, which are better than the conventional solar collectors' performance.

2.5 Parameter evaluation of the PVT system

For water-type photovoltaic thermal modules, a great deal of efforts have been paid to enhance the heat transfer from absorber to water. A satisfying heat transfer is obtained by leading the heat-collecting medium through a thin channel over the full width of the absorber. Chow et al. (2006) built a thermosyphon system with a PVT module based on an extruded aluminium channel absorber with a W/D ratio of 1 to obtain an optimal heat transfer to the fluid. De Vries (1998) indicated that the yearly yield of a PVT system could be raised by 2% by using a water channel underneath the cells instead of a sheet-and-tube construction.

For an unglazed PVT collector, Hendrie (1982) described a grooved cover surface, which is coated with a low-emissivity film. Due to recirculation areas caused by the grooves, the effective surface for heat transfer can be reduced. She claims that whereas large ratios lead to large fin losses, small ratios (less than 2) are able to reduce the heat loss by 20%-25%. Depending on the emissivity of the surface, the thermal efficiency is between 50% and 30%. However, the feasibility of such a scheme is doubtful. Apart from examining the thermal properties, attention should also be paid to cost and soiling, as well as possible inhomogeneous illumination of the PV. Zondag et al. (2003) compared a conventional PV module, an unglazed PVT module and a glazed PVT module. The average annual electrical efficiency was found to be 7.2%, 7.6% and 6.6% respectively. Since a glass with the transparency of 92% was used in the calculations, the reduction in electrical performance for the glazed PVT compared to a conventional PV module is exactly what one would expect from the additional reflection losses, which means that for the glazed PVT the additional temperature effect cancelled over the year, while for the unglazed PVT the

temperature effect was positive. They found that for the case of domestic water heating, the increase in annual thermal performance (35%-38%) could not compensate for the loss in electrical performance (6.6%-5.8%) and the more complicated manufacturing and handling cost. Krauter (2003) has been developing an unglazed integrated solar home system, in which a PV laminate is connected to a triangular water tank. The tank serves to cool the PV by means of an 'extended heat capacity'. Typically, at high irradiance a PV temperature reduction of about 20℃ is reported relative to a conventional solar home system, which leads to a 9%-12% increase in electrical yield, depending on the stratification. The stratification in the tank causes a temperature difference of about 6℃ between the upper and the lower PV module. In a later prototype the battery storage is placed at a cooled triangular space at the centre of the storage and the PV is shifted to the lower part of the tank to improve the PV performance.

The radiative characteristics of the top cover are of importance. The spectra of infrared transmission for various covering materials are presented by Bansal et al. (1985). Since a typical absorber has temperatures in the range of 30℃-70℃, this corresponds with wavelengths of 9.6mm-8.4mm. It would be even better if the emission of the top cover could also be reduced, e.g. by a spectrally selective coatings for the top glass that would reflect the infrared back to the absorber. However, the problem of such coatings at present is the reduced transmission in the solar part of the spectrum. The glass database in the LBNL program WINDOW gives 76% solar transmission at best for a glazing of 30% emissivity, while a glazing of 5% emissivity would have a transmission of 60%. Although in theory spectrally selective glazing has a substantial potential for increasing the thermal efficiency of a

PVT collector, for commercially available spectrally selective glazing the transmission is too low to increase the PVT performance. Although the transmissions are presently too low for PVT applications and it will be difficult to increase the transmission substantially, the research may be promising for the future.

2.6 Experimental investigation of the BIPVT system

Several investigations of the BIPVT system have been carried out previously. Bergene et al. (1995), for instance, proposed a detailed model of a PVT system and examined its performance. The simulation results indicated that the overall efficiency of a PVT system could reach 60%-80%. Huang et al. (2001) proposed a primary, energy-saving efficiency scheme, which considers different energy grades between electrical and thermal energies for evaluation of the energy-saving capacity of a PV/T system. Similarly, Tripanagnostopoulos et al. (2002) analyzed the performance of different types of PVT systems, including water-type PVT systems with or without glazing, air-type PVT systems with or without glazing and PVT systems with or without booster diffuse reflectors. The conclusion implied that the PVT systems with glazing could increase thermal efficiency but would reduce electrical efficiency. In addition, the systems with booster diffuse reflectors could achieve an electrical output increase by 16% compared with those without booster diffuse reflectors. He et al. (2006) studied the PVT module adapted with a flat-box absorber design and reported a daily thermal efficiency of approximately 40% in cases with natural water circulation. Ji et al. (2007) have done experiments on a flat-box aluminum-alloy photovoltaic and water-heating system designed for natural circulation and found its daily electrical efficiency is 10.15%, the characteristic daily thermal efficiency exceeds 45%, the characteristic daily total efficiency is above

52% and the characteristic daily primary-energy saving is up to 65%. In addition to these, various other studies on the PVT system have been conducted in recent years (Arvind et al., 2006; Fraisse et al., 2007; Robles-Ocampo et al., 2007; Pei et al., 2008a,b; Sarhaddi et al., 2010).

2.7 Summary

This chapter mainly presents a literature review on the BIPV system and the BIPVT system considering several aspects. A review of numerous studies about the application of the BIPV systems has been made, mainly focusing on the energy performance and the typical projects of the shading-type BIPV system. Secondly, in addition to the estimation of its energy performance, the studies about the configuration optimization and experimental investigation are also referred.

It is found that although a number of reports have been published for the BIPVT and BIPVT applications, there are still problems to be solved, especially for its application in high-rise buildings. In Hong Kong, most of the buildings are high-rise buildings. Most people live in small to medium flats. There is not enough roof area for locating solar collectors for solar energy application on the roofs of the buildings. If the BIPV panel or the BIPVT panel can be used on vertical façades of such high-rise buildings, the less roof are problem can be solved for solar energy applications. This project is to evaluate a BIPV system and a BIPVT system designed for a typical residential application of a high-rise building in Hong Kong.

CHAPTER 3: MODEL OF SHADING-TYPE BIPV CLADDINGS

3.1 Introduction

In general, the shading-type BIPV claddings are oriented at the position that can receive the most desirable solar energy to obtain the maximum electricity generation. At the same time, a great amount of solar heat entering the windows can be prevented and the cooling load of the building can be reduced by the shading effect of the shading-type BIPV claddings. These benefits make buildings become more energy efficient. However, contradiction between the electricity generation and the cooling load reduction occurs. It is obvious that the PV modules produce the greatest shading effect when they are placed horizontally. However, this position is not the best for PV modules to obtain the most desirable electricity generation. It is difficult for engineers to select the optimum tilt angle of PV modules for a particular building. Thus, it is worth setting up a simulation model to evaluate the effects of different tilt angles of PV modules on the energy saving in order to maximize the saving.

3.2 The solar radiation on a tilt surface

The electricity power generated by photovoltaic (PV) systems is directly related to the solar energy received by the PV panels, while the PV panels can be placed at any orientations and at any tilt angles, but most local observatories only provide solar radiation data on a horizontal surface. Thus, an estimation of the total solar radiation incident on the PV module surface is needed. Generally, the total solar radiation on a

tilt surface is calculated by adding the beam, diffuse and reflected solar radiation components on the tilt surface together.

3.2.1 Beam radiation on a tilt surface

The beam solar radiation that reaches a surface is related to the various solar angles and local latitude. In order to establish the relationship between the tilted angles and the solar radiation on the corresponding surface, one should start from solar geometry.

According to Duffie et al. (1996), for a tilted surface with tilt angle (β), the angle of incidence of beam radiation (θ) is given by:

$$\begin{aligned}\cos\theta = &\sin\delta\sin\varphi\cos\beta - \sin\delta\cos\varphi\sin\beta\cos\gamma \\ &+ \cos\delta\cos\varphi\cos\beta\cos\omega \\ &+ \cos\delta\sin\varphi\sin\beta\cos\gamma\cos\omega \\ &+ \cos\delta\sin\beta\sin\gamma\sin\omega\end{aligned} \tag{3-1}$$

As shown in Equation (3-1), the beam solar radiation incidence angle is a function of a series of solar geometry angles. φ is the local latitude, which equals to 22.3° N for Hong Kong, deg. ω is the hour angle, which represents the angle between the meridian of the sun and the local meridian, deg. γ is called surface azimuth angle, which is the angle between the vertical plane containing the normal to wall and the vertical plane running north-south, deg. The surface azimuth is measured from the south, which is negative when the normal of the surface is to the east of south but positive when the sun is to the west of south. δ is the solar declination which defines the angle between the sun-earth line and the equatorial plane, deg. It varies from +23.5° to -23.5° throughout a year. On the equinoxes, δ is 0° while on summer

solstice and winter solstice δ is +23.5° and -23.5° respectively. Accurate values of δ on a particular day can be determined by the following equation by inputting the day number n:

$$\delta = 23.45 \sin\left(\frac{360 \cdot (284 + n)}{365}\right) \tag{3-2}$$

For a horizontal surface, the tilted angle β equals 0°. The angle of incidence is the zenith angle of the sun, which is denoted by θ_h. Equation (3-1) becomes:

$$\cos\theta_h = \cos\delta\cos\phi\cos\omega + \sin\delta\sin\phi \tag{3-3}$$

For a tilted surface, a relationship between the angle of incidence and the tilted angle was described by Duffie et al. (1996). They stated that the surfaces with slope β have the same angular relationship to beam radiation as a horizontal surface at the location that having latitude of (φ- β). For a surface facing south, and replacing φ with (φ- β) in Equation (3-3) yields:

$$\cos\theta = \cos\delta\cos(\varphi - \beta)\cos\omega + \sin\delta\sin(\varphi - \beta) \tag{3-4}$$

The beam solar radiation on a tilted surface can be obtained by multiplying a ratio R_b to the horizontal beam solar radiation. The ratio R_b is defined as the ratio of beam radiation on a tilted surface to horizontal surface. It can be expressed in terms of the angle of incidence and the zenith angle of the sun as follows:

$$R_b = \frac{G_{bt}}{G_{bh}} = \frac{G_{bn}\cos\theta}{G_{bn}\cos\theta_h} = \frac{\cos\theta}{\cos\theta_h} \tag{3-5}$$

where G_{bh} is the horizontal beam radiation, W/m^2; G_{bn} is the direct normal radiation to the surface, W/m^2. As a result, modifying Equation (3-5), beam radiation on a tilted surface can be evaluated by:

$$G_{bt} = G_{bh} \cdot R_b = G_{bh} \cdot \frac{\cos\theta}{\cos\theta_h} \tag{3-6}$$

By using Equation (3-6), the beam component of the solar radiation of an inclined surface can be determined.

3.2.2 Diffuse solar radiation on a tilt surface

Diffuse radiation on a tilted surface is the most difficult component to be modeled accurately due to its spatial distribution. Many previous studies have been conducted on the mathematical modeling of diffuse radiation on a slope. These models differ in the assumed diffuse radiance distribution at different states of cloudiness. It is vital to choose a suitable model for the diffuse radiation in order to reduce the error. According to the comparison between the models and the on-site measurement carried out by Fung (2006), the model by Perez was found to be the most accurate among the other models in general.

Thus, the Perez model (Perez et al., 1990) is used for calculating the diffuse solar radiation on a tilt surface as follows:

$$G_{dt} = G_{dh}\left(\cos^2\left(\frac{\beta}{2}\right)(1-F_1) + F_1\left(\frac{f_1}{f_2}\right) + F_2\sin(\beta)\right) \tag{3-7}$$

F_1 and F_2 are circumsolar and horizontal brightening coefficients given by:

$$F_1 = F_{11}(\varepsilon) + F_{12}(\varepsilon)\Delta + F_{13}(\varepsilon)\theta_h \tag{3-8}$$

$$F_2 = F_{21}(\varepsilon) + F_{22}(\varepsilon)\Delta + F_{23}(\varepsilon)\theta_h \tag{3-9}$$

where F_{11}, F_{12}, F_{13}, F_{21}, F_{22} and F_{23} are named as Perez coefficients. For the Perez coefficients, there are many sets of values from different studies (Perez et al., 1987; 1990). In this Chapter, the newest set of coefficients (Perez et al., 1990) is applied as shown in Table 3.1.

Table 3.1 The Perez model coefficients for solar radiation calculation

ε	F_{11}	F_{12}	F_{13}	F_{21}	F_{22}	F_{23}
1-1.065	-0.008	0.588	-0.062	-0.06	0.072	-0.022
1.065-1.23	0.13	0.683	-0.151	-0.019	0.066	-0.029
1.23-1.5	0.33	0.487	-0.221	0.055	-0.064	-0.026
1.5-1.95	0.568	0.187	-0.295	0.109	-0.152	-0.014
1.95-2.8	-0.873	-0.392	-0.362	0.226	-0.462	0.001
2.8-4.5	1.132	-1.237	-0.412	0.288	-0.823	0.056
4.5-6.2	1.06	-1.6	-0.359	0.264	-1.127	0.131
6.2-	0.678	-0.327	-0.25	0.156	-1.377	0.251

ε and Δ are respectively the sky clearness and the sky brightness and defined as follows:

$$\varepsilon = \frac{(G_{bh} + G_{dh})/G_{dh} + 1.041\theta_h^3}{1.041\theta_h^3} \tag{3-10}$$

$$\Delta = \frac{G_{dh}}{G_o} = \frac{G_{dh}}{1353\left[1 + 0.033\cos\left(\frac{360n}{365}\right)\right]\cos\theta_h} \tag{3-11}$$

The ratio f_1/f_2 determines the angular location of the circumsolar region and can be expressed as:

$$\frac{f_1}{f_2} = \frac{\max[0, \cos\theta_t]}{\max[\cos 85, \cos\theta_h]} \tag{3-12}$$

where θ_t and θ_h is the incidence angle of a tilt surface and a horizontal surface, deg.

3.2.3 Ground reflected solar radiation on a tilt surface

The reflected component of solar radiation includes all the reflected radiation from other surfaces in the surroundings. In general, it is not possible to calculate the reflected energy from the surfaces in detail because of the changing solar radiation incident on them, and their changing reflectance. In order to calculate the reflected term, it is assumed that all the surrounding surfaces are condensed into one large horizontal, diffusely reflecting ground. The radiation reflected from this composite "ground" contributes to the reflected component.

The inclined surface with tilted angle β has a view factor to the ground of (1-cosβ)/2. If the ground has a reflectance of ζ for the total solar radiation, the reflected radiation from the ground, G_{grt}, can be written as:

$$G_{grt} = (G_{bh} + G_{dh})\zeta\left(\frac{1-\cos\beta}{2}\right) \tag{3-13}$$

The ground reflectance ξ is assumed to be 0.2 for the Hong Kong weather where there is no snow. For other situations, for example if there is a fresh snow cover, the value should be 0.7.

3.2.4 Total solar radiation on a tilt surface

For a tilt surface, the total solar radiation (G_{tt}) is the sum of the beam solar radiation (G_{bt}), the diffuse solar radiation (G_{dt}) and the ground reflected solar radiation (G_{grt}) and is expressed as:

$$G_{tt} = G_{bh} \cdot R_b + G_{dh}\left(\cos^2\left(\frac{\beta}{2}\right)(1 - F_1) + F_1\left(\frac{f_1}{f_2}\right) + F_2 \sin(\beta)\right) + (G_{bh} + G_{dh}) \cdot \zeta \cdot \frac{1-\cos(\beta)}{2}$$

(3-14)

When the tilted angle β of an inclined surface equals to 90°, this inclined surface can be known as a vertical surface. The total radiation of the vertical surface can be written as:

$$G_{tv} = G_{bh} \cdot R_b + G_{dh}\left(\frac{1-F_1}{2} + F_1\left(\frac{f_1}{f_2}\right) + F_2\right) + \frac{1}{2} \cdot \zeta \cdot (G_{bh} + G_{dh}) \qquad (3\text{-}15)$$

3.2.5 Beam and diffuse solar radiation on a horizontal surface

As can be seen from the above analysis, the total and diffuse solar radiation components on horizontal surface are necessary in order to calculate the solar radiations on a tilt surface.

Although the total horizontal solar radiation can be obtained from the local observatory, the beam and diffuse solar radiation components on a horizontal surface are not readily available. Therefore, a correlation between horizontal diffuse and horizontal total solar radiation is required.

A model based on local measured data was developed by Li et al. (2001) to simulate the relationship between the horizontal diffuse radiation (G_{dh}) and horizontal total radiation (G_{th}) for Hong Kong conditions:

$$\frac{G_{dh}}{G_{th}} = \begin{cases} 0.976 & k_T \le 0.15 \\ -1.589k_T^2 + 0.036k_T + 0.996 & 0.15 < k_T \le 0.7 \\ 0.23 & k_T > 0.7 \end{cases} \quad (3\text{-}16)$$

The above correlation involves the sky clearness, k_T, which is defined as the ratio of the total horizontal radiation (G_{th}) to the extraterrestrial radiation. By using Equation (3-16), the diffuse solar radiation on a horizontal surface (G_{dh}) can be calculated. Thus, the horizontal beam solar radiation (G_{bh}) can also be obtained.

3.3 Thermal and electrical models of the PV module

3.3.1 Dynamic heat transfer model of PV module

As known in Figure 3.1, a PV module mainly consists of five layers (from top to bottom): front glass, EVA sheet, silicon cell, EVA sheet and TPT back sheet. If ρ_p, C_p and l_p are the lumped density, specific heat capacity and thickness of the PV module, then

$$\rho_p C_p l_p = \rho_{fg} C_{fg} l_{fg} + \rho_{sc} C_{sc} l_{sc} + 2\rho_{\mathrm{EVA}} C_{EVA} l_{EVA} + \rho_{TPT} C_{TPT} l_{TPT} \quad (3\text{-}17)$$

where ρ_{fg}, ρ_{sc}, ρ_{EVA} and ρ_{TPT} are the density of the front glass, silicon cell, EVA and TPT, respectively, kg/m^3. C_{fg}, C_{sc}, C_{EVA} and C_{TPT} are the specific heat of the front glass, silicon cell, EVA sheet and TPT back sheet, respectively, J/(kg·K). l_{fg}, l_{sc}, l_{EVA} and l_{TPT} are the thickness of the front glass, silicon cell, EVA sheet and TPT back sheet, respectively, mm.

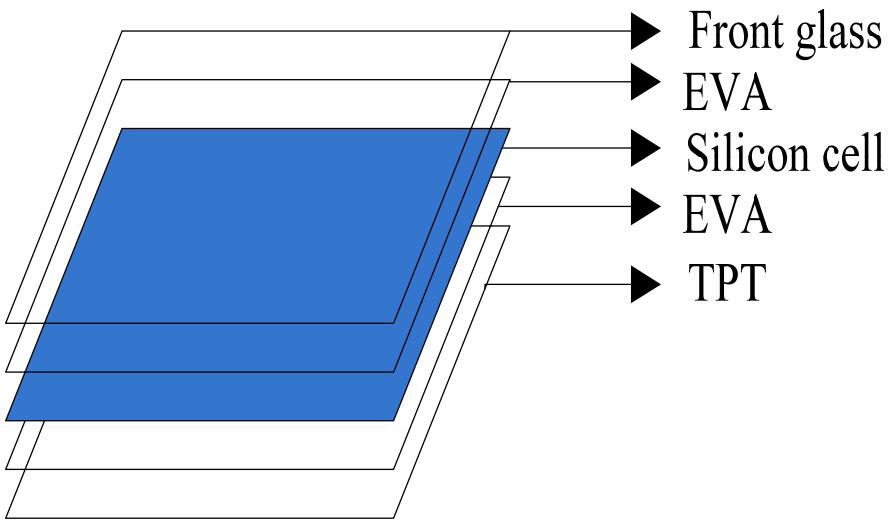

Figure 3.1 Structure of a PV module

The heat balance equation of the PV module is expressed as:

$$\rho_p C_p l_p \frac{\partial T_p}{\partial t} = (1-\eta)G_p + h_o(T_o - T_p) + h_{p-s}(T_s - T_p) + h_{p-w}(T_w - T_p) \qquad (3\text{-}18)$$

where T_p, T_o, T_s and T_w are the temperature of the PV module, outdoor air, sky and concrete wall, respectively, K. G_p is the total solar radiation absorbed by the PV module. η is the energy efficiency of the PV module. h_o is the outside convective heat transfer coefficient, W/(m^2·K). $h_{p\text{-}s}$ is the radiant heat transfer coefficient between the PV module and the sky, W/(m^2·K). $h_{p\text{-}w}$ is the radiant heat transfer coefficient between the PV module and the wall, W/(m^2·K).

The solar radiation absorbed by PV modules is described as:

$$G_p = \alpha_{sc}\left(\tau_{b-fg}G_{bt} + \tau_{d-fg}G_{dt} + \tau_{gr-fg}G_{grt}\right) \tag{3-19}$$

where $\tau_{b\text{-}fg}$, $\tau_{d\text{-}fg}$ and $\tau_{gr\text{-}fg}$ is the transmittance of the front glass for the beam, diffuse and ground reflected solar radiation, respectively. α_{sc} is the absorptance of the silicon cells. G_{bt}, G_{dt} and G_{grt} are, respectively, the beam, diffuse and ground reflected solar radiation incident on the tilt surface where PV modules are installed, W/m^2.

The long wave radiant heat transfer coefficient between the concrete wall and the PV module is defined as:

$$h_{p-w} = \sigma \frac{\left(T_p + T_w\right)\left(T_p^2 + T_w^2\right)}{\frac{1}{\varepsilon_w A_w} + \frac{1}{X_{wp} A_w} + \frac{1}{\varepsilon_p A_p}} \tag{3-20}$$

where σ is the Stefan-Boltzmann's constant, 5.67×10^{-8}W/(m^2·K^4). ε_p and ε_w are the emittance respectively for the PV modules and concrete wall. X_{wp} is the view factor between the concrete wall and the PV module.

The long wave radiant heat transfer coefficient between the PV module and the sky is calculated as:

$$h_{p-s} = \sigma\varepsilon_p\left(T_s + T_p\right)\left(T_s^2 + T_p^2\right) \tag{3-21}$$

where T_s is the temperature of the sky, K.

3.3.2 Electrical model of PV module

The energy efficiency of the PV module can be determined using the following linear model (Huang et al. 1999):

$$\eta = \eta_r \left(1 - 0.0045\left(T_p - 298.15\right)\right) \tag{3-22}$$

where η_r is the energy efficiency of the PV module on the standard test condition.

3.4 Thermal model of the window

3.4.1 Dynamic heat transfer model of window

The transient heat transfer of the window can be analyzed by solving the heat balance equation. As there is sunlight passing through the glazing, in addition to conduction, the solar radiation absorbed by the glazing should be included in the equation. The heat transfer balance equation is:

$$\rho_g C_g l_g \frac{\partial T_g}{\partial t} = G_g + h_o\left(T_o - T_g\right) + h_{g-s}\left(T_s - T_g\right) + h_{i,g}\left(T_i - T_g\right) + \sum_{j=1}^{5} h_{g-j}\left(T_j - T_g\right) \tag{3-23}$$

where ρ_g, C_g and l_g are respectively the density, specific heat capacity and thickness of the glazing. T_i is the indoor air temperature, K. $h_{i,g}$ is the convective heat transfer coefficient of the inside surface of window, W/(m^2·K).

The long wave radiant heat transfer coefficient between the glazing and the sky is given by the Stefan-Boltzmann's law:

$$h_{g-s} = \sigma \varepsilon_g \left(T_s + T_g\right)\left(T_s^2 + T_g^2\right) \tag{3-24}$$

where ε_g is the emittance of the glazing.

The long wave radiant heat transfer coefficient between the glazing and the internal envelope is calculated as:

$$h_{g-j} = \sigma \frac{\left(T_j + T_g\right)\left(T_j^2 + T_g^2\right)}{\frac{1}{\varepsilon_g A_g} + \frac{1}{X_{gj} A_g} + \frac{1}{\varepsilon_j A_j}} \tag{3-25}$$

where T_j is the temperature of the internal envelope named as J, K. ε_j is the emittance of the internal envelope named as J and X_{gj} is the view factor between the glazing and the internal envelope named as J.

The total solar radiation absorbed by the glazing can be described as:

$$G_g = \alpha_{bg} G_{bv} + \alpha_{dg} G_{dv} + \alpha_{grg} G_{grv} \tag{3-26}$$

where α_{bg}, α_{dg} and α_{grg} are respectively the absorptance of the glazing for the beam, diffuse and ground reflected part of solar radiation. G_{bv}, G_{dv} and G_{grv} are the beam, diffuse and ground reflected solar radiation incident on the vertical surface, respectively, W/m^2.

If part of the window is shaded by an overhang, the beam solar radiation from the sun is intercepted before reaching the window. In the meantime, the diffuse solar radiation received by the window can also be affected by the overhang (Utzinger et

al, 1979). Thus, the total solar radiation absorbed by a partly shaded window can be expressed as:

$$G_g^{'} = \alpha_{bg} G_{bv} \cdot F_u + \alpha_{dg} G_{dv} \cdot F_{o-s} + \alpha_{grg} G_{grv} \tag{3-27}$$

where $F_{o\text{-}s}$ is the view factor from the overhang to the sky and determined by the geometry and relative position of the window and the overhang. F_u is the ratio of beam solar radiation received by a partly shaded window to that received by an unshaded window.

3.4.2 Calculation of F_u

The most significant effect of the overhang is to intercept the beam solar radiation from the sun before it reaches the window. The ratio of beam solar radiation received by a partly shaded window to that received by an unshaded window, F_u, can be defined as:

$$F_u = \frac{A_u}{A_w} \tag{3-28}$$

where A_u and A_w are the area of the unshaded window and the whole window, respectively, m^2.

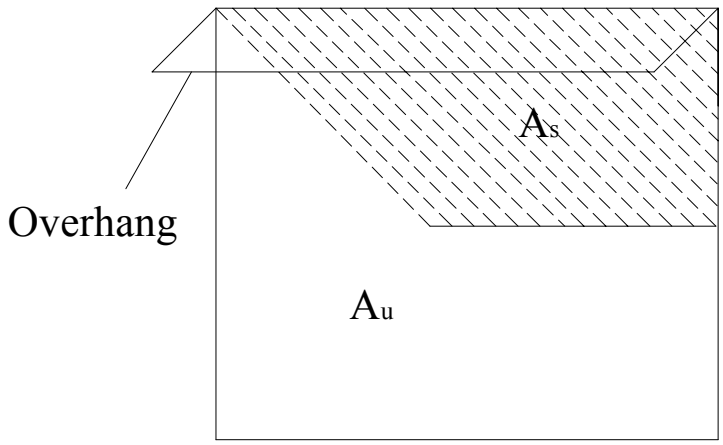

Figure 3.2 Schematic of shaded window

The value of F_u at any time not only depends on the dimensions of the overhang and the window but also on the incidence angle of the beam solar radiation entering through the window. In order to calculate the value of F_u, the shadow of the overhang projected on the window should be determined first. In the orthogonal coordinates (as shown in Figure 3.3), *X*, *Y*, *Z* represents the direction of south, east and solar zenith, respectively. The parallelogram *OMCD* represents the window and the parallelogram *ABCD* presents the overhang.

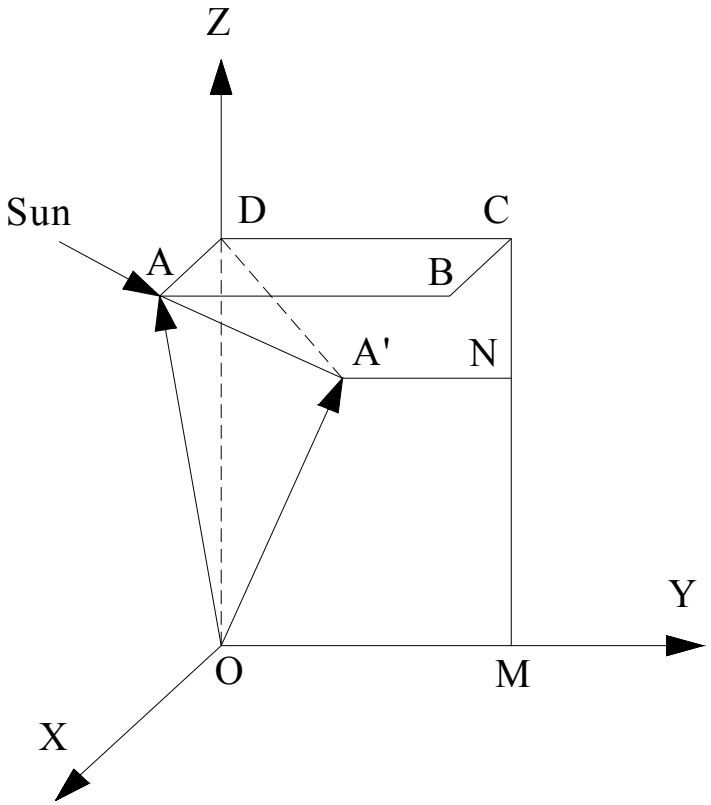

Figure 3.3 The orthogonal coordinates

At a particular moment, the position of the Sun can be determined by the zenith angle (θ_h) and the surface-solar azimuth angle (γ), so that the unit vector of the Sun, $\overline{V_s}$, can be expressed as:

$$\overline{V_s} = [\sin\theta_h \cdot \cos\gamma, -\sin\theta_h \cdot \sin\gamma, \cos\theta_h]^T \tag{3-29}$$

As shown in Figure 3.4, the vector $\overline{OA}$ can be presented as $\left[L_o, 0, H_g\right]^T$. Supposing that the projection of point A on the window is at point A', the vector $\overline{OA'}$ can be found by employing the vector algebra law:

$$\overline{OA'} = \overline{OA} + \Pi \cdot \overline{V_s} \tag{3-30}$$

where Π is a constant and can be written as:

$$\Pi = -\frac{L_o}{\sin\theta_h \cos\gamma} \tag{3-31}$$

Thus, the vector $\overline{OA'}$ can be expressed as:

$$\overline{OA'} = \left[0, L_o \tan\gamma, H_g - \frac{L_o}{\tan\theta_h \cos\gamma}\right] \tag{3-32}$$

If the position of point A' can be determined, the area of quadrilateral $A'NCD$ can be calculated. Therefore, the value of F_u can be obtained.

3.5 Thermal model of concrete wall

The concrete wall is modeled as one dimensional slab of the finite thickness. It is assumed that the thermophysical properties of the concrete wall are homogeneous, isotropic and independent of temperature. The transient heat transfer of the concrete wall can be described as follows:

$$\rho_w C_w \frac{\partial T_w}{\partial t} = \lambda_w \frac{\partial^2 T_w}{\partial x^2} \quad \left(0 < x < l_w\right) \tag{3-33}$$

$$-\lambda_w \frac{\partial T_w}{\partial x}\Big|_{x=0} = h_{w-p}\left(T_p - T_w\right) \tag{3-34}$$

$$-\lambda_w \frac{\partial T_w}{\partial x}\Big|_{x=l_w} = h_{i,w}\left(T_i - T_w\right) + \sum_{j=1}^{5} h_{w-j}\left(T_j - T_w\right) \tag{3-35}$$

where λ_w is the thermal conductivity of the concrete wall, W/(m·K). $h_{i,w}$ is the convective heat transfer coefficient of the inside surface of wall, W/(m^2·K).

The long wave radiant heat transfer coefficient between the concrete wall and the internal envelope is defined as:

$$h_{w-j} = \sigma \frac{\left(T_j + T_w\right)\left(T_j^2 + T_w^2\right)}{\frac{1}{\varepsilon_w A_w} + \frac{1}{X_{wj} A_w} + \frac{1}{\varepsilon_j A_j}} \tag{3-36}$$

where X_{wj} is the view factor between the concrete wall and the internal envelope named as j.

3.6 Calculation of convective heat transfer coefficient

The outside convective heat transfer coefficient depends on the speed and direction of the wind blowing over the outside surface of the building external envelope. The correlations developed by Loveday et al. (1996) are used as follows:

$$h_o = 16.21 v_o^{0.452} \tag{3-37}$$

$$v_o = 0.68 v_r - 0.5 \; (20^\circ \le \varphi \le 160^\circ) \tag{3-38}$$

$$v_o = 0.157 v_r - 0.027 \; (\varphi \le 20^\circ \quad \text{or} \quad \varphi \ge 160^\circ) \tag{3-39}$$

where φ is the incidence angle of the wind and v_r is the local wind speed.

The outside surface of the concrete wall, where PV modules are installed, is mainly in leeward side. Thus, the outside convective coefficient can be simplified as:

$$h'_{o,w} = 16.21\left(0.157 v_r - 0.027\right)^{0.452} \tag{3-40}$$

Supposed that the inside surface of the building external envelope is the laminar regime, the inside convective heat transfer coefficient of wall and window are calculated as:

$$h_{i,g} = 1.332\left(\frac{\left|T_g - T_i\right|}{H_g}\right)^{0.25} \tag{3-41}$$

$$h_{i,w} = 1.332\left(\frac{\left|T_w - T_i\right|}{H_w}\right)^{0.25} \tag{3-42}$$

where H_g and H_w are the height of the window and wall, m.

3.7 Optical model of the glazing

For one cover glazing, the absorptance and transmittance can be approximated by the following models proposed by Duffie et al. (1996):

$$\alpha_g = 1 - \exp\left(-\frac{K_g l_g}{\cos\left(\theta_2\right)}\right) \tag{3-43}$$

$$\tau_g = \frac{1}{2} \cdot \exp\left(-\frac{K_g l_g}{\cos\left(\theta_2\right)}\right) \cdot \left(\frac{1 - r_1}{1 + r_1} + \frac{1 - r_2}{1 + r_2}\right) \tag{3-44}$$

where K_g and l_g are the extinction coefficient and thickness of the glazing, respectively. θ_2 is the fraction angle when sunlight passing through the glazing and defined as:

$$\theta_2 = \arcsin\left(\frac{\sin\theta_1}{1.526}\right) \tag{3-45}$$

r_1 and r_2 are respectively the perpendicular and parallel component of unpolarized solar radiation and described as follows:

$$r_1 = \left[\frac{\sin(\theta_2 - \theta_1)}{\sin(\theta_2 + \theta_1)}\right]^2 \tag{3-46}$$

$$r_2 = \left[\frac{\tan(\theta_2 - \theta_1)}{\tan(\theta_2 + \theta_1)}\right]^2 \tag{3-47}$$

The values of the incidence angle, θ_1, are different for beam, diffuse and ground reflected solar radiation. For the beam solar radiation, $\theta_{1,b}$ depends on the angles of declination (δ), latitude (φ), tilt (β), surface azimuth (γ) and hour (ω) and is calculated by Equation (3-2). For the diffuse and ground reflected solar radiation, the incidence angles only have relationship to the tilt angle. The incident angles of the diffuse and ground reflected solar radiation are calculated using models proposed by Duffie et al. (1996):

$$\theta_{1,d} = 90 - 0.5788\beta + 0.002693\beta^2 \tag{3-48}$$

$$\theta_{1,gr} = 59.68 - 0.1388\beta + 0.001497\beta^2 \tag{3-49}$$

3.8 Cooling load calculation of window and concrete wall

The cooling load of the concrete wall is described as:

$$Q_w(t) = \left(T_w(t)\big|_{x=l_w} - T_i\right) A_w h_{i,w} \tag{3-50}$$

The cooling load through the window consists of three parts including the cooling load produced by the convective heat gain, beam solar heat gain and diffuse solar heat gain, as shown in follows:

$$Q_{g,c}(t) = \left(T_g(t) - T_i\right) A_g h_{i,g} \tag{3-51}$$

$$Q_{g,b}(t) = \sum_{i=0}^{23} q_{g,b}(t-i) r_i \tag{3-52}$$

$$Q_{g,d}(t) = \sum_{i=0}^{23} 0.46 q_{g,d}(t-i) n_i + 0.54 q_{g,d}(t) \tag{3-53}$$

where r and n are the Radiant time series (RTS) factors respectively for the solar and nonsolar part. When the type of window is chosen, the values of RTS factors can be found in ASARE Hand Book 2009. $q_{g,b}$ and $q_{g,d}$ is respectively the beam and diffuse solar heat gain transmitting through the glazing and can be determined by:

$$q_{g,b} = \tau_{bg} G_{bv} A_g \tag{3-54}$$

$$q_{g,d} = \left(\tau_{dg} G_{dv} + \tau_{grg} G_{grv}\right) A_g \tag{3-55}$$

where τ_{bg}, τ_{bg} and τ_{bg} are transmittance of the glazing for the beam, diffuse and ground reflected solar radiation, respectively. A_g is the area of the glazing, m^2. G_{bv},

G_{dv} and G_{grv} are, respectively, the beam, diffuse and ground reflected solar radiation exposed on a vertical surface, W/m^2.

3.9 Calculation of combined electrical energy

As mentioned above, the annual electricity generation and cooling load reduction produced by the shading-type BIPV claddings contribute to the total electricity saving of buildings. It is necessary to analyze the combined effects of these two contributions and to evaluate the optimum position of the shading-type BIPV claddings so that the maximum electricity saving is achieved. By using the COP of the HVAC system, the cooling load reduction of windows and concrete walls can be converted into the corresponding electricity consumption reduction. Thus, the combined electrical energy of the shading-type BIPV claddings is calculated as:

$$E_{comb} = E_{pv} + E_{g+w} = E_{pv} + \frac{Q_{g+w}}{COP} \tag{3-56}$$

where E_{pv} is the electrical power produced by the PV module, W. E_{g+w} is the electrical power due to cooling load reduction of the window and concrete wall, W. Q_{g+w} is the cooling load reduction of the window and concrete wall, W.

3.10 Numerical resolution

The dynamic heat transfer equations presented above are solved using the explicit finite difference method. The derivations have been discretized as follows:

$$\left(\frac{\partial T}{\partial t}\right)_{m,k} = \frac{T_m^{k+1} - T_m^k}{\Delta t} \tag{3-57}$$

$$\left(\frac{\partial^2 T}{\partial x^2}\right)_{m,k} = \frac{T_{m-1}^k - 2T_m^k + T_{m+1}^k}{\Delta x^2} \tag{3-58}$$

As iteration is involved in solving discretized equations, initial conditions are required. The initial temperature distributions of the glazing, concrete wall and PV module are expressed as follows:

$$T_g(0) = \frac{T_o(0) + T_i}{2} \tag{3-59}$$

$$T_w(x,0) = T_0(0) - \frac{T_0(0) - T_i}{l_w} x \tag{3-60}$$

$$T_p(0) = T_o(0) \tag{3-61}$$

3.11 Summary

In this chapter the simulation model of the shading-type BIPV system is developed for estimating its energy performance. Firstly, the calculation of the solar radiation on a tilt surface is introduced. Secondly, the heat balance equation of the BIPV module, window and concrete wall are set up on the dynamic heat transfer method. Finally, the determination of the cooling load and the conversion of the cooling load into the electrical energy are also referred.

CHAPTER 4: ENERGY PERFORMANCE OF SHADING-TYPE BIPV CLADDINGS

4.1 Introduction

Building Integrated Photovoltaic (BIPV) is a PV application close to being capable of delivering electricity at less than the cost of grid electricity to end users in certain peak demand niche markets (Norton et al., 2010). Compared with PV systems, one of the important advantages of BIPV systems is that PV modules can replace conventional building materials. The savings in the purchase and installation of conventional materials can lower the net cost of the BIPV systems. PV modules provide fully integrated electricity generation while also serve as part of the weather protective building envelopes. If the BIPV systems are properly designed, the cooling load of building envelopes on which PV modules are integrated into can also be eliminated. Apart from the electricity generation of PV modules, the cooling energy consumption reduction due to cooling load reduction of building envelopes should also be regarded as parts of the total electricity saving when the energy performance of the BIPV systems is evaluated.

4.2 System description

In this Chapter, the annul energy performance of the shading-type BIPV claddings (as shown in Figure 4.1) was conducted on the basis of the dynamic simulation model (described in chapter 3) and the hourly TMY weather data of Hong Kong. Figure 4.1 shows the schematic of the shading-type BIPV claddings. PV modules are installed on concrete walls between two adjacent windows. The dimension of the

windows is 4.5m × 1.5m. The height of the concrete walls is 1.7m. The ratio of the height of the concrete walls installed with PV modules to the total height of the concrete walls is defined as the wall utilization fraction (R). In this chapter, the wall utilization fractions vary from 20% to 100% at 20% increment.

In the simulation the polycrystalline silicon PV module is used and its energy efficiency is 16%. The width of the PV module is 4.5m, as the same as the width of window. The length of the PV module depends on the wall utilization fraction and tilt angle.

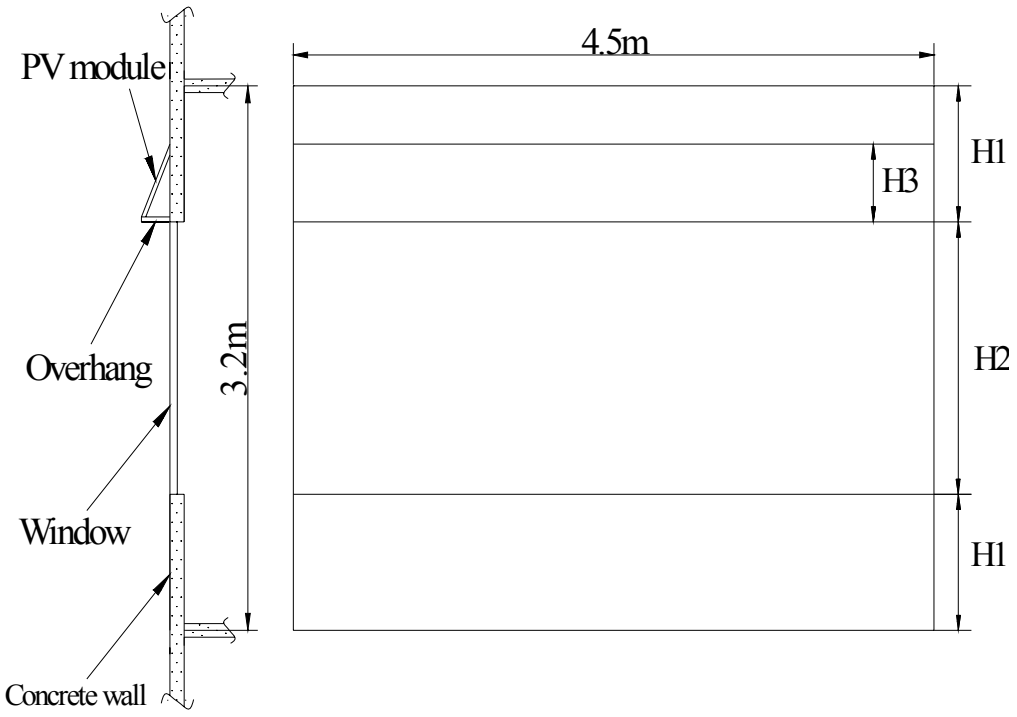

Figure 4.1 The schematic of the shading-type BIPV claddings

A maximum length of 1.5m for the overhang is adopted because it is the maximum projection from an external wall that can be exempted from the Gross Floor Area and Site Coverage calculation (Incentives for Green Buildings of Hong Kong, 2001). Thus, different tilt angles were selected for different wall utilized fractions to make

the overhang length be smaller than 1.5m. Table 4.1 lists different values of the overhang length for different wall utilization fractions and tilt angles.

Table 4.1 Length of overhangs

Length of overhangs	Wall utilization fraction (R)				
Tilt angle (β)	20%	40%	60%	80%	100%
20°	0.93m				
30°	0.59m	1.18m			
40°	0.41m	0.81m	1.22m		
50°	0.29m	0.57m	0.86m	1.14m	1.43m
60°	0.20m	0.39m	0.59m	0.78m	0.98m
70°	0.12m	0.25m	0.37m	0.50m	0.62m
80°	0.06m	0.12m	0.18m	0.24m	0.30m

4.3 Simulation results and discussions

The annual simulation of the energy performance of shading-type BIPV claddings is conducted on basis of the simulation models referred in Chapter 3 and the hourly TMY weather data of Hong Kong (Lu et al., 2004). Each contribution of the total electricity saving of shading-type BIPV claddings, such as PV electricity generation, window cooling load reduction and concrete wall cooling load reduction, has been analyzed in this section.

4.3.1 Electrical power of PV modules

The annual electricity generation per unit PV area for different surface azimuth angles is shown in Figure 4.2. The maximum electricity generation of 76.7kWh/m^2

occurs when PV modules are installed on south-facing facades at the tilt angle of 10°. If the east-facing PV modules have to be installed vertically, the annual electricity generation is 43.2kWh/m^2, decreased by 43.8% compared with the maximum value. In general, PV modules produce more electricity annually at smaller tilt angles than at larger ones. The annual electricity generation of PV modules decreases sharply when tilt angles exceed 40°. When tilt angles are smaller than 60°, the ascending order of annual electricity generation is -90°, -45°, 90°, 45° and 0°. In contrary, the ascending order of the annual electricity generation becomes -90°, -45°, 90°, 0° and 45°. Thus, the orientations of south and southwest facades are two better choices for PV module installation. The optimum tilt angles of PV modules are 10° for both south and southwest facades.

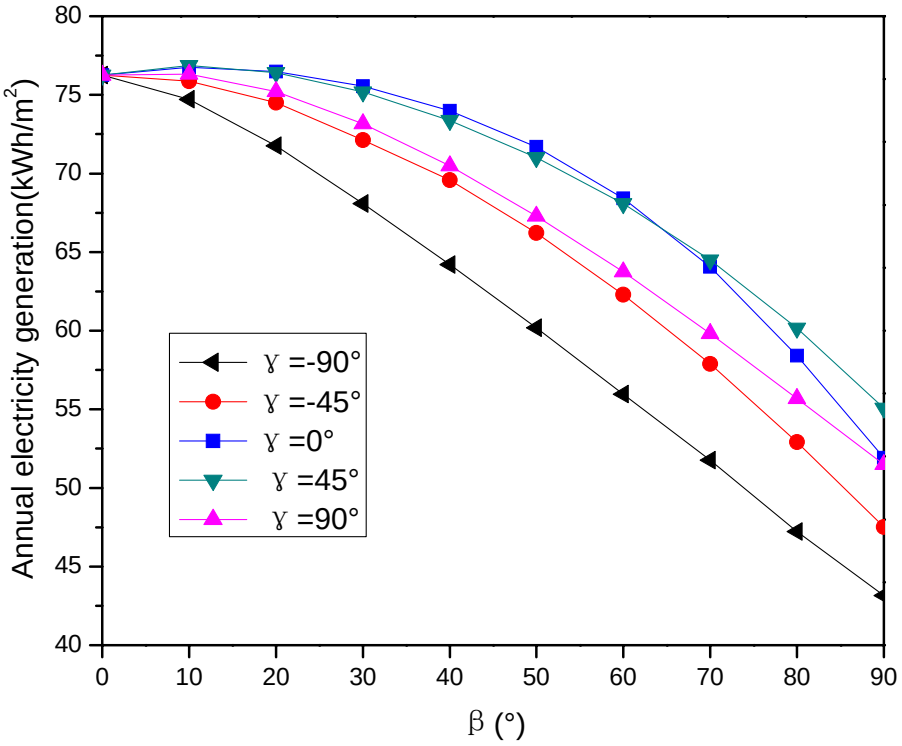

Figure 4.2 Annual electricity generation per unit PV area

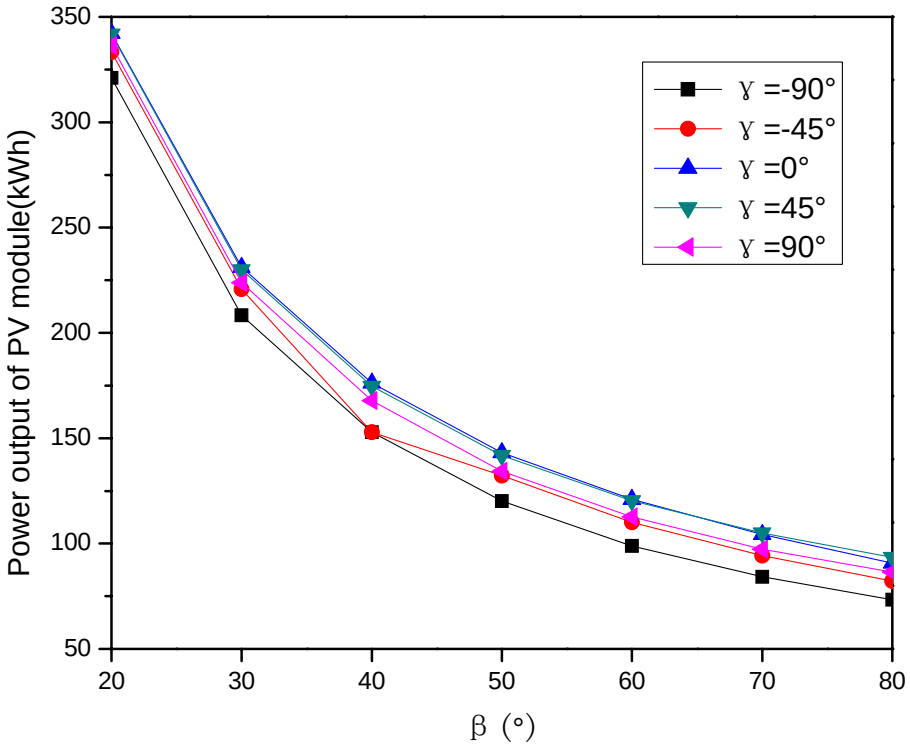

Figure 4.3 Annual power output of PV modules (R=20%)

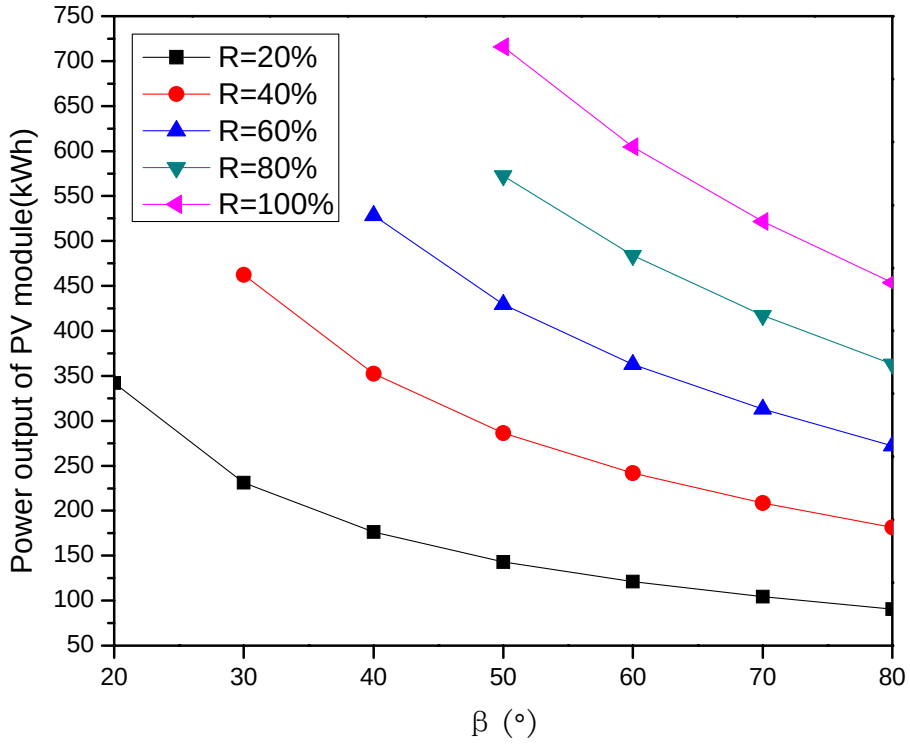

Figure 4.4 Annual power output of south-facing PV modules

Figures 4.3 and 4.4 present the annual power output of PV modules for different orientations and wall utilization fractions. In comparison of Figures 4.3 and 4.4, it is concluded that the wall utilization fractions have more significant effect on the power output of PV modules than that of surface azimuth angles. As indicated in Figure 4.4, the south-facing PV modules can produce the maximum power output of 715.7kWh with the tilt angle of 50° and the wall utilization fraction of 100%. Correspondingly, the overhang length is 1.43m, which is also the biggest overhang length used in this chapter.

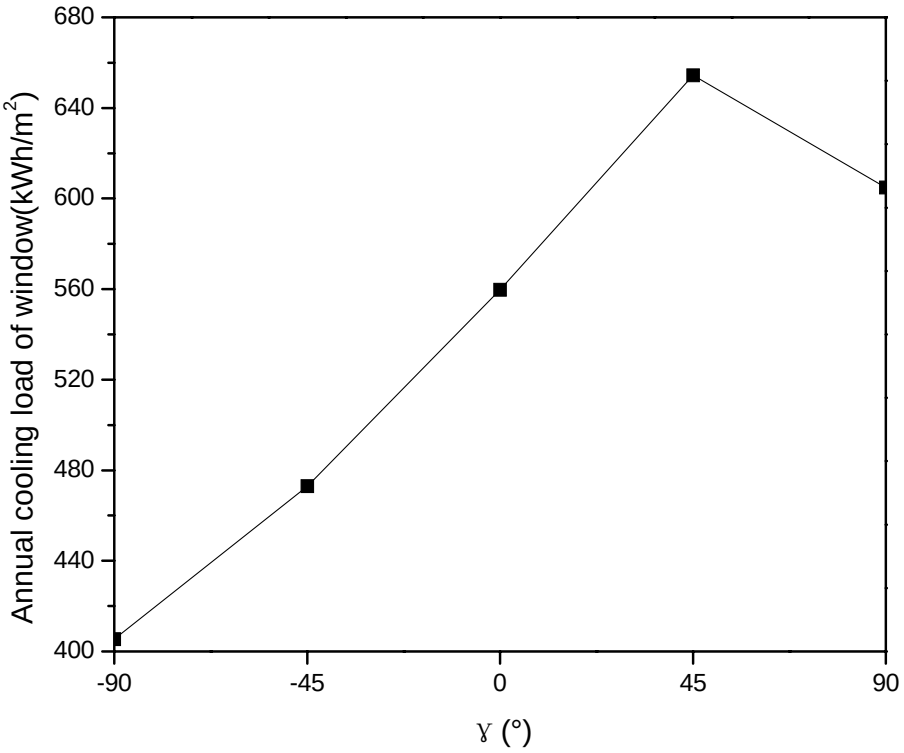

Figure 4.5 Annual cooling load per unit window area

4.3.2 Cooling load reduction of windows and concrete walls

As shown in Figure 4.5 and 4.6, the variations of cooling load per unit area of windows and concrete walls have the same trend when the surface azimuth angles change from -90° to 90°. Both southwest-facing windows and concrete walls can

lead to more cooling load than other orientations. It can also be inferred that the annual cooling load of the concrete walls can be neglected compared with that of windows.

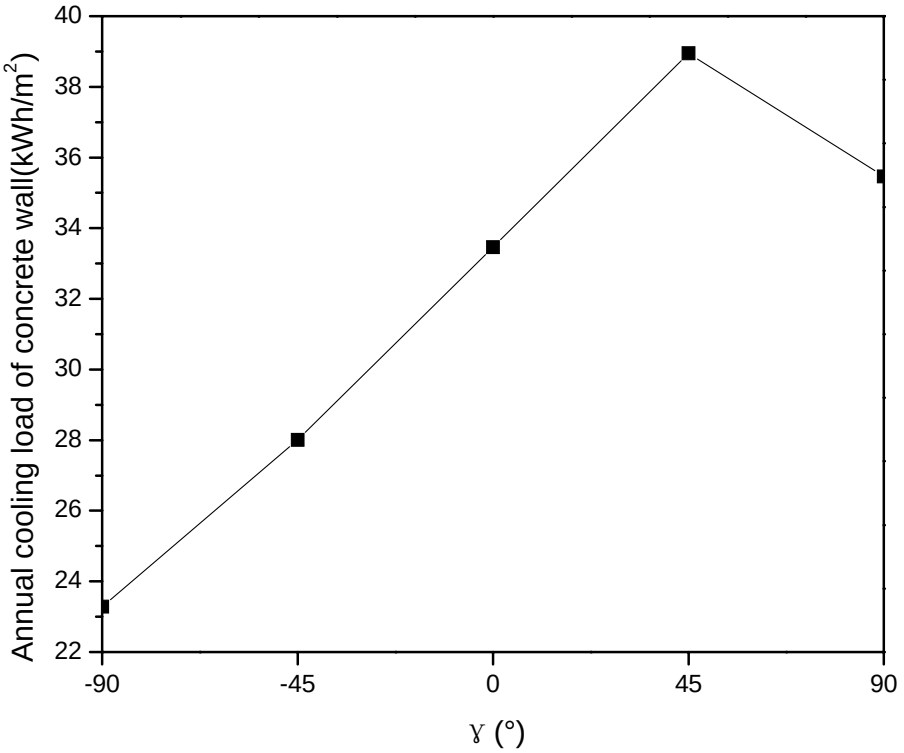

Figure 4.6 Annual cooling load per unit concrete wall area

Figure 4.7 and 4.8 present the annual cooling load reduction and cooling load reduction ratio of windows when the wall utilization fraction is 20%. It can be observed from Figure 4.7 that the cooling load reduction of the southwest-facing windows is the largest, while that of the east-facing windows is the smallest. As illustrated in Figure 4.8, there is no significant difference among the window cooling load reduction ratios of all five orientations, particularly at the larger tilt angles. In addition, the south-facing windows have larger cooling load reduction ratio than other orientations.

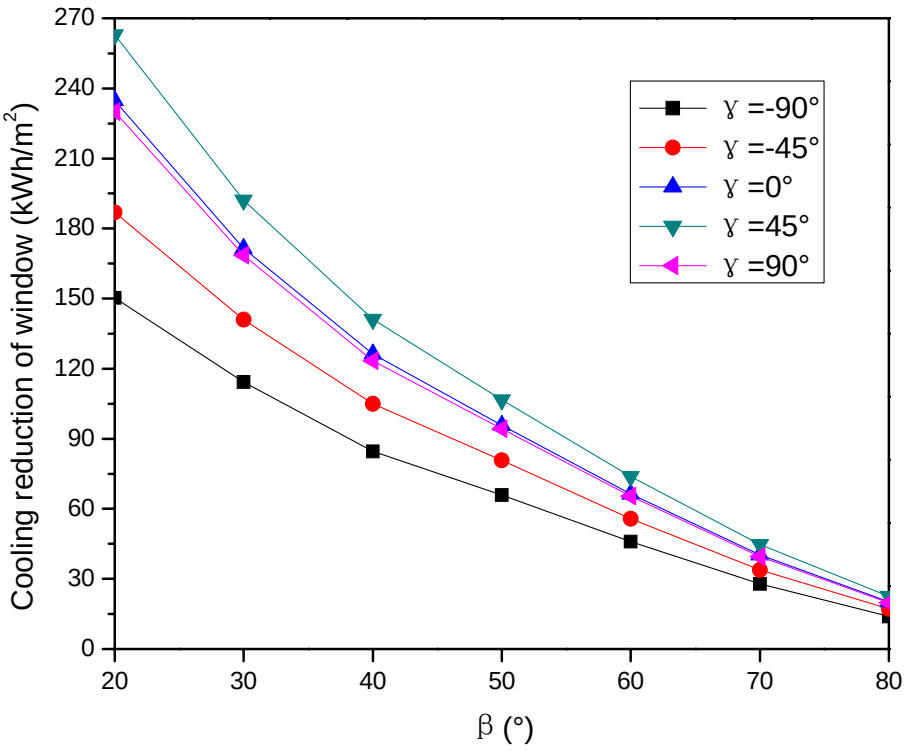

Figure 4.7 Cooling load reduction per unit window area (R=20%)

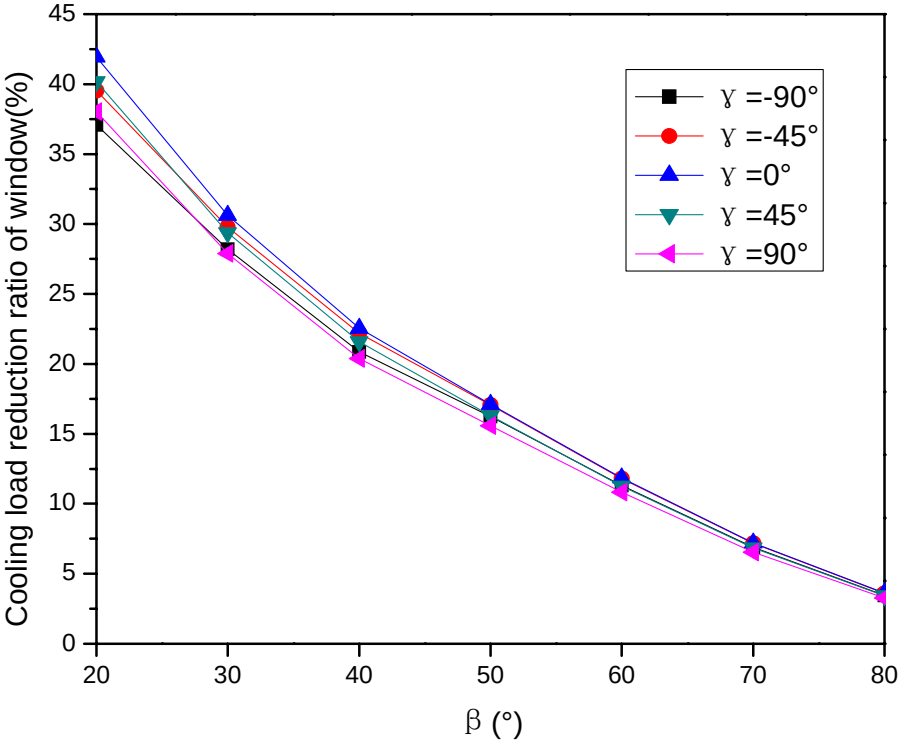

Figure 4.8 Cooling load reduction ratio of windows (R=20%)

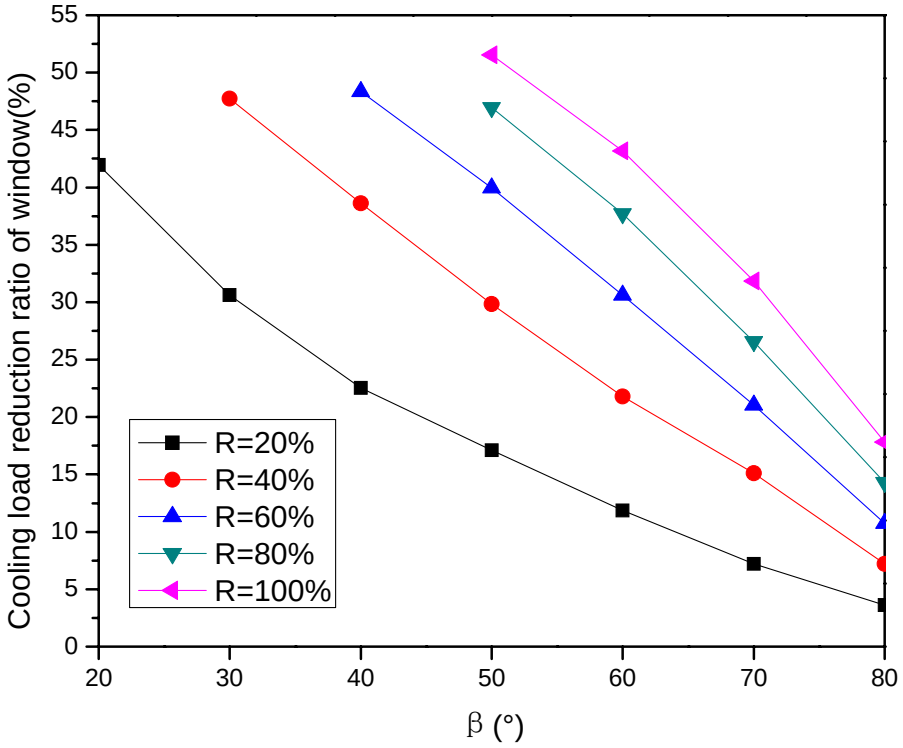

Figure 4.9 Cooling load reduction ratio of south windows

Figure 4.9 shows the annual cooling load reduction ratio of south windows. It can be seen that when the wall utilization fractions increase from 20% to 100%, the cooling load reduction ratio increases and the growth rate decreases as wall utilization fractions are larger. The cooling load reduction ratio is as high as 51.6% when the tilt angle equals 50° and the wall utilization fraction is 100%. While the tilt angle increases to 80°, the cooling load reduction ratio decreases to 17.8%. Thus, the shading-type BIPV claddings with small tilt angles are more effective for window cooling load reduction. In addition, the effect of tilt angles on window cooling load reduction ratio is more significant than that of surface azimuth angles.

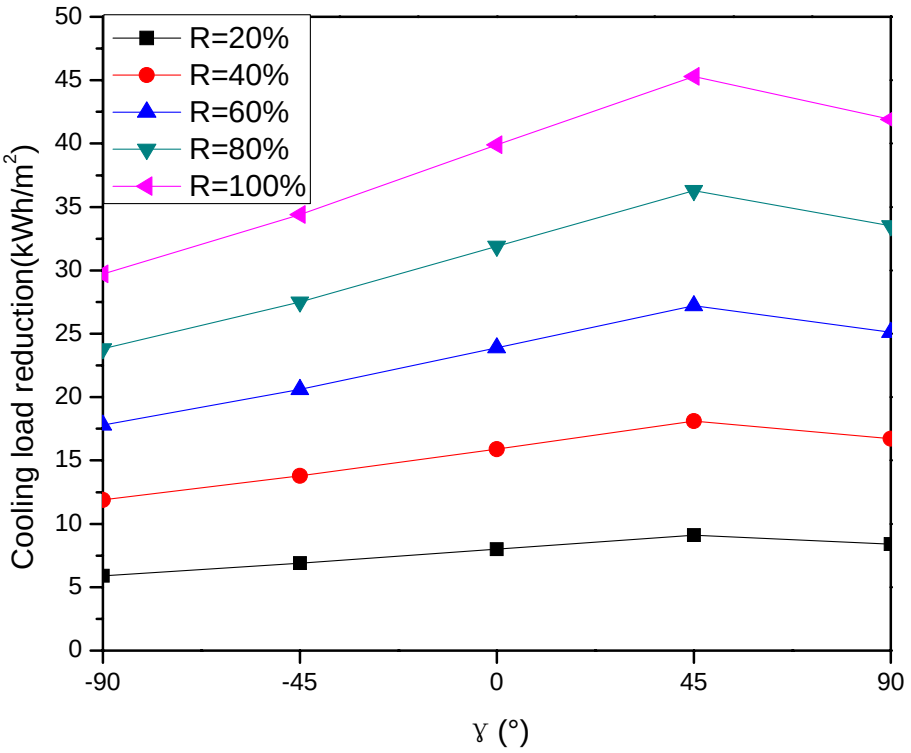

Figure 4.10 Cooling load reduction per unit concrete wall area

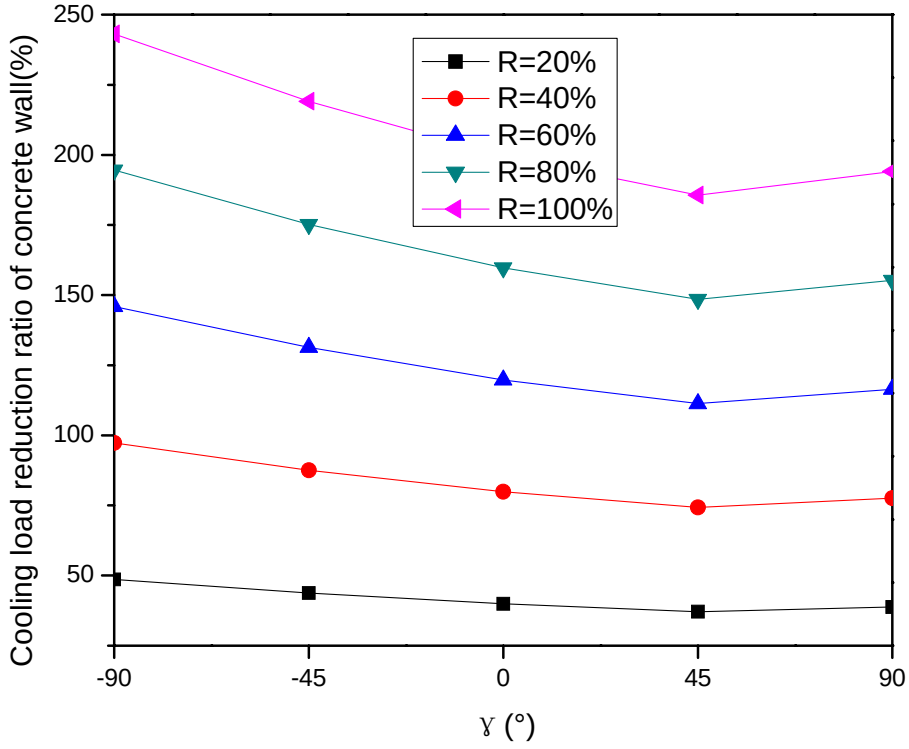

Figure 4.11 Cooling load reduction ratio of concrete walls

In comparison of Figures 4.6 with 4.10, it can be seen that the cooling load and the cooling load reduction of the concrete walls have the same variation trend and can

reach their maximum values when the surface azimuth angle equals 45°. Figure 4.11 shows that the annual cooling load reduction ratios of the concrete walls are very large. The minimum value of cooling load reduction ratios is 37.1%, while the maximum value is as high as 243.2%. When the wall utilization fractions are larger than 60%, the cooling load reduction ratios of the concrete walls are all higher than 100%. In addition, it is indicated that the ascending order of annual cooling load reduction ratio of the concrete walls is 45°, 90°, 0°, -45° and -90°.

4.3.3 Combined electrical energy

Supposing that the building where the shading-type BIPV claddings are installed is cooled by an air cooled HVAC system, the COP is set to be 2.8 (Yik et al., 2001). According to Equation (3-55), the total electricity saving of the shading-type BIPV claddings at different orientations can be determined.

Since the initial cost of PV modules is high, the annual electricity saving per unit PV area is utilized to evaluate the energy performance of the shading-type BIPV claddings. Figures 4.12-4.16 show the simulation results of the annual electricity saving with different wall utilization fractions and orientations. In comparison of Figures 4.12-4.16, it is seen that as wall utilization fractions increase, the amount of annual electricity saving produced by the shading-type BIPV claddings decreases. When the wall utilization fractions are smaller, such as 20%, 40% and 60%, the maximum annual electricity saving does not occur at the smallest tilt angle. While the wall utilization fractions are larger, such as 80% and 100%, the PV modules at smaller tilt angles can produce more electricity saving than that of larger ones. Table

4.2 summarizes these optimum tilt angles for different orientations and wall utilization fractions.

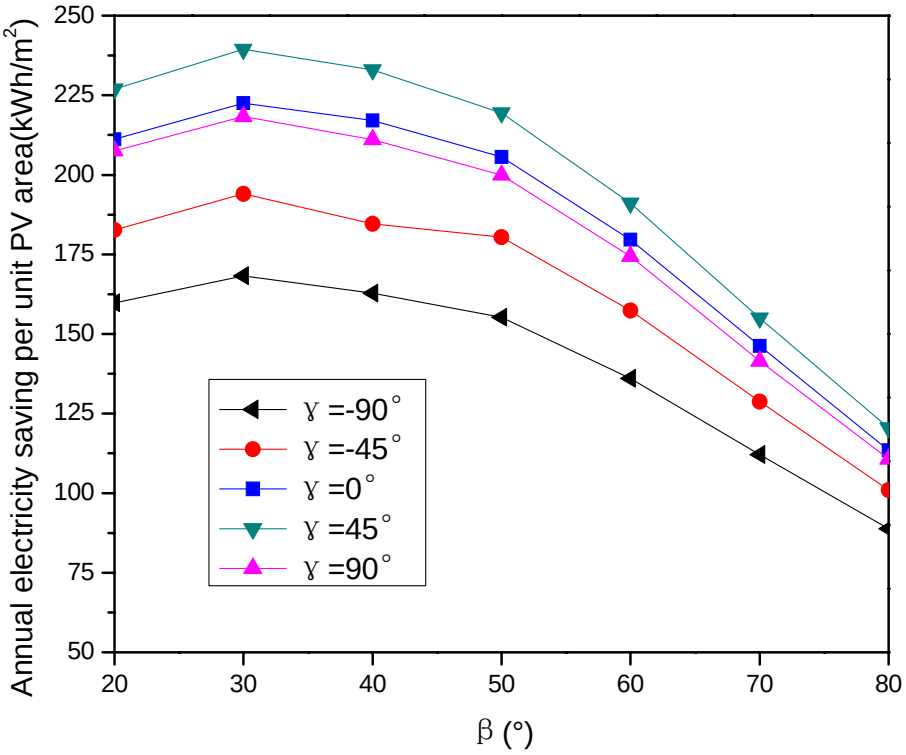

Figure 4.12 Annual electricity saving per unit PV area (*R*=20%)

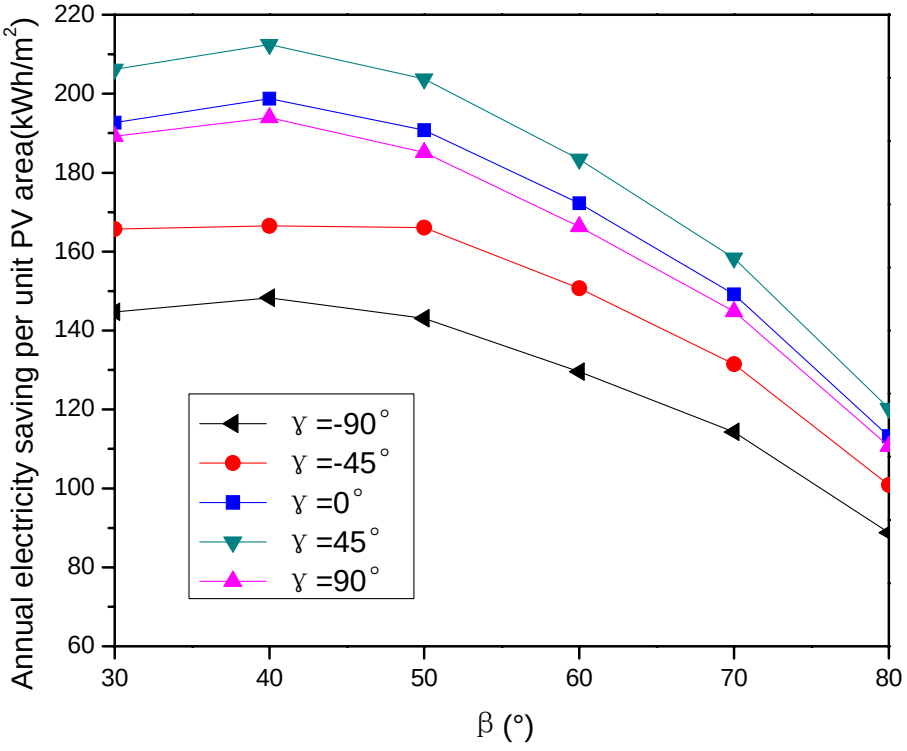

Figure 4.13 Annual electricity saving per unit PV area (*R*=40%)

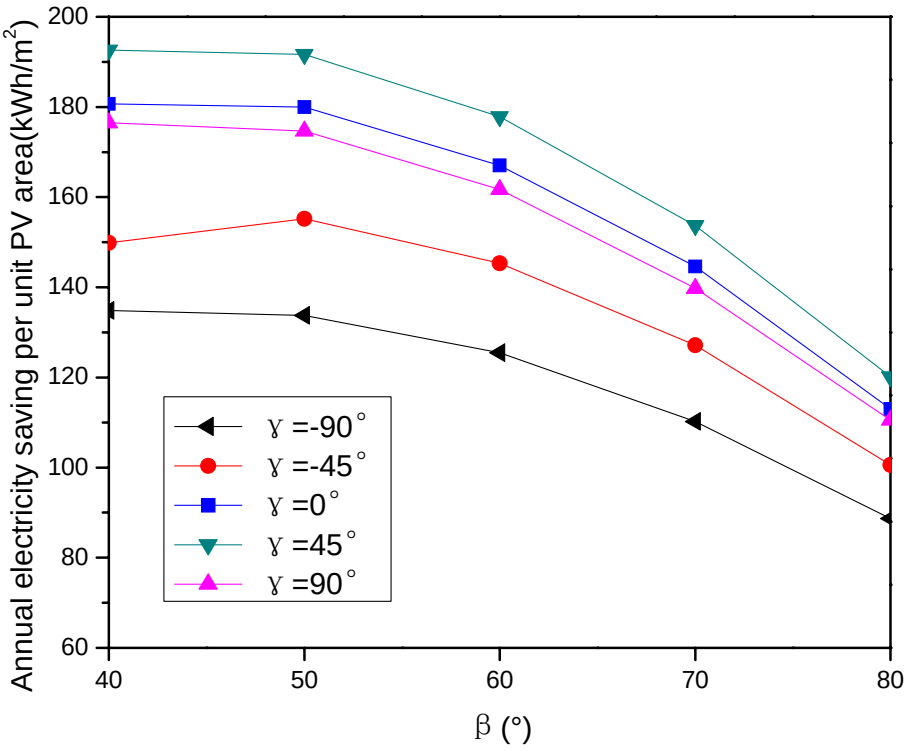

Figure 4.14 Annual electricity saving per unit PV area (*R*=60%)

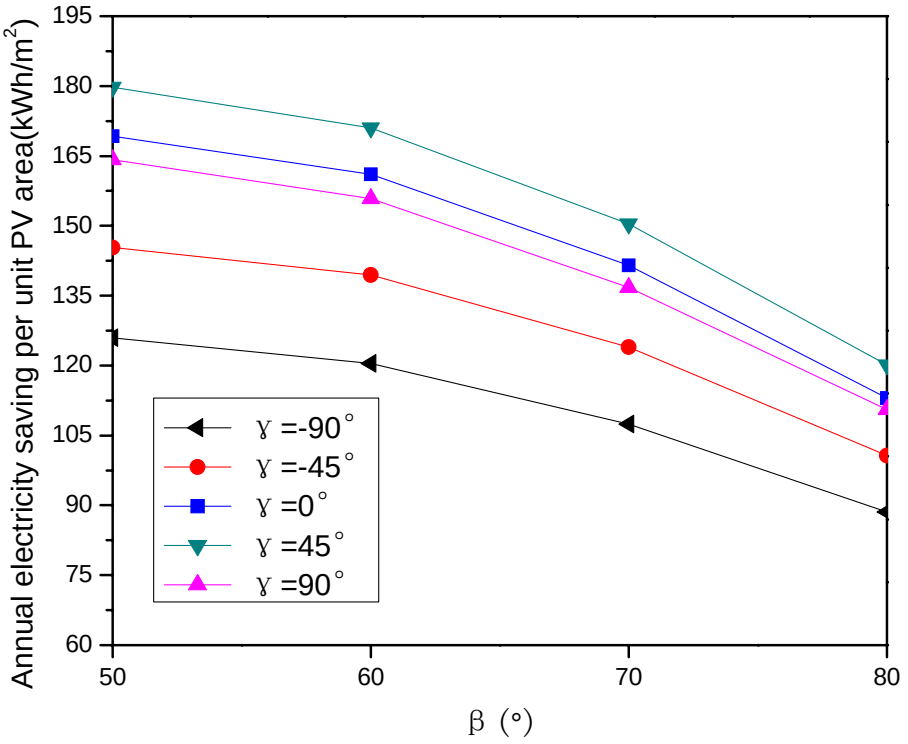

Figure 4.15 Annual electricity saving per unit PV area (*R*=80%)

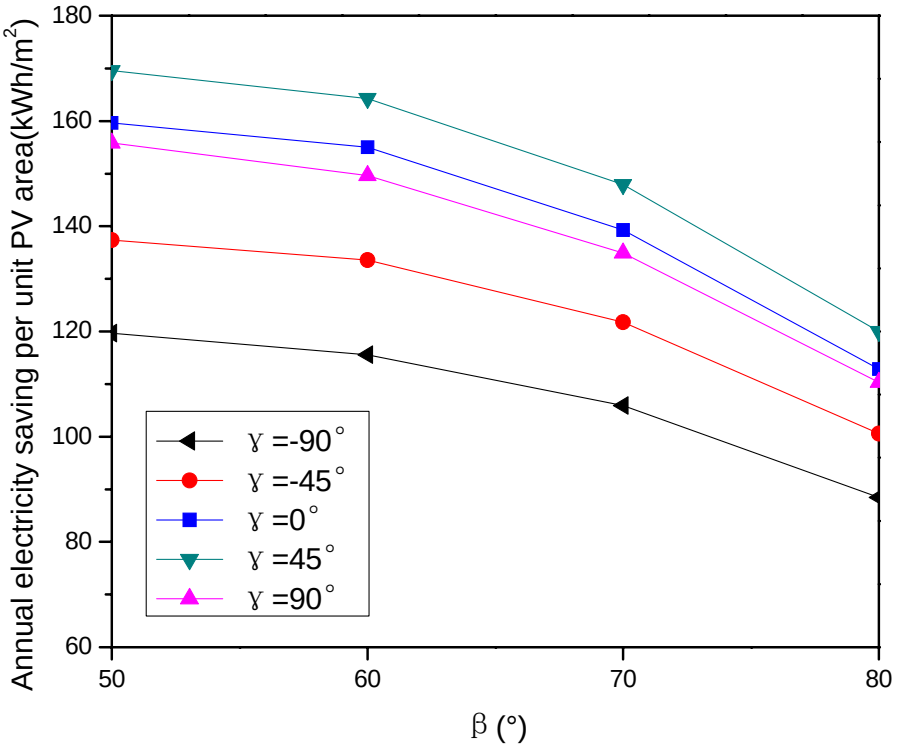

Figure 4.16 Annual electricity saving per unit PV area (*R*=100%)

Table 4.2 Optimum tilt angles for different orientations and wall utilization fractions

Optimum tilt angle	Wall utilization fraction				
Surface azimuth angle	20%	40%	60%	80%	100%
-90°	30°	40°	40°	50°	50°
-45°			50°		
0°					
45°			40°		
90°					

It is observed from the curves the southwest-facing BIPV claddings can produce more electricity saving than that of other orientations. The maximum electricity saving per unit PV area is 239.5kWh/m^2 when the shading-type BIPV claddings

have the surface azimuth angle of 45°, the tilt angle of 30° and the wall utilization fraction of 20%. The east-facing BIPV claddings with the tilt angle of 80° and the wall utilization fraction of 100% produce the minimum electricity saving of 88.5kWh/m^2, lowered by 63% compared with the maximum value. In addition, the maximum electricity saving per unit PV area is twice more than the maximum electricity generation of the PV modules. The shading-type BIPV systems can produce much more energy benefits than that of other PV systems.

4.4 Summary

In this chapter, the impact of building orientations, inclinations and wall utilization fractions on the energy performance of the shading-type BIPV claddings is discussed in terms of annual power output of PV modules and cooling load reduction of windows and concrete walls. Some specific findings from this case study are described as follows:

(1) If the annual electricity generation per unit PV area is concerned, the orientations of south and southwest are two better choices for PV module installation for the weather in Hong Kong. The maximum electricity generation per unit PV area is 76.8kWh/m^2 when the PV modules are installed on south façades at the tilt angle of 10°.

(2) The shading-type BIPV claddings have significant effect on cooling load reduction of windows and concrete walls. The maximum cooling load reduction ratios are 51.6% and 243.2% respectively for windows and concrete walls.

(3) When the area of PV modules is considered, the maximum electricity saving of the shading-type BIPV claddings is 239.5kWh/m^2, which is twice more than the maximum electricity generation of the PV modules.

(4) Different optimum tilt angles of the shading-type BIPV claddings are obtained for different orientations and wall utilization fractions. In this case study, the optimum tilt angles for different designs vary from 30° to 50°. When installed with smaller wall utilization fractions, the shading-type BIPV claddings are more cost-effective than that with larger wall utilization fractions.

The simulation results indicate that the shading-type BIPV claddings can significantly increase the total energy benefits relative to PV modules. It is thus a good choice to apply the shading-type BIPV systems in Hong Kong. In addition, these simulation results are good references for the design of integrating PV modules into buildings.

CHAPTER 5: MODELING OF THE BIPTV HOT WATER SYSTEM WITH NATURAL CIRCULATION

5.1 Introduction

In many high-rise buildings, there is not enough area for locating solar collectors for solar energy application on the roofs of the buildings. If the BIPV panel can be used on vertical façades of such high-rise buildings, the problem of the less roof area can be solved for solar energy applications. However, the energy efficiency of the PV module is lower than 20%, that is to say, more than 80% of the absorbed solar energy is converted into heat and wasted. The combination of the BIPV module and the thermal absorber can use the wasted heat to heating water. Thus, the total energy efficiency of the BIPVT module is higher than that of the BIPV module. The BIPVT hot water system has a much shorter economic payback period than the BIPV system. Application of the BIPVT hot water system is worth detailed investigation. A dynamic simulation model for the BIPVT hot water system with natural circulation was proposed in this chapter.

As shown in Figure 5.1, the BIPVT hot water system mainly consists of a BIPVT module and a thermal storage tank. Since the system is designed for natural circulation, there is no need to have a pump. Such a system is simple and more economical for small system. Its disadvantage is that natural circulation is only suitable for small system.

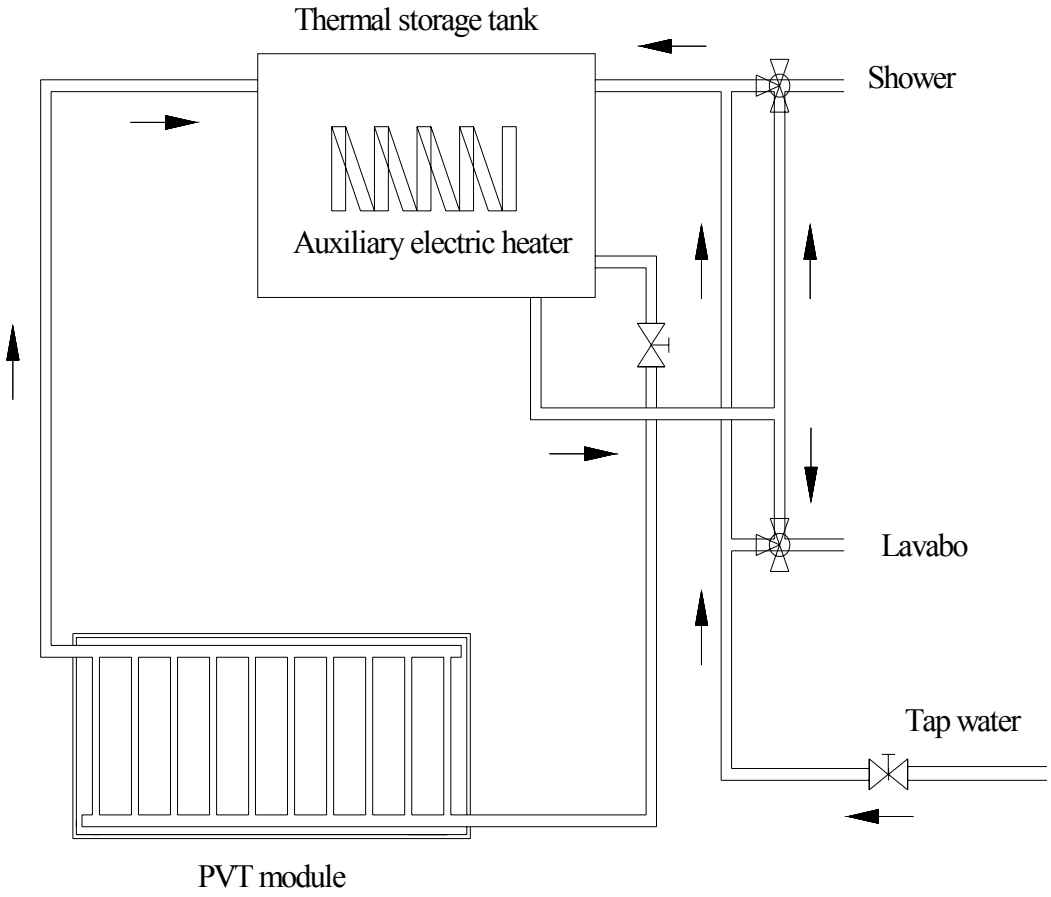

Figure 5.1 Schematic diagram of the BIPVT hot water system

Figure 5.2 shows that the BIPVT modules are installed on the concrete walls between windows of two adjacent floors. The BIPVT modules can prevent parts of sunlight from exposing on the window (bellow of the BIPVT module) and concrete wall (behind of the BIPVT module). The impact of the BIPVT module on the cooling load reduction of the window and concrete wall has been investigated in Chapter 3 and 4. Thus the cooling load reduction effect of the BIPVT module is not repeated in this chapter.

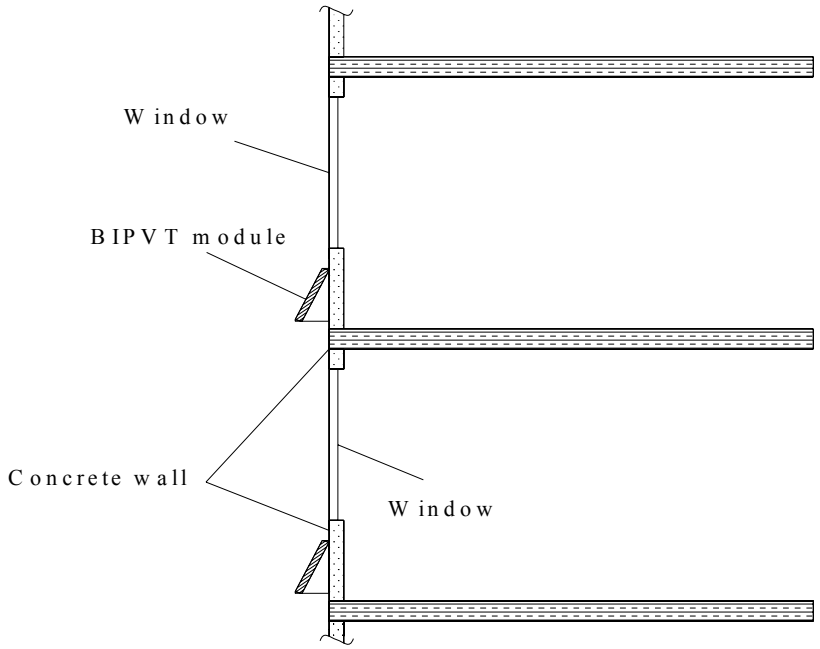

Figure 5.2 The schematic of BIPVT modules installation

Figure 5.3 shows the front view and cross section of the BIPVT module. It is known that the BIPVT module is made of seven layers, including cover glass, PV module, silicon gel, thermal absorber, water tube, thermal insulation material and metal frame. There is an air gap between the covering glass and PV module. The cover glass and air gap are both designed to eliminate the heat loss from the front surface of the PV module. Silicon gel is utilized to strengthen the thermal contact between the PV module and thermal absorber. The thermal insulation material aims to reduce the heat loss from the back surface of the thermal absorber. Generally, water tubes are attached evenly on the back surface of the thermal absorber in order to make sure that the temperature distribution of each water tube is uniform.

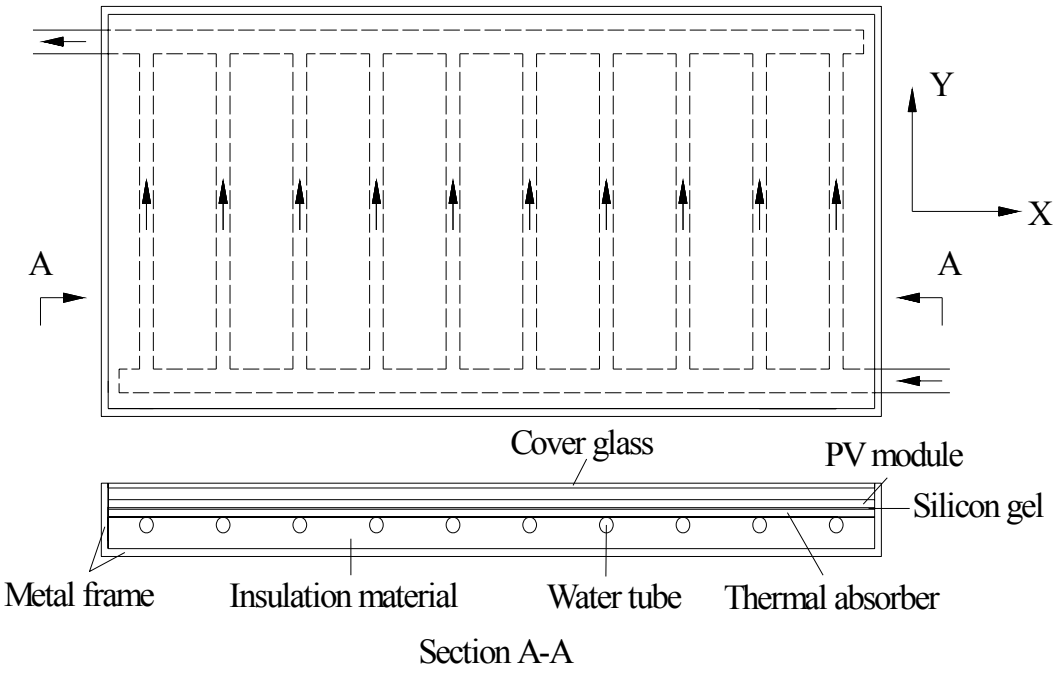

Figure 5.3 Front view and cross section of the BIPVT module

5.2 Dynamic heat transfer model of the BIPVT system

5.2.1 The covering glass

The dynamic heat balance equation on the covering glass is described as:

$$\rho_{cg} C_{cg} l_{cg} \frac{\partial T_{cg}}{\partial t} = G_{cg} + h_o \left(T_o - T_{cg}\right) + h_{cg-s} \left(T_s - T_{cg}\right) + \left(h_{r,p-cg} + h_{c,p-cg}\right)\left(T_p - T_{cg}\right) \quad (5\text{-}1)$$

where ρ_{cg} is the density of the covering glass, kg/m^3; C_{cg} is the specific thermal capacity of the covering glass, J/(kg·K); l_{cg} is thickness of the covering glass, m. T_{cg} is the temperature of the covering glass, K. G_{cg} is the solar radiation absorbed by the covering glass, W/m^2. $h_{cg\text{-}s}$ is the long wave radiant heat transfer coefficient between the covering glass and sky, W/(m^2·K). $h_{r,p\text{-}cg}$ and $h_{c,p\text{-}cg}$ are the radiant and convective heat transfer coefficients between the PV module and covering glass, W/(m^2·K).

The total solar radiation absorbed by the covering glass can be described as:

$$G_{cg} = \alpha_{bcg} G_{bt} + \alpha_{dcg} G_{dt} + \alpha_{grcg} G_{grt} \tag{5-2}$$

where α_{bcg}, α_{dcg} and α_{grcg} are the abosorptance of the covering glass for the beam, diffuse and ground reflected parts of solar radiation, respectively.

The long wave radiant heat transfer coefficient between the outside surface of the covering glass and the sky is given by the Stefan-Boltzmann's law as:

$$h_{cg-s} = \sigma \varepsilon_{cg} \left(T_s + T_{cg}\right)\left(T_s^2 + T_{cg}^2\right) \tag{5-3}$$

where ε_{cg} is the emissivity of the covering glass.

The long wave radiant heat transfer coefficient between the inside surface of the covering glass and the PV module is expressed as:

$$h_{r,p-cg} = \sigma \frac{\left(T_p + T_{cg}\right)\left(T_p^2 + T_{cg}^2\right)}{\frac{1}{\varepsilon_p} + \frac{1}{\varepsilon_{cg}} - 1} \tag{5-4}$$

where ε_p is the emissivity of the PV module.

The inside convective heat transfer coefficient between the inside surface of the cover glass and the PV module is calculated by using the following models (Duffie et al., 2006):

$$h_{c,p-cg} = \frac{Nu\lambda_a}{l_a} \tag{5-5}$$

$$Nu = 1 + 1.44\left(1 - \frac{1708}{Ra\cdot\cos\beta}\right)^{+}\left(1 - \frac{1708(\sin 1.8\beta)^{1.6}}{Ra\cdot\cos\beta}\right) + \left(\left(\frac{Ra\cdot\cos\beta}{5830}\right)^{1/3} - 1\right)^{+} \tag{5-6}$$

$$Ra = \frac{g\mathrm{B}l_a^3}{\gamma k_a}\left(T_p - T_g\right) \tag{5-7}$$

where l_a is the thickness of the air gap, m. β is ranging from 0° to 75°. The "+" exponent means that only a positive value of the term in the brackets is to be used and zero is used if the term is negative. g is gravitational constant, m/s^2. B is the volumetric coefficient of expansion. λ_a, k_a and γ are, respectively, the thermal conductivity, thermal diffusivity and kinematic viscosity of air in the air gap.

5.2.2 The PV module

The temperature distribution of the PV module on its cross section is calculated by solving a two dimensional dynamic heat transfer equation:

$$\rho_p C_p l_p \frac{\partial T_p}{\partial t} = \lambda_p \frac{\partial^2 T_p}{\partial x^2}dx + \lambda_p \frac{\partial^2 T_p}{\partial y^2}dy + (1-\eta)G_p + \left(h_{c,p-cg} + h_{r,p-cg}\right)\left(T_{cg} - T_p\right) + \frac{T_c - T_p}{R_{si}} \tag{5-8}$$

where R_{si} is the thermal conductive resistance of the silicon gel, (m^2·K)/W. T_c is the temperature of the thermal absorber, K.

The solar radiation absorbed by the PV module is described by:

$$G_p = \alpha_p\left(\tau_{bg}G_{bt} + \tau_{dg}G_{dt} + \tau_{grg}G_{grt}\right) \tag{5-9}$$

where α_p is the absorptance of the PV module's front surface.

5.2.3 The thermal absorber

According to different heat transfer phenomenon, the thermal absorber is divided into two parts: the thermal absorber without water tubes and the thermal absorber attached with water tubes. The temperature of the thermal absorber without water tubes is calculated by solving the following equation:

$$\rho_c C_c l_c \frac{\partial T_c}{\partial t} = \lambda_c \frac{\partial^2 T_c}{\partial x^2} dx + \lambda_c \frac{\partial^2 T_c}{\partial y^2} dy + \frac{T_p - T_c}{R_{si}} + \frac{T_o - T_c}{R_{in}} \tag{5-10}$$

The heat balance equation of the thermal absorber attached with water tubes is expressed by:

$$\rho_c C_c l_c \frac{\partial T_c}{\partial t} = \lambda_c \frac{\partial^2 T_c}{\partial x^2} dx + \lambda_c \frac{\partial^2 T_c}{\partial y^2} dy + \frac{T_p - T_c}{R_{in}} + \frac{T_f - T_c}{\left(\frac{1}{h_f \pi d_i} + \frac{dy}{2\pi\lambda_{wt}} \log\left(\frac{d_o}{d_i} \right) + \frac{R_B}{w_B} \right) dy} \tag{5-11}$$

where ρ_c is the density of the thermal absorber, kg/m^3; C_c is the specific thermal capacity, J/(kg·K); l_c is the thickness of the thermal absorber, m; λ_c is the thermal conductivity of the thermal absorber, W/(m·K). T_f is the water temperature in the water tubes, K. d_o and d_i are the external and internal diameter of water tubes, m. R_{in} and R_B are, respectively, the thermal conductive resistances of the thermal insulation material and the bond, (m^2·K)/W. λ_{wt} is the thermal conductivity of the water tube wall, W/(m·K). w_B is the width of the bond and its value is no less than one eighth of

the external diameter of the water tube to obtain good thermal contact between the thermal absorber and the water tube, m.

The heat transfer coefficient from each water tube to water is calculated using the following models (Bejan, 1993):

$$h_f = 4.364\frac{\lambda_f}{d_i}\,(\mathrm{Re} \le 2300) \tag{5-12}$$

$$h_f = 0.023\,\mathrm{Re}^{0.8}\,\mathrm{Pr}^{0.4}\,\frac{\lambda_f}{d_i}\,(\mathrm{Re} > 2300) \tag{5-13}$$

where *Re* and *Pr* are, respectively, the Reynolds number and the Prandtl number of water in the water tubes. h_f is the convective heat transfer coefficient inside the water tubes, W/(m^2·K). λ_f is the thermal conductivity of water in the water tubes, W/(m·K).

5.2.4 The water tubes

When the water tubes are placed in parallel, the flow rate in each water tube is assumed the same. The heat balance equation of water in each water tube can be described by:

$$\frac{\pi d_i^2}{4}\rho_f C_f \frac{\partial T_f}{\partial t} = \frac{\pi d_i^2}{4}\lambda_f \frac{\partial^2 T_f}{\partial y^2} + \frac{T_c - T_f}{\dfrac{1}{h_f \pi d_i} + \dfrac{1}{2\pi\lambda_{wt}}\log\left(\dfrac{d_o}{d_i}\right) + \dfrac{R_B}{w_B}} - \frac{\pi d_i^2}{4}\rho_f C_f V_f \frac{\partial T_f}{\partial y} \tag{5-14}$$

where ρ_f is the water density of the water tubes, kg/m^3; C_f is the specific thermal capacity of water in the water tubes, J/(kg·K); V_f is the water flow rate of in each water tube, m^3/s.

5.2.5 The connecting pipe

There are two connecting pipes in the BIPVT hot water system. One is the supply water pipe which is connected to the outlet of the thermal storage tank and the inlet of the PVT module and the other is the return water pipe which is connected to the outlet of the PVT module and the inlet of the water tank. By neglecting the thermal capacity of the two connecting pipes and the heat loss to the surrounding, the heat balance equations of the supply water pipe and return water pipe are expressed as follows:

$$\frac{\pi d_{cp}^2}{4}\rho_{swp}C_{swp}\frac{\partial T_{swp}}{\partial t}=\frac{\pi d_{cp}^2}{4}\lambda_{swp}\frac{\partial^2 T_{swp}}{\partial L_{swp}^2}-\frac{\pi d_{cp}^2}{4}\rho_{swp}C_{swp}V_{cp}\frac{\partial T_{swp}}{\partial L_{swp}} \tag{5-15}$$

$$\frac{\pi d_{cp}^2}{4}\rho_{rwp}C_{rwp}\frac{\partial T_{rwp}}{\partial t}=\frac{\pi d_{cp}^2}{4}\lambda_{rwp}\frac{\partial^2 T_{rwp}}{\partial L_{rwp}^2}-\frac{\pi d_{cp}^2}{4}\rho_{rwp}C_{rwp}V_{cp}\frac{\partial T_{rwp}}{\partial L_{rwp}} \tag{5-16}$$

where ρ_{swp} and ρ_{rwp} are, respectively, the density of water in supply water pipe and return water pipe, kg/m^3; C_{swp} and C_{rwp} are, respectively, the thermal capacity of water in supply water pipe and return water pipe, kJ/(kg·K); λ_{swp} and λ_{rwp} are, respectively, the thermal conductivity of water in supply water pipe and return water pipe, W/(m·K). L_{swp} and L_{rwp} are the length of the supply water pipe and return water pipe, m. d_{cp} is the internal diameter of the connecting pipes, m; V_{cp} is the water flow rate of the connecting pipes, m^3/s.

If the number of water tubes is N, the flow rate of connecting pipe, V_{cf}, is expressed as follows:

$$V_{cp}=N\cdot V_f \tag{5-17}$$

5.2.6 The thermal storage tank

Supposing that the water temperature in the thermal storage tank is uniform and the heat loss between its surfaces and surroundings is neglected due to good insulation, the heat balance equation of water in the thermal storage tank is expressed as

$$\rho_w V_w C_w \frac{\partial T_{wt}}{\partial t} = \frac{\pi d_i^2}{4} N v_{cp} \left(\rho_{rwp} C_{rwp} T_{rwp} - \rho_w C_w T_w \right) \tag{5-18}$$

where T_{wt} is the temperature of water in the thermal storage tank, K; V_{wt} is the volume of water in the thermal storage tank, m^3. d_{cp} is the internal diameter of the connecting pipe, m; v_{cp} is water flow rate of the connecting pipes, m^3/s.

5.3 Flow rate determination

In this thesis, the BIPVT hot water system is designed for natural circulation. For natural circulation, the flow rate in each water tube is determined when the buoyant head equals the friction loss. The buoyant head and friction loss of the BIPVT hot water system are described as follows:

$$H_t = \left(\rho_w - \rho_f \right) \cdot \Delta H \tag{5-19}$$

$$H_f = \xi_f \frac{V_f^2}{2g} + f_f \frac{L_f}{d_i} \frac{V_f^2}{2g} + \xi_{swp} \frac{V_{cp}^2}{2g} + f_{swp} \frac{L_{swp}}{d_{cp}} \frac{V_{cp}^2}{2g} + \xi_{rwp} \frac{V_{cp}^2}{2g} + f_{rwp} \frac{L_{rwp}}{d_{cp}} \frac{V_{cp}^2}{2g} \tag{5-20}$$

where ΔH is the vertical distance between the barycentre of the PVT module and the thermal storage tank, m. L_f is the length of each water tube, m. ξ_f, f_f, ξ_{swp}, f_{swp}, ξ_{rwp} and f_{rwp} are loss coefficients and friction factors, respectively, for the water tubes, the supply water pipe and the return water pipe.

5.4 Combined electrical power and thermal energy

In order to compare the combined energy performance of the BIPVT system, the water heat gain is converted into electrical energy by introducing the energy efficiency of a electric heater. In this case study, the hot water design temperature in the thermal storage tank is set as 45℃. A supplemental electric heater is used when water temperature is lower than the set point in the evening when hot water is used for shower. The combined equivalent electrical energy generation can be expressed as follows:

$$E_{comb} = E_p + E_{hw} = E_p + \frac{q_{hw}}{\eta_e} = E_p + q_{hw} \tag{5-21}$$

where E_p is the total electrical power output of the PVT modules, J. E_{hw} is the electrical power output due hot water production, J. q_{hw} is the water heat gain in the thermal storage tank, J. η_e is the energy efficiency of the electric heater and its value of 100% is used in this study.

The electrical energy efficiency, thermal energy efficiency and combined energy efficiency of the BIPVT hot water system are described as follows:

$$\eta_p = \frac{E_p}{G_{tt} A_p} \tag{5-22}$$

$$\eta_{hw} = \frac{E_{hw}}{G_{tt}} = \frac{q_{hw}}{G_{tt} A_p} \tag{5-23}$$

$$\eta_{comb} = \frac{E_{comb}}{G_{tt} A_p} \tag{5-24}$$

5.5 Summary

This chapter developed a simulation model for estimating the energy performance of the BIPVT hot water system. Firstly, the heat balance equations of several main components of the BIPVT hot water system, including the covering glass, the PV module, the thermal absorber, the water tubes, the connecting pipes and the thermal storage tank have been proposed on the basis of the dynamic heat transfer method. Secondly, the water flow rate of the BIPVT water system under natural circulation mode is determined by the buoyant head and the friction loss of such a system. Finally, the water heat gain is converted into the electrical energy generation in order to evaluate the total energy benefits of the BIPVT hot water system.

CHAPTER 6: EXPERIMENTAL INVESTIGATION OF THE PVT HOT WATER SYSTEM WITH NATURAL CIRCULATION

6.1 Introduction

A series of well recorded experiments were carried out in order to examine the validity of the simulation models developed in this study. The experimental study was carried out in the Solar Simulation Lab of the Department of Buildings Services Engineering, The Hong Kong Polytechnic University. An experimental rig has been set up in the lab. The measured data from the experiments were employed to verify the corresponding simulation results. In this chapter, the detailed descriptions of the experimental test rig and its major components are presented. That is followed by the analysis of the experimental results.

6.2 Experimental set-up

This study aims to investigate the energy performance of the BIPVT hot water system with natural circulation and validate the simulation model presented in the preceding chapter. An indoor experimental testing facility in The Hong Kong Polytechnic University was set up during the testing period for the above mentioned purposes. This experimental rig allows changing of solar radiation levels and makes comparison easier among different operational conditions with same solar irradiation level. The test maybe difficult to be performed under outdoor testing conditions as weather conditions, i. e. solar radiation, changes from time to time. In previous

literature, researchers attempted to find similar weather conditions among all test data collected for their comparison purposes, which may introduce some errors in the comparison.

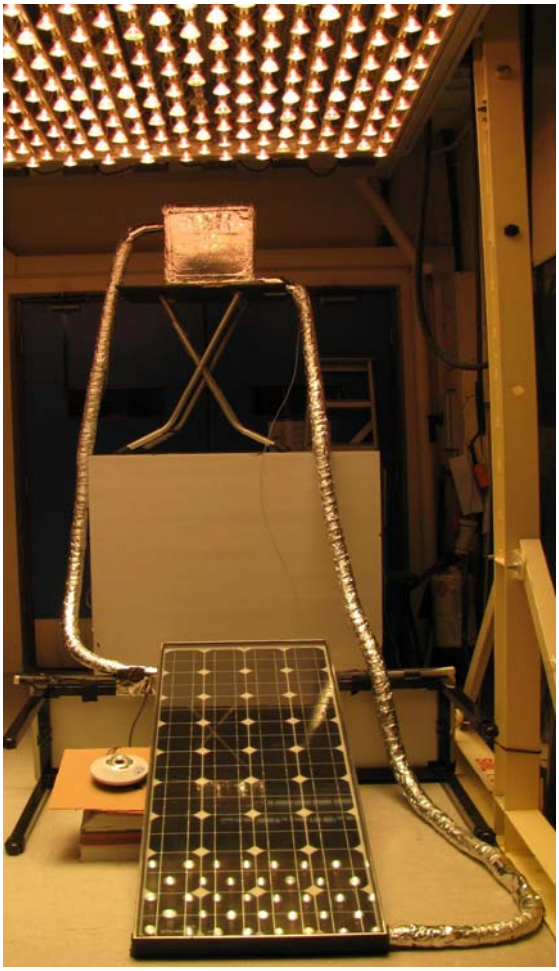

Figure 6.1 Photo of the test rig in the Solar Simulation Lab

The photo of the test rig is shown in Figure 6.1. The experimental rig consists of a PVT module, a thermal storage tank, a flow meter and a solar simulator which provides simulated light to the module surface. The PVT module with the tilt angle of 20° is under the exposure of the solar simulator. Heat transfer by convection and radiation occurs on the surface of the PVT module. Heat absorbed by the PVT module increases its temperature and part of the heat is transmitted through the

module. The thermal storage tank is made of plastic and its volume is 0.027m^3. The schematic of the PVT hot water system is shown in Figure 6.2.

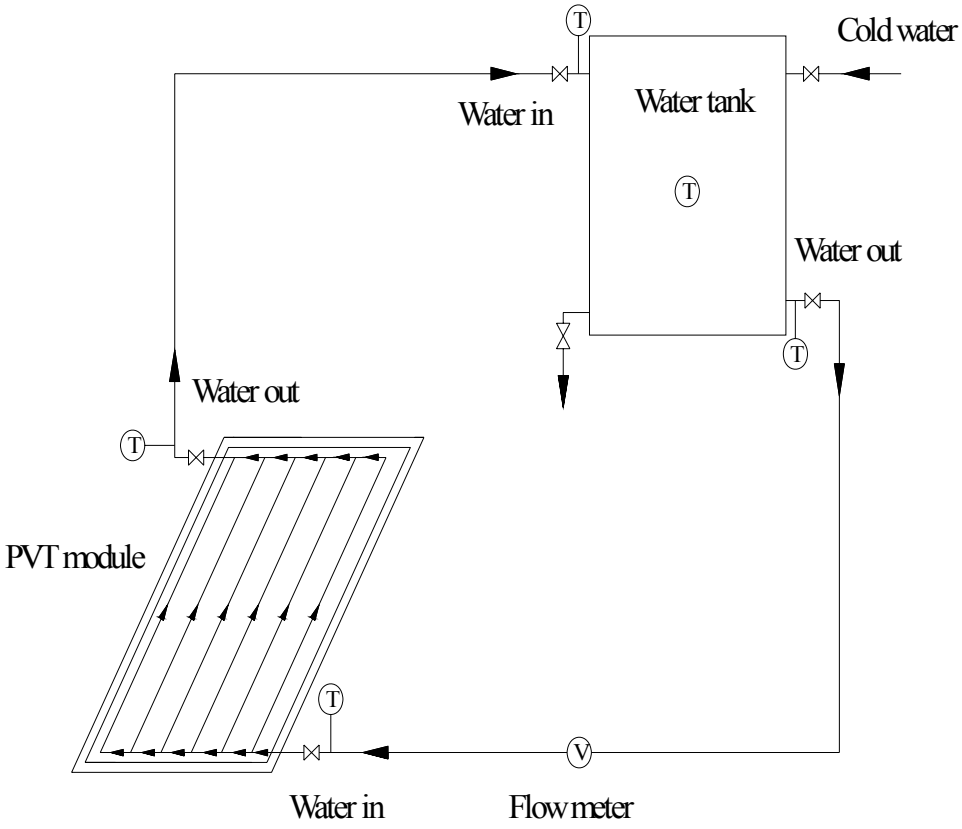

Figure 6.2 Schematic of the PVT hot water system

6.2.1 The PVT module

As shown in Figure 6.3, the PVT module integrated with monocrystalline silicon solar cells is used for this application in order to explore the energy performance of the PVT hot water system. The energy efficiency for monocrystalline silicon cells is higher compared with polycrystalline silicon solar cells and amorphous silicon solar cells. The technical data for this PVT module is listed in Table 6.1

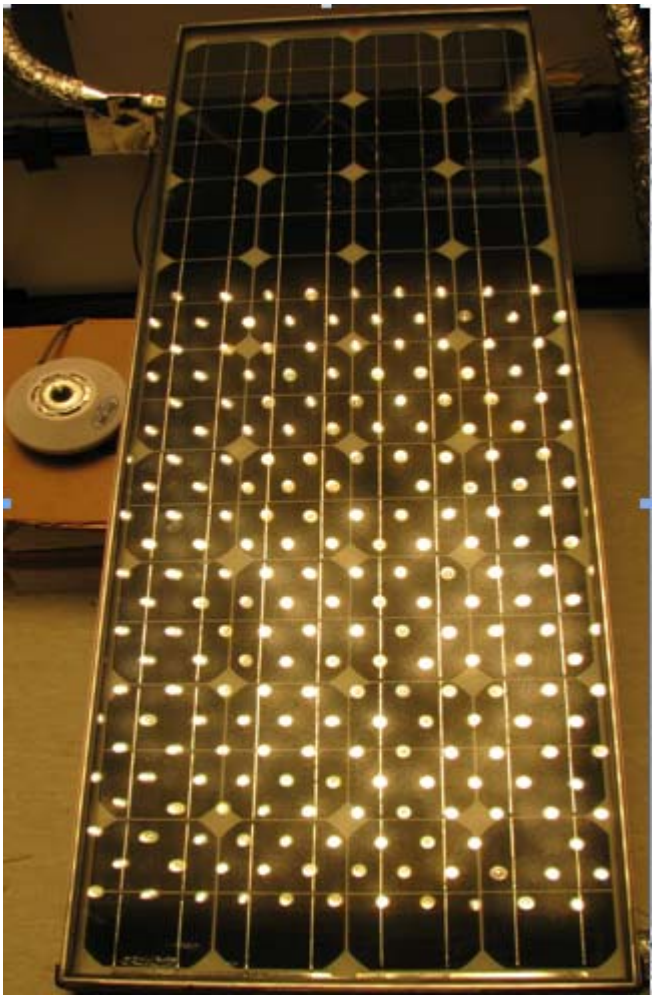

Figure 6.3 Photo of the test rig in the Solar Simulation Lab

Table 6.1 Basic parameters of the PVT module

Cover glass	
Thickness	5mm
Glass type	Toughened glass
Air gap	
Thickness	16mm
PV module	
Dimensions (L × W × H)	1.59 m × 0.54 m × 0.005m
Solar cell type	Monocrystalline silicon

PV efficiency	16.0%
Max power(W)	100W
Max power voltage(V)	17.5V
Max power current (A)	5.77 A
Open circuit voltage (V)	21.5V
Short circuit current (A)	6.28A
Silicon gel	
Thickness	2mm
Thermal conductivity	0.8W/(m·K)
Thermal absorber	
Material	Copper
Thickness	3mm
Water tube	
Number	6
Material	Copper
Internal diameter	14mm
Thermal insulation	
Material	Glass fiber
Thickness	25mm

6.2.2 The Solar simulator

A solar simulator (as shown in Figure 6.4) with a 3-phase lamp array is employed to imitate necessary solar irradiation for the photovoltaic tests. The light source

(2m×2m) is based on proven steady-state Halogen Dichroic system, which is made of 363×75 W lamps powered by 12VDC. The standard steady-state solar simulator can simulate the sunlight in a variety of conditions, with radiation from zero to approximately 1300 W/m^2. As the number of the lamps is large and the diffuse angle of the light is quite high, the solar radiation flux on the PV module is quite uniform.

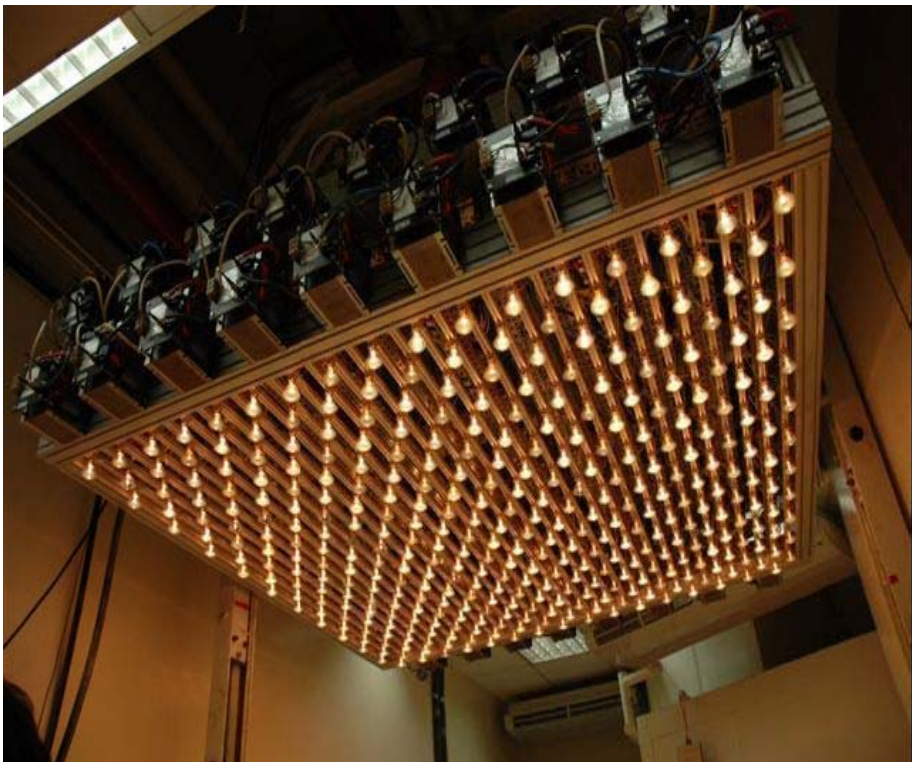

Figure 6.4 Photo of the solar simulator in the Solar Simulation Lab

6.2.3 The GL800 data logger

The ambient air temperature, the inlet and outlet temperature of water in the thermal storage tank and the PVT module, the temperature of the back surface of the PVT module, the temperature of the thermal absorber, the temperature of external surface of the water tube, the temperature of the back surface of the PVT module and the

water flow rate were logged at constant time interval through a Midi Data Logger – GL800 (as shown in Figure 6.5).

Figure 6.5 Photo of the GL800 data logger

The GL800 midi data logger accepts voltage, temperature, humidity, pulse and logic signals. The sensors are connected via rear mounted screw terminals. With its channel-to-channel isolation, the wiring errors or overloaded channels will not affect neighboring channels, due to its channel-to-channel isolation. Its built-in 12.0MB non-volatile memory retains data even if the power supply is interrupted. The software of the data logger provides real-time waveform monitoring, data upload and data export to spreadsheets. The detailed information of the data logger is listed in Table 6.2.

Table 6.2 Specification of the GL800 data logger

Number of Channels	20 Channels (Expandable to 200)
Input Method	Scanning
Input Types	Voltage, Current, Thermocouple, RTD, Humidity
Voltage Input Ranges	±20mV to ±50 V, ±1 to 5V (4 to 20 mA)
Voltage Measurement Ranges	20mV,50mV,100mV,200mV,500mV, 1V,2V,5V,10V,20V,50V, 1-5 Volts FS
Thermocouple Input Types	K, J, E, T, R, S, B, N, W
RTD Input Types	PT100 and JPT100
Internal Memory Capacity	12.0 MB
Sampling Interval	100 ms to 1 Hour
Alarm Function	Analog, Logic or Pulse
Operating Environment	Temperature: 0 to 45°C
	Humidity: 5 to 85% RH
Certifications	CE, RoHS, China RoHS
Software Compatibility	Windows 2000/XP
Power Supply	100 to 240 VAC, 50/60 Hz AC Adapter (Included)
	DC Input (8.5 to 24VDC), Battery Pack (Optional)
Dimensions	232mm x 152mm x 50mm
Weight	990g (Battery and AC Adapter excluded)

6.2.4 The I-V curve tracer MP-170

The MP-170 (as shown in Figure 6.6) is a state-of-the-art instrument to measure the I-V curve characteristics of PV modules to evaluate the electrical performance of the PV modules and systems. Especially designed to measure 10W PV modules to 10kW PV systems, the MP-170 has a measurement range of up to 1000V making it well suited for larger voltage PV arrays. It is very cost effective, compact and portable. It includes a solar irradiance sensor, two temperature sensors, and failure analysis functions.

Figure 6.6 Photo of the MP-170

The Sensor Unit is equipped with a pyranometer with a silicon detector and comes with a calibration certificate. Solar irradiance and temperatures can be measured remotely. Coupled with its internal capabilities to display the differential coefficient and magnification of the I-V curve, the MP-170 is very effective for failure diagnosis of the PV array. With a built in keyboard, LCD, and functional diagnostics, the

MP-170 can be operated without a PC. The enhanced measurement and analysis software package for PC operation works with Windows 2000/XP and it has functions of text data saving, graphical representation, auto continuous measurement, as well as additional analysis capabilities. The detailed information is listed in Table 6.3.

Table 6.3 Specifications of the MP-170 I-V curve tracer

Measurement range	Voltage: 10V - 1000V
	Current: 1A - 20A
	Power: 10W - 10kW
Data points	400 points / I-V curve
Data storage	300 IV curves (Internal Memory)
Input	Tester: PV module/array x 1(2 cables to PV string)
	Sensor Unit: Pyranometer or reference cell, Thermocouple x 2
Interface	USB x 1(PC), RS-485 x 1(Sensor Unit)
Measurement parameters	I-V curve, Pm, Isc, Voc, FF, Ipm, Vpm, Solar irradiance, Temperature x 2, STC conversion, Differential coefficient of I-V curve
Dimensions	Tester: W:230mm x L:300mm x H:160mm
	Sensor Unit: W:210mm x L:85mm x H:55mm
Weight	Tester: 3.0 kg, Sensor Unit: 0.48 kg, Battery Box: 0.75 kg
Power supply	Tester: D size battery x 4 or AC adapter DC9V, 1.3A
	Sensor Unit: 006P type battery x 1 (9V)
PC Operating system	Windows 2000/XP

6.3 Thermal property of the PVT hot water system

6.3.1 Stability of the solar radiation

Figure 6.7 shows that the solar radiation exposed on the tilt surface during the measurement period. In the measurement period of 5 hours, solar radiation ranges from 499.29W/m^2 to 514.54W/m^2. The relative error between the measured values and the average value (508.41W/m^2) is within 2%. The solar radiation produced by the solar simulator is very stable.

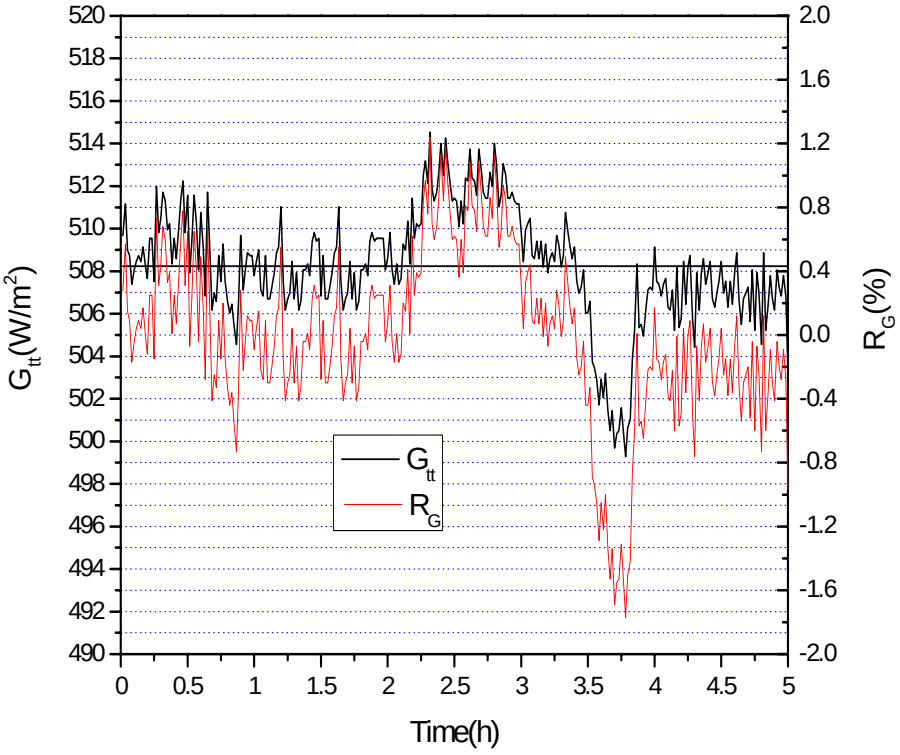

Figure 6.7 Solar radiations on a tilt surface

6.3.2 Thermal contact

Good thermal contact between the PV module, thermal absorber and water tubes plays an important role in the thermal performance of the PVT module. Figure 6.8

shows the temperature of the PV module, thermal absorber and water tube. At the beginning, the temperature of the PV module, thermal absorber and water tube is 28.5℃, 27.5℃ and 26℃. The maximum temperature difference between the PV module and the thermal absorber is 2.6℃. And the maximum temperature difference between the thermal absorber and the water tube is 4.1℃. It is concluded that the PVT module has good thermal contact although improvement is still needed.

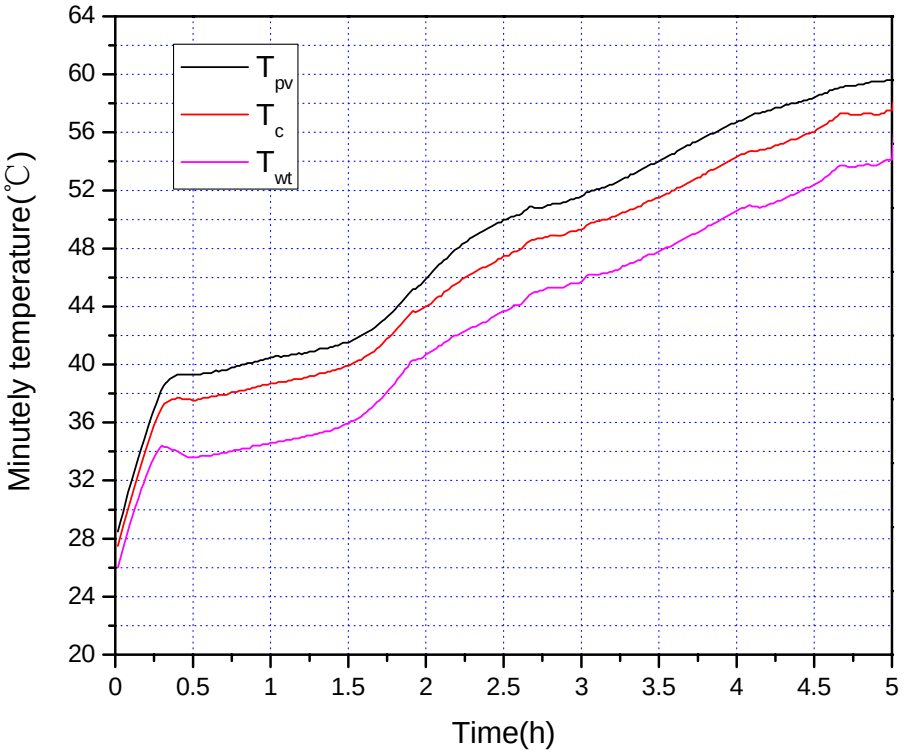

Figure 6.8 Temperatures of PV module, thermal absorber and water tube

6.3.3 Thermal insulation

In the BIPVT hot water system, there are thermal insulation materials utilized in three parts: between the thermal absorber and the metal frame, outside the connecting pipes and outside the thermal storage tank. The function of these thermal insulation materials is to preventing the heat loss from the hot water to ambient air.

Figure 6.9 gives the water temperature of the thermal absorber, ambient air and the back surface of the metal frame. At the start of the measurement, the temperature of the thermal absorber and the metal frame is 27.5℃ and 22.4℃. At the end of the measurement period, the thermal absorber temperature reaches up to 57.5℃, 25.4℃ higher than the temperature of the metal frame. In addition, the maximum temperature difference of the metal frame and ambient air is as low as 4.7℃.

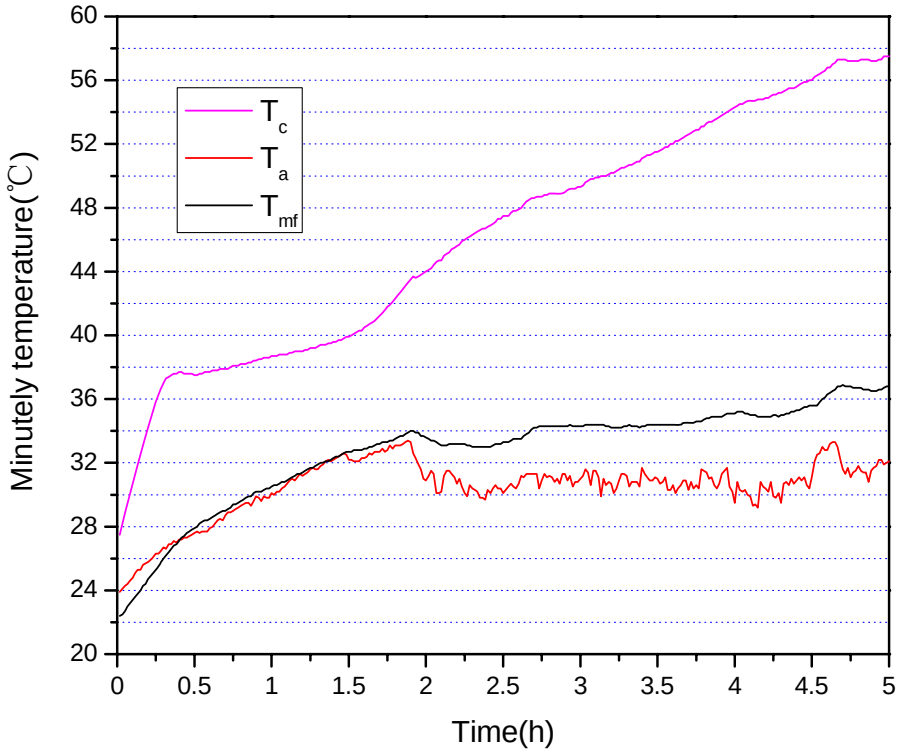

Figure 6.9 Temperature of thermal absorber, ambient air and the back surface of metal frame

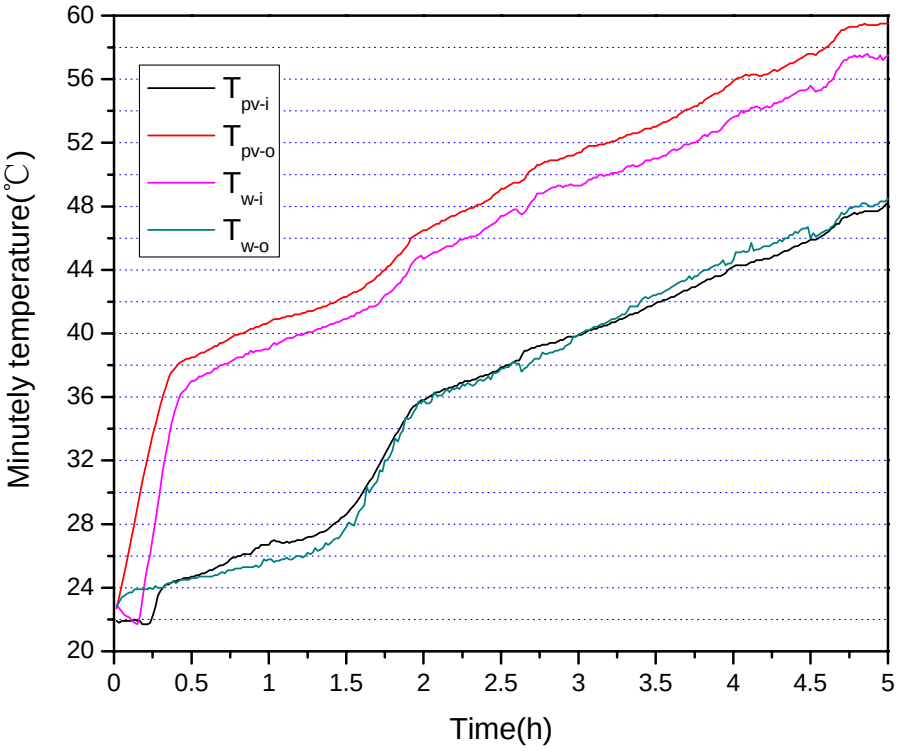

Figure 6.10 Measurement data of water temperature

Figure 6.10 gives the water temperature of inlet and outlet of the PVT module and thermal storage tank. It can be seen from Figure 6.10 that the water temperature difference between the inlet and outlet of the water pipe is in the range of -2.2~1.4℃. At the beginning, say in 0.5h, there is no significant circulation of water. The water temperature difference between the inlet and outlet of the return water pipe is as large as 7.7℃. Then, the water temperature difference decreases to 1.3℃~2.5℃.

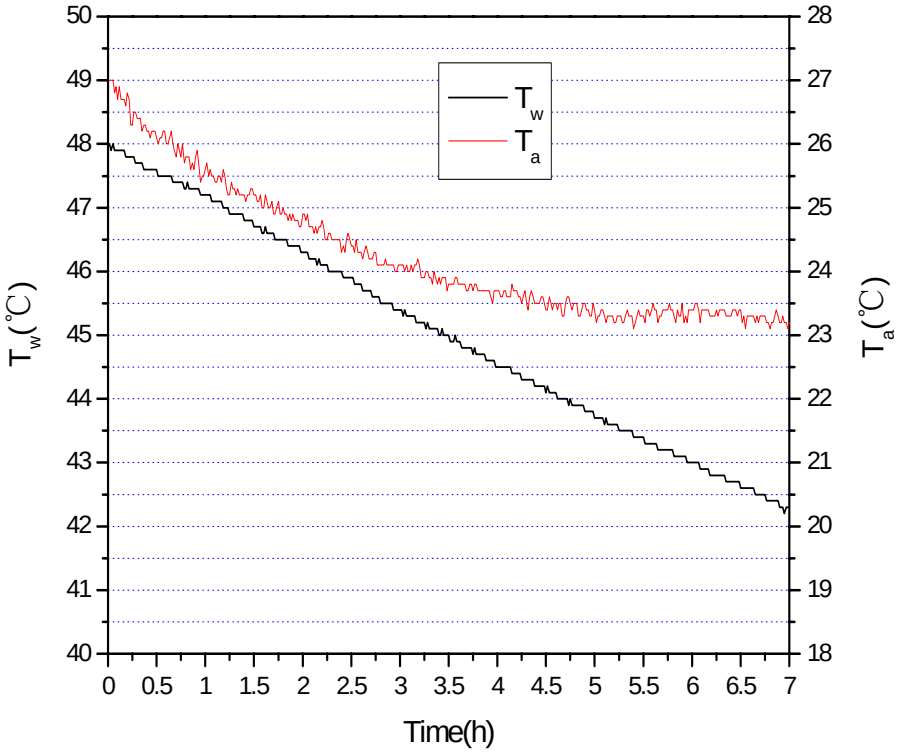

Figure 6.11 Temperatures of water in the thermal storage tank

Figure 6.11 presents the temperature of water in the middle of the thermal storage tank. It shows that the water temperature decreases from 48.0℃ to 42.3℃ in 7 hours. The water temperature reduction is about 0.8℃ per hour. In one word, the thermal insulation material of the PVT module, connecting pipes and thermal storage tank performs well.

6.4 Energy performance of the PVT hot water system

6.4.1 Electrical energy efficiency

Figures 6.12 and 6.13 show the electrical power output at the maximum power point and the corresponding electrical efficiency of the PVT module. Because of the good stability of the solar simulator, the reduction of the electrical power and electrical

efficiency both depends on the temperature increase of the PVT module. As the temperature of PVT module increases from 28.5℃ to 59.6℃, the electrical power is 31.9W, lowered by 15.2% compared with the power output of 37.6W at the start of the experiment. During the same period, the relative reduction ratio of the electrical efficiency is 15.1%, which is almost as same as the relative reduction ratio of electrical power. This also proves that the minor variation of the solar radiation is neglected.

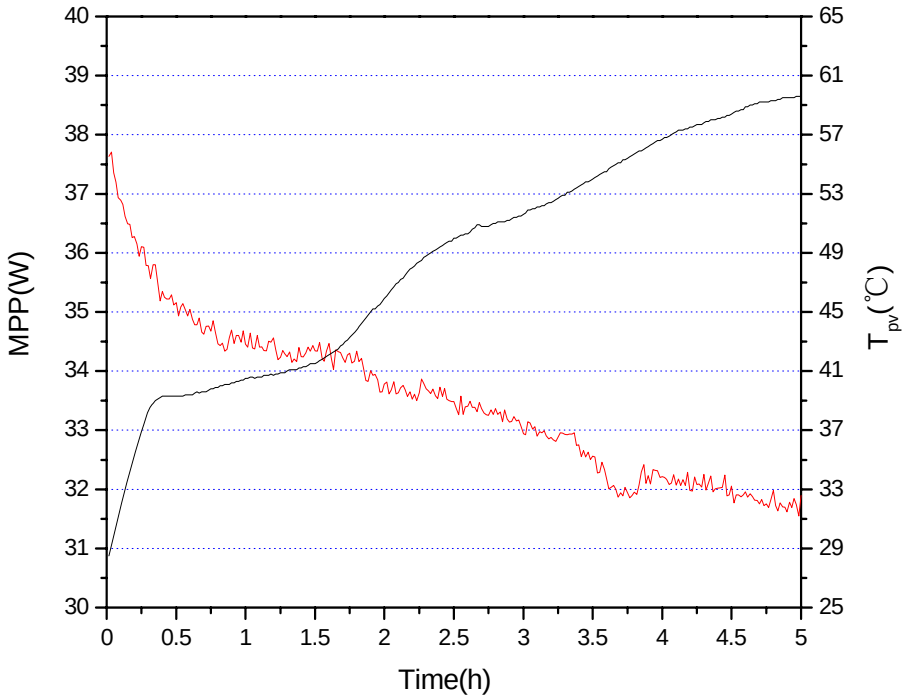

Figure 6.12 Maximum power of BIPVT module

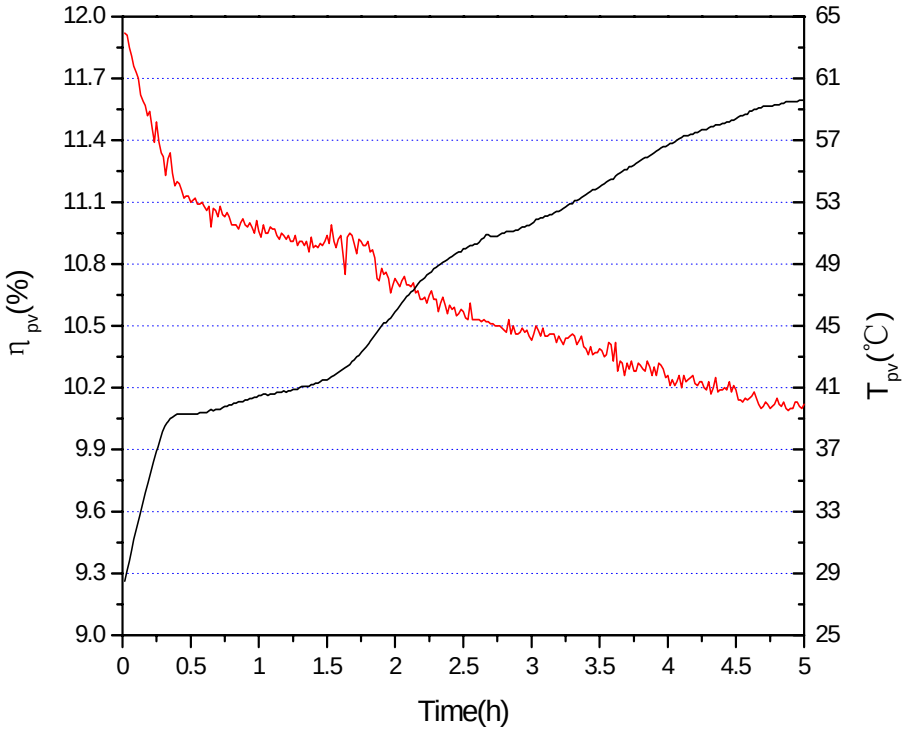

Figure 6.13 Electrical efficiency of BIPVT module

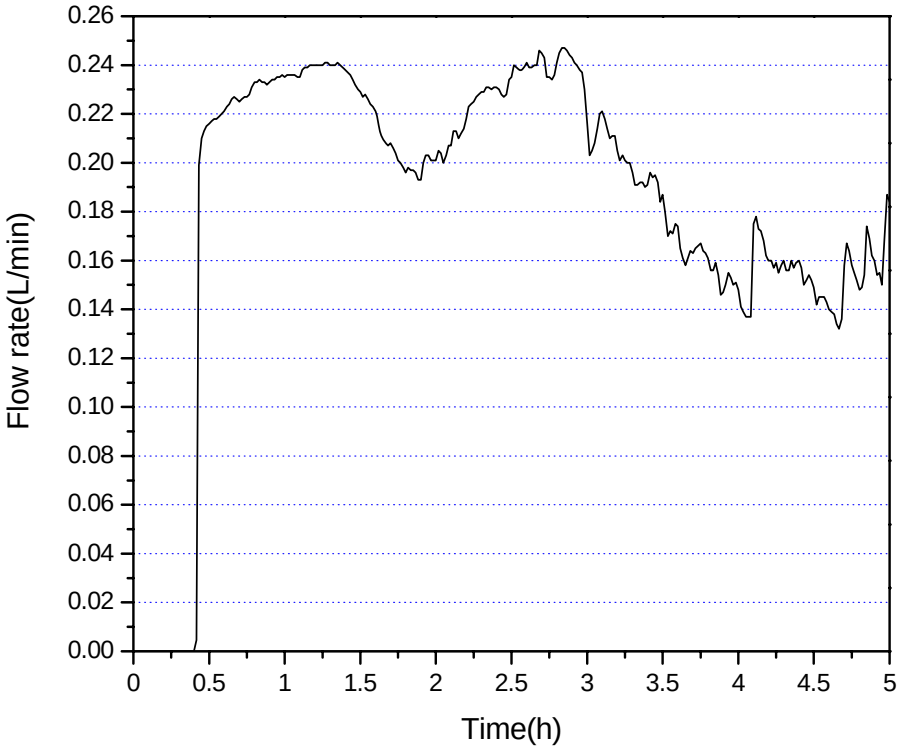

Figure 6.14 Flow rate of water in connecting pipe

6.4.2 Thermal efficiency

The measurement data of flow rate is presented in Figure 6.14. It shows that the flow rate increases form 0 to 0.20L/min suddenly at the time of 25min after the beginning of the experiment. In the whole period of the experiment, the maximum value of the flow rate is about 0.24L/min while the minimum flow rate is 0.13L/min.

Figure 6.15 gives the measured thermal efficiency of the PVT module and the BIPVT hot water system. Although the thermal efficiency of the PVT hot water system is lower than that of the PVT module, the variation trends of these two measurement data are coincident. The maximum thermal efficiency of the PVT module and the BIPVT hot water system are, respectively, 52.4% and 51.3%.

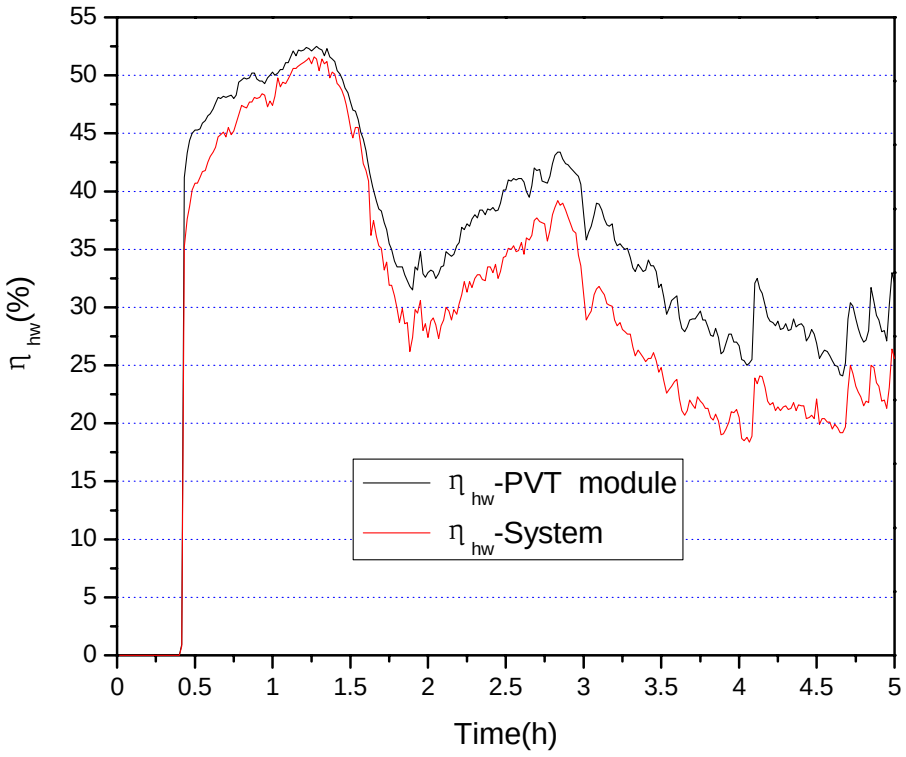

Figure 6.15 Thermal efficiencies of the PVT module and the PVT hot water system

6.5 Effect of varied parameters

6.5.1 Different solar radiation levels

The experimental data of the PVT hot water system under solar radiation of 508.41W/m^2 and 364.81W/m^2 are presented in Figures 6.16-6.19. It is indicated from Figure 6.16 that the solar radiation has more significant effect on the electrical performance of the PVT module than that of the temperature of PV module. As shown in Figure 6.17, it is 25min and 107min respectively for the solar radiation of 508.41W/m^2 and 364.81W/m^2 that the flow rate is not equal to 0. It indicates that the solar radiation has obvious influence on the flow rate of natural circulation.

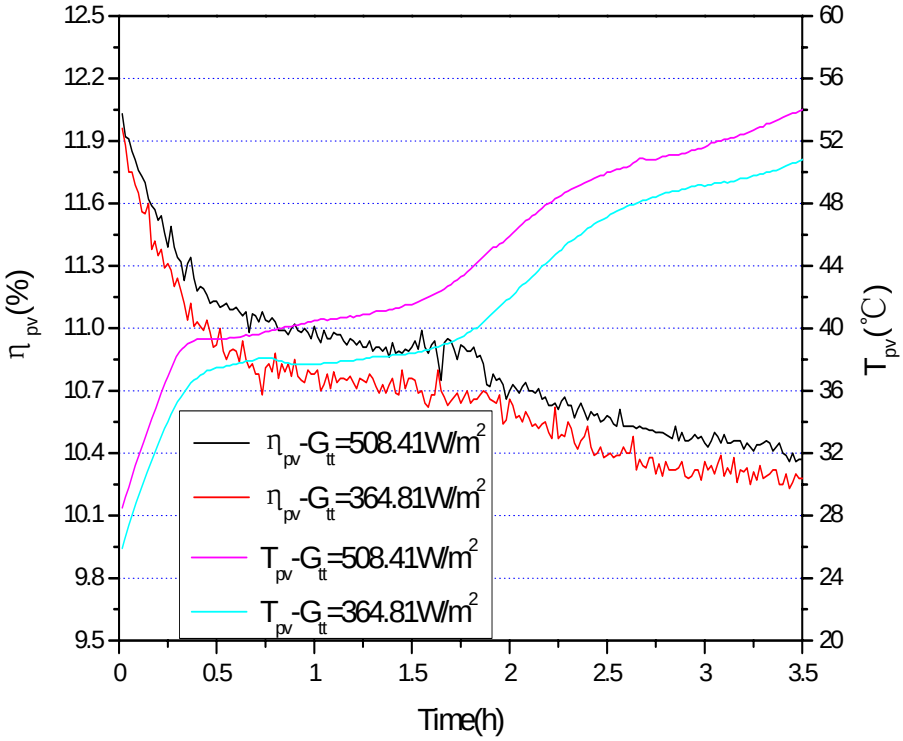

Figure 6.16 Electrical efficiency of the PVT module

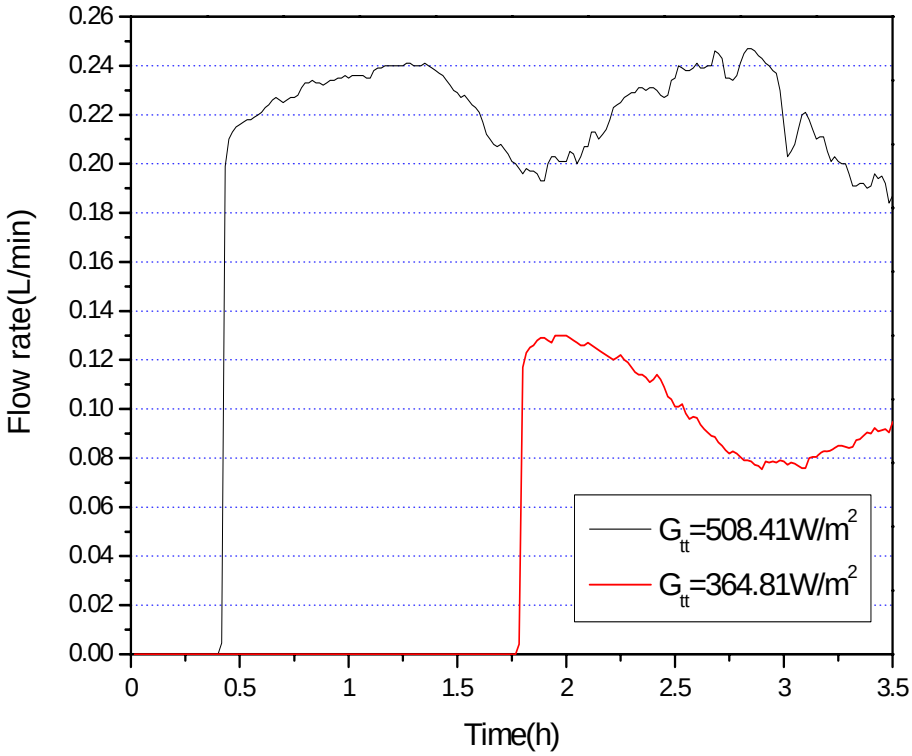

Figure 6.17 Flow rate of water for different solar radiation

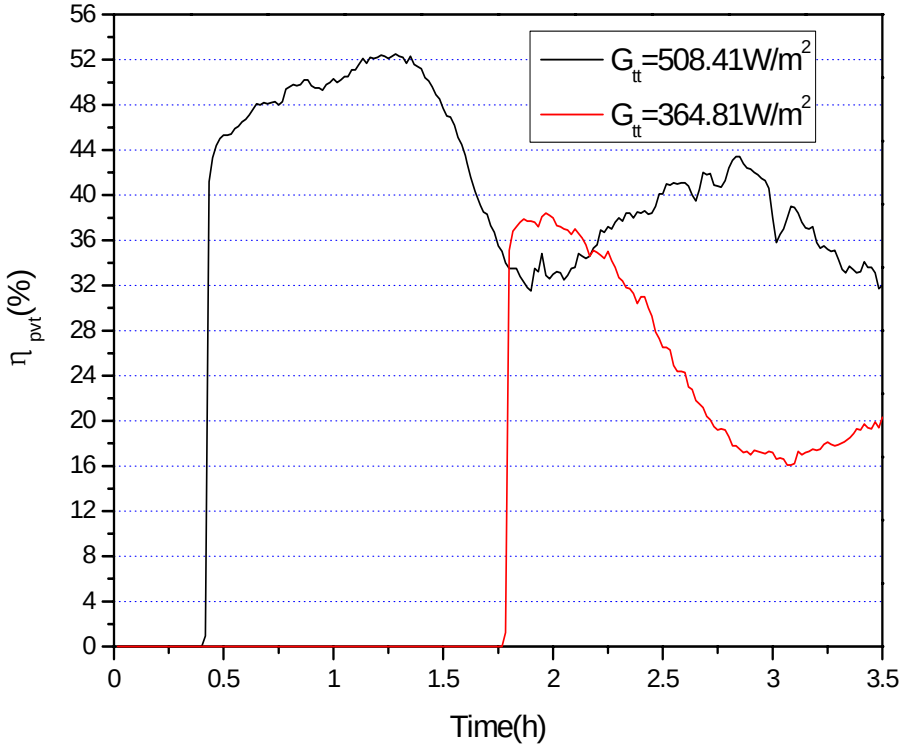

Figure 6.18 Thermal efficiency of the PVT module

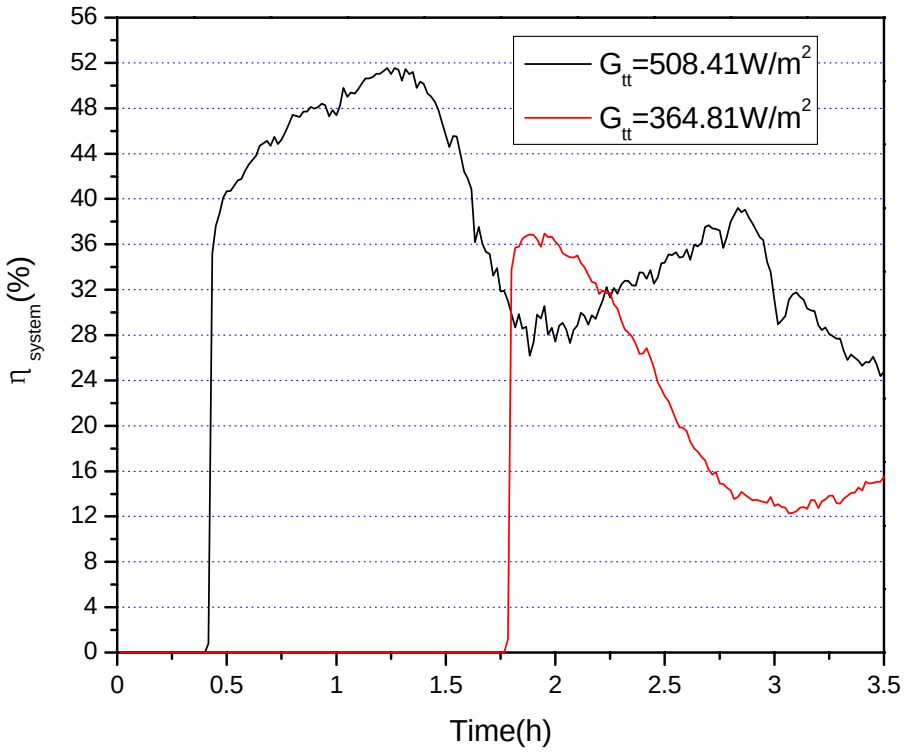

Figure 6.19 Thermal efficiency of the PVT hot water system

The thermal efficiency of the PVT module and the system are presented in Figures 6.18 and 6.19. The reduction of the thermal efficiency is very obvious when the solar radiation decreases from 508.41W/m^2 to 364.81W/m^2.

6.5.2 Different vertical distances of barycenters

Figure 6.20 shows the electrical efficiency of the PVT module with the vertical distance of 1.7m and 1.9m. The solar radiation has more significant effect on the electrical performance of the PVT module than that of the temperature of the PV module.

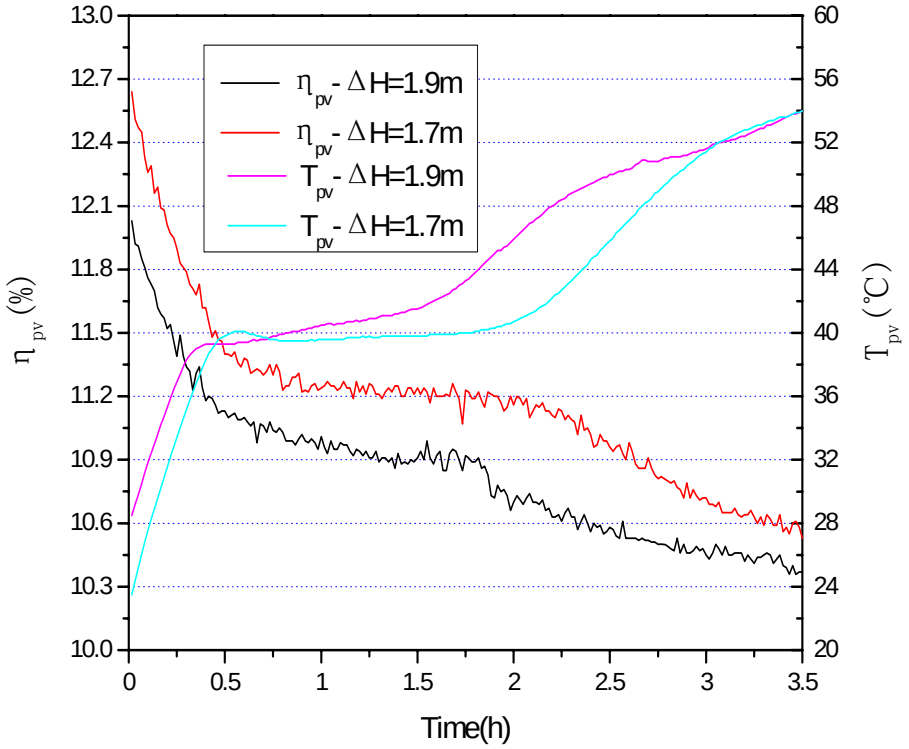

Figure 6.20 Electrical efficiency of PVT module

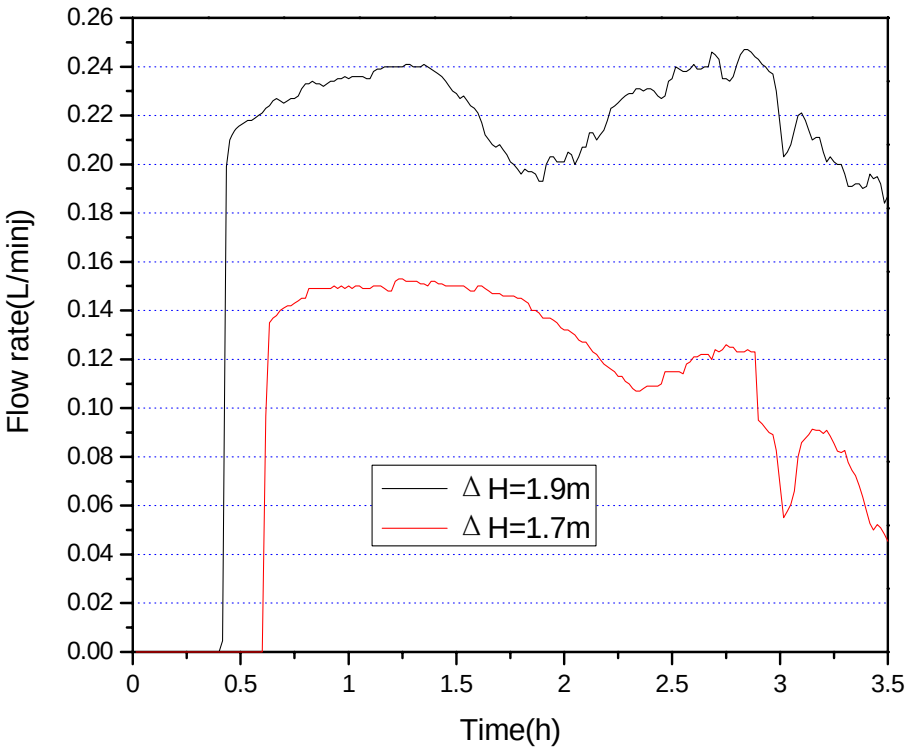

Figure 6.21 Flow rate of water for different ΔH

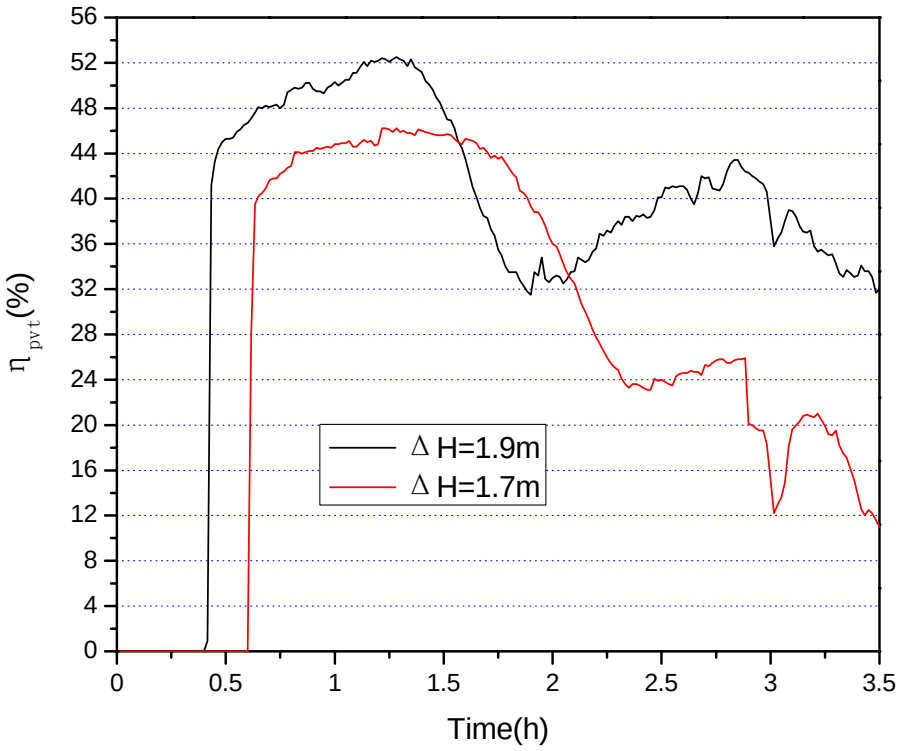

Figure 6.22 Thermal efficiency of the PVT module

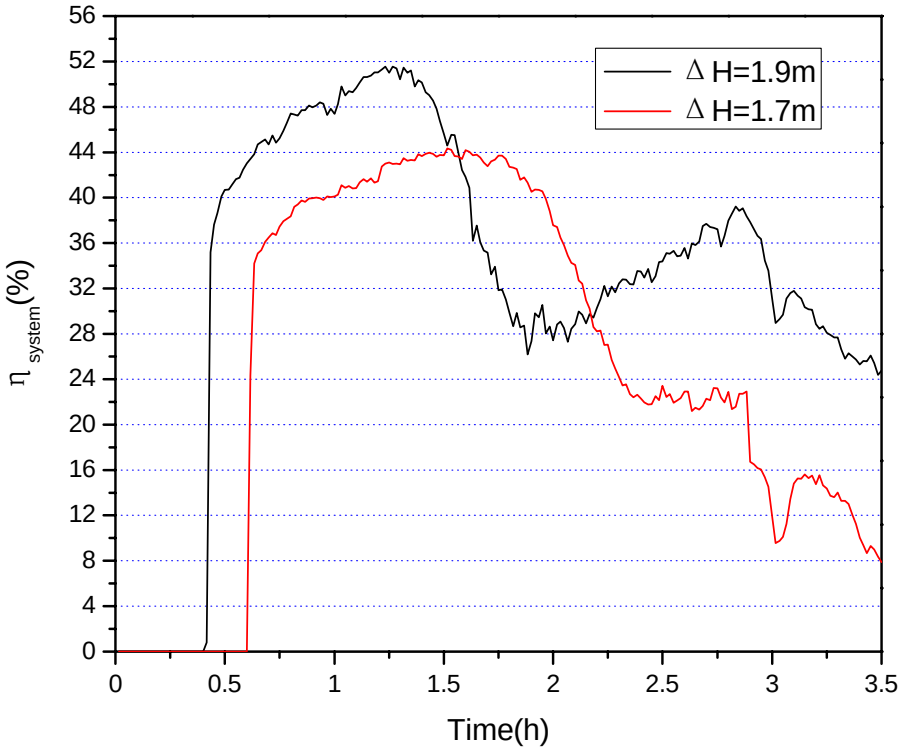

Figure 6.23 Thermal efficiency of the PVT hot water system

As shown in Figure 6.21, after 25min and 37min, respectively, for the vertical distance of 1.7m and 1.9m, the flow rate is higher than 0. It concludes that the effect of vertical distance on the flow rate of natural water circulation is not significant.

Figures 6.22 and 6.23 show the thermal efficiency of the PVT module and the system with respect to different vertical distances. It indicates that the thermal efficiency also decreases as the vertical distance decreases. The reduction ratio becomes larger and larger when time is longer.

6.6 Simulation validation

The measured data obtained from the experimental rig were used to verify the accuracy of the above simulation model of the PVT hot water system. The power output of the PVT module and the water temperature of the thermal storage tank were recorded in every minute. The results are reported in Figures 6.24 and 6.25. From Figure 6.24, it is evident that the simulation values of the minutely power output have good agreement with the experiment data. The relative errors rang from -3.0% to + 3.0% during the whole measurement period. Figure 6.25 gives the minutely variation of simulation and experiment values of the water temperature in the thermal storage tank. Although at the beginning there are very large deviation between the simulation data and the experiment data, the deviation is eliminated gradually with respect to time. When the measurement time is longer than 2.5h, the relative errors become to be within the range of -3%~+3%. It is indicated that the comparison of the simulation and experiment values of the power output and water temperature can support the validity of the present models utilized in this paper.

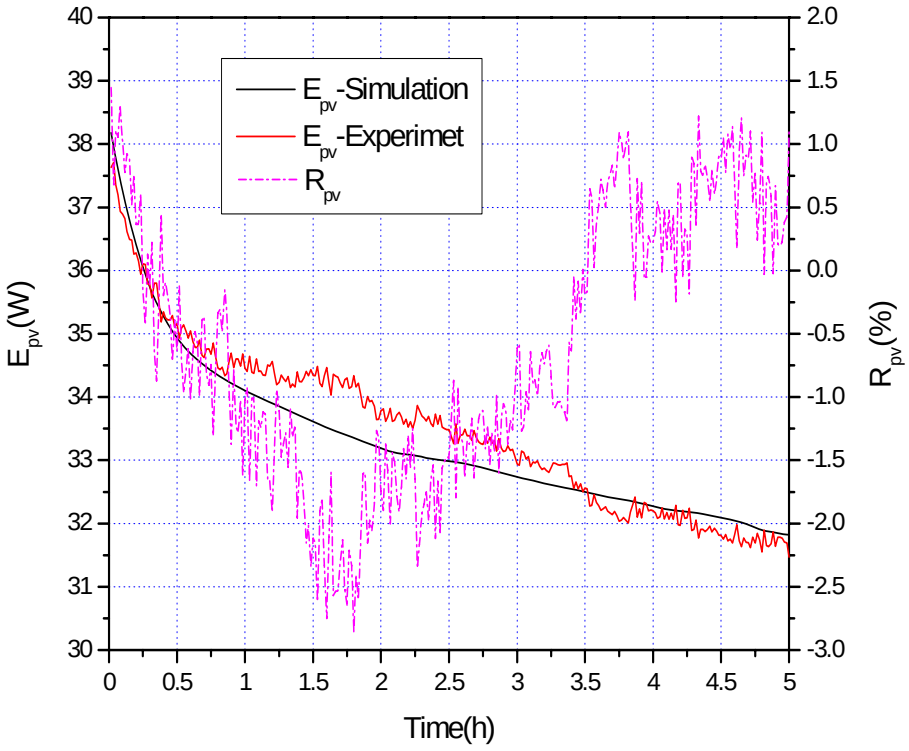

Figure 6.24 Minutely variation of PV power output-simulation and experiment

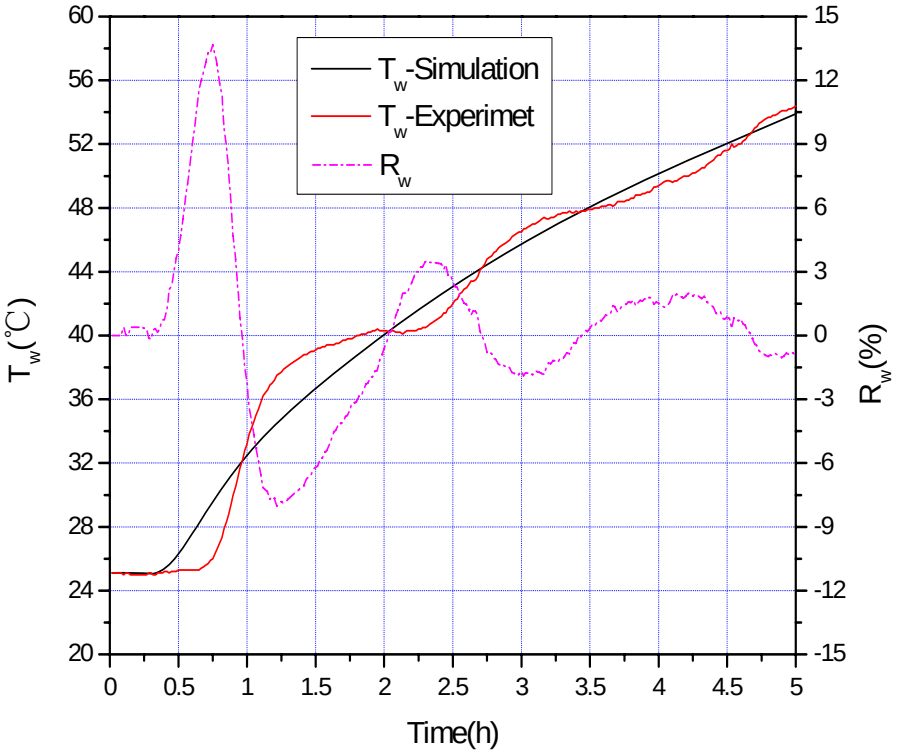

Figure 6.25 Minutely variation of water temperature-simulation and experiment

6.7 Summary

In this chapter, a number of indoor measurements were carried out in order to examine the validity of the simulation models and the energy performances of the PVT hot water system. The laboratory measurements using developed test rig and existing equipment in the Solar Simulation Lab of the Hong Kong Polytechnic University were performed. Experiment data indicate that the PVT module has good thermal contact and thermal insulation. The thermal storage tanks and connecting pipes are also in good insulation. Comparison among a variety of operational modes for the BIPVT hot water system, i.e. different solar radiation and different vertical distance of barycenters, were carried out and results were analyzed in detail. It is found that the electrical efficiency mainly depends on the temperature of the PV module. Both the solar radiation and the vertical distance of barycenters show nearly no influence on the electrical performance of the PVT module. For thermal performance of the PVT module and the PVT hot water system, the effect of the solar radiation is more significant than that of the vertical distance of barycenters. In addition, the accuracy of the simulation model was validated by the experimental data. The simulation model is qualified for analyzing the energy performance of the PVT hot water system.

CHAPTER 7: PARAMETER ESTIMATION OF PVT HOT WATER SYSTEM

7.1 Introduction

The energy performance of the PVT module is affected by both configuration parameters and operation parameters. There are eleven configuration parameters are discussed in this chapter, including the thickness of cover glass, the thickness of air gap, the thermal conductivity and thickness of silicon gel, the material and thickness of thermal absorber, the internal diameter and spacing of water tubes, the thickness of thermal insulation material, the volume of thermal storage tank and the vertical distance of barycenters.

In order to estimate the impact of design parameters of the PVT hot water system on its electrical performance, thermal performance and total combined performance, the term of variation ratio is introduced in this chapter and defined as follows:

$$\mathrm{V}R_p = \frac{E_p - E_{p-base}}{E_{p-base}} \times 100\% \tag{7-1}$$

$$VR_{hw} = \frac{E_{hw} - E_{hw-base}}{E_{hw-base}} \times 100\% = \frac{q_{hw} - q_{hw-base}}{q_{hw-base}} \times 100\% \tag{7-2}$$

$$VR_{comb} = \frac{E_{comb} - E_{comb-base}}{E_{comb-base}} \times 100\% \tag{7-3}$$

where VR_p, VR_{hw} *and* VR_{comb} are the variation ratios, respectively, for electrical power output, water heat gain and combined electrical energy. $E_{p\text{-}base}$, $E_{hw\text{-}base}$ *and* $E_{comb\text{-}base}$ are, respectively, the electrical power output, water heat gain and combined electrical energy of the base design, W.

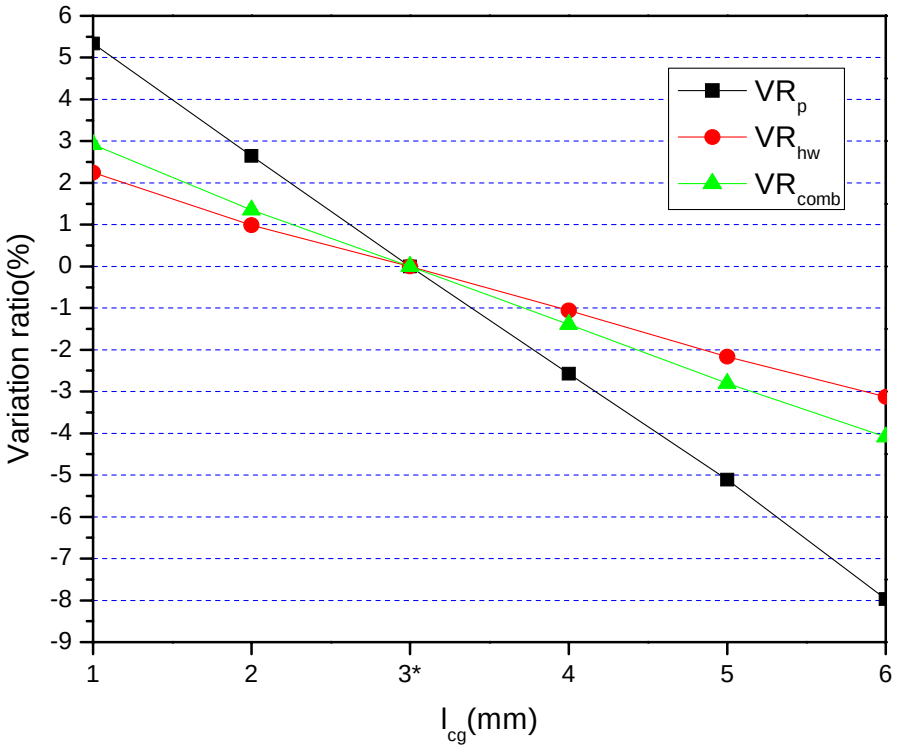

Figure 7.1 Variation ratios with respect to cover glass thickness

7.2 Effect of parameters

7.2.1 Thickness of covering glass (l_{cg})

The variation ratios with respect to the thickness of the cover glass are shown in Figure 7.1. As the cover glass thickness increases, the electrical power and water heat gain both decrease. The effect of the cover glass thickness on electrical power is more significant than that of hot water heat gain. If the combined electrical energy generation is considered, the cover glass thickness of 1mm is the best choice. However, the thinner the glass is, the more brittle it is. Because it is the smallest

thickness of toughened glass, the cover glass with the thickness of 3mm is a preferable choice.

7.2.2 Thickness of air gap (l_a)

Figure 7.2 shows the impact ratios for varied thickness of air gap. As the thickness of air gap increases, the electrical power decreases while the water heat gain increases. Comparing with the electrical power, the air gap thickness has more influence on the water heat gain. The PVT module with thicker air gap can produce more combined electrical energy. In the basic design, the air gap thickness is 15mm. When the air gap thickness changes from 15mm to 5mm, 25mm and 35mm, the variation ratios of the combined electrical energy are -4.29%, 0.87% and 2.24%, respectively. Thus the air thickness of 15mm is more cost-effective by considering the initial cost and the thickness of the PVT module.

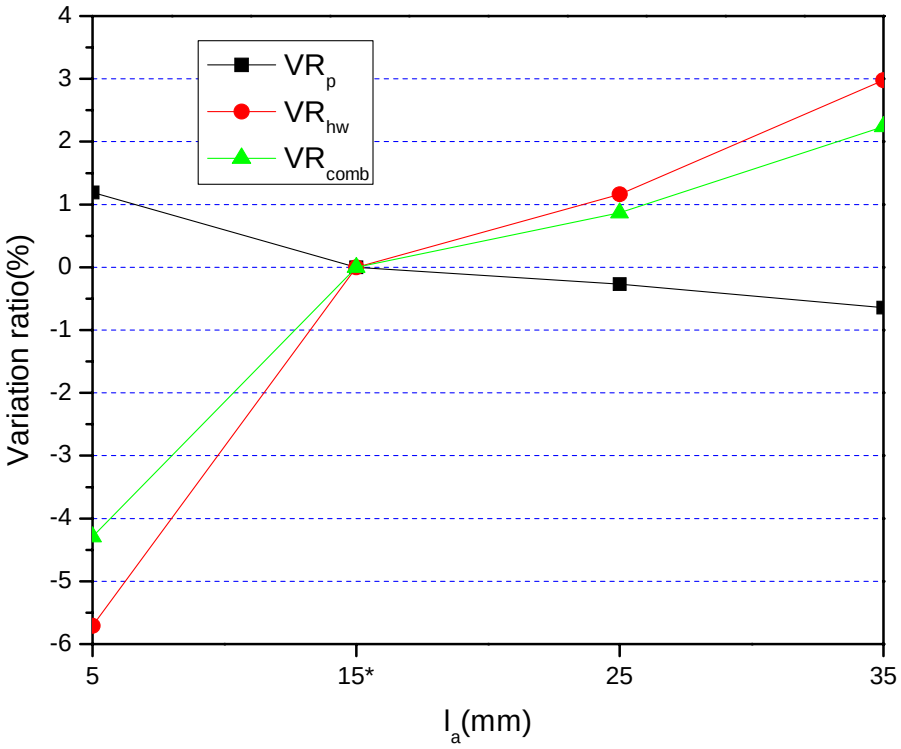

Figure 7.2 Variation ratios with respect to air gap thickness

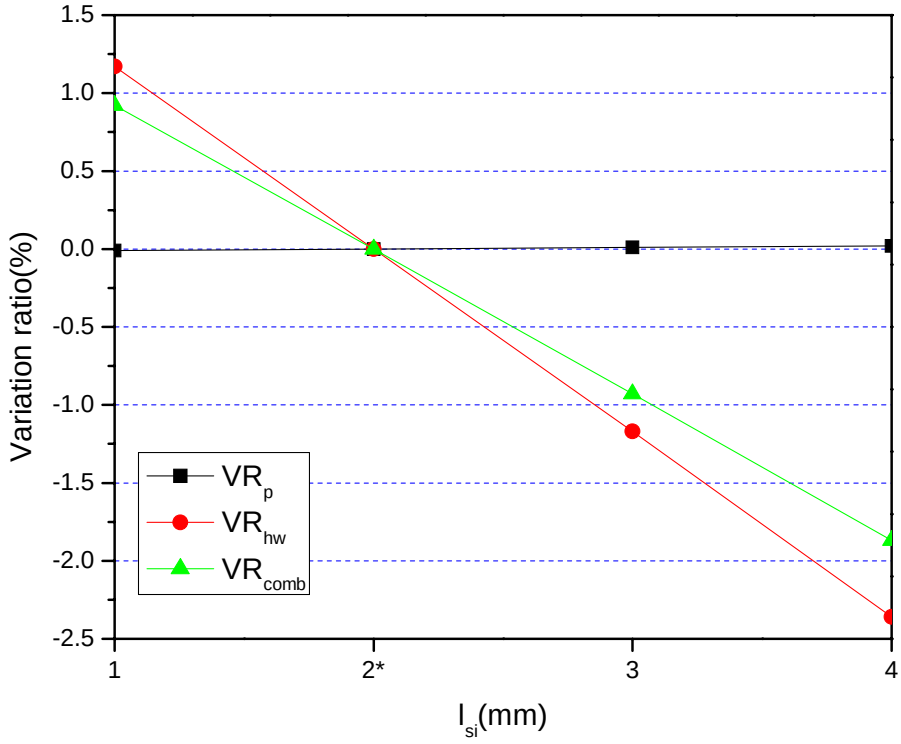

Figure 7.3 Variation ratios with respect to silicon gel thickness

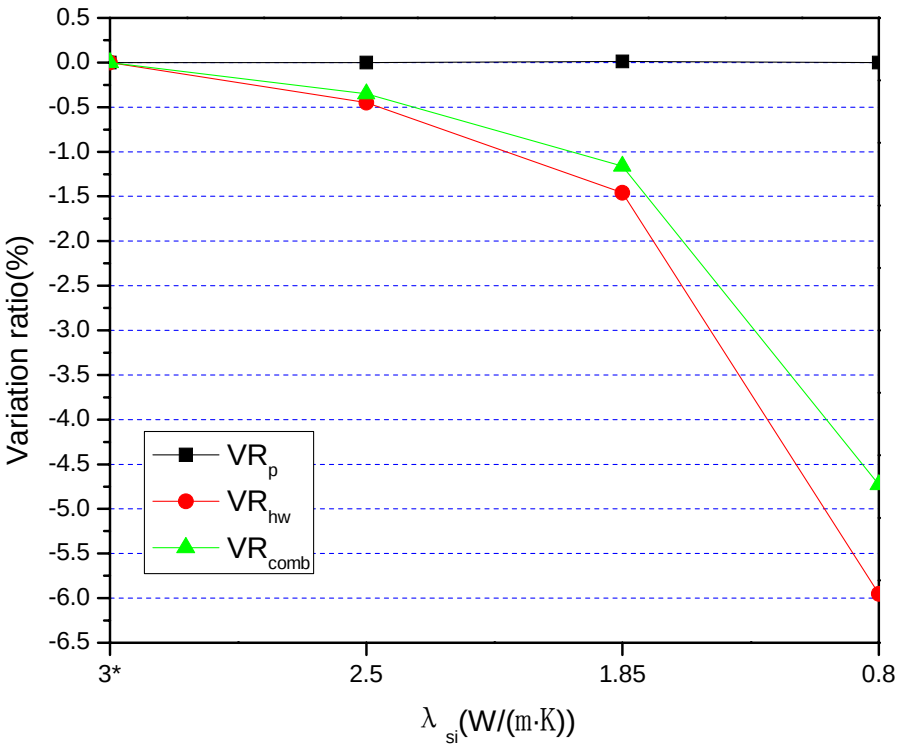

Figure 7.4 Variation ratios with respect to silicon gel conductivity

7.2.3 Thickness and conductivity of silicon gel (l_{si} & λ_{si})

Silicon gel is used to combine the PV module and thermal absorber. The proper utilization of the silicon gel can effectively eliminate the thermal contact resistance between the PV module and thermal absorber. From Figures 7.3 and 7.4, it indicates that both the thickness and thermal conductivity of the silicon gel have no impact on the electrical performance of the PVT module. For the water heat gain, the silicon gel conductivity has more significant impact than that of the silicon gel thickness. It also shows that the smaller the silicon gel thickness is or the larger the silicon gel conductivity is, the more the water heat is gained. Therefore, the optimum values for the thickness and thermal conductivity of the silicon gel are 1mm and 3.0W/(m·K) when the combined electrical energy is concerned. On the other hand, the price of the silicon gel rises quickly as its thermal conductivity increase from 0.8W/(m·K) to 3.0W/(m·K). If the thermal conductivity of the silicon gel decreases from 3.0W/(m·K) to 1.85W/(m·K), the combined electrical energy is only lowered by 1.16%. Thus the silicon gel with thermal conductivity of 1.85W/(m·K) is more effective.

7.2.4 Thickness and material of thermal absorber (l_c & M_c)

The thermal absorber is used to collect the heat produced by the PV module and transfer the heat to water in water tubes. The variation ratios for different thickness and material of the thermal absorber are presented in Figures 7.5 and 7.6. From Figures 7.5 and 7.6, there are nearly no evident influence of the thickness and material of the thermal absorber on the energy performance of the PVT module including electrical power and water heat gain since the variation ratios are within

±1.0%. The aluminum is used as thermal absorber in this case because of its lowest price and density.

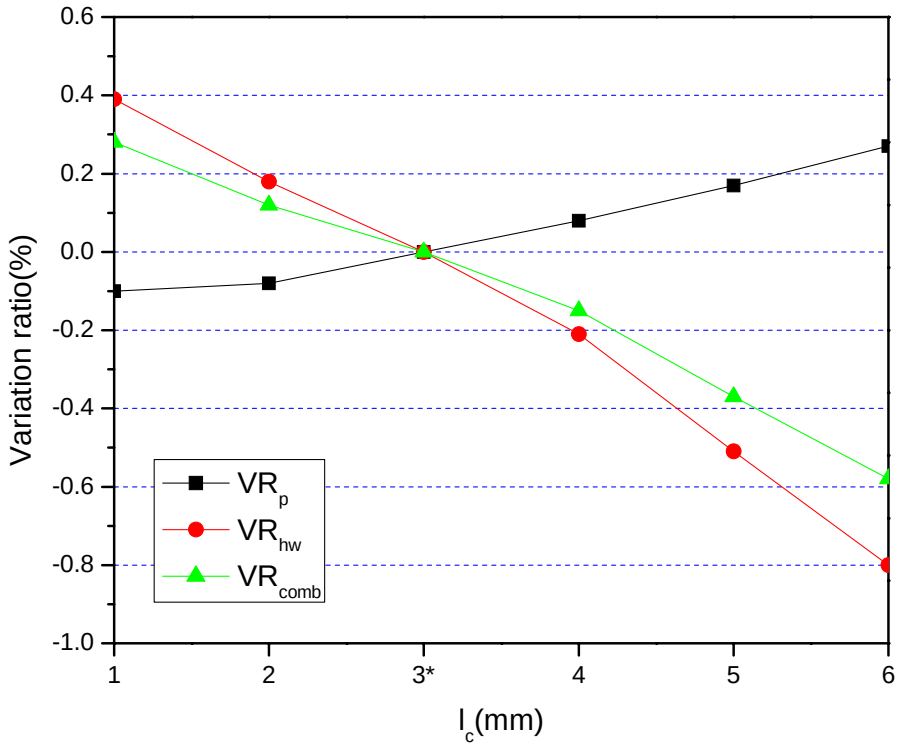

Figure 7.5 Variation ratios with respect to thermal absorber thickness

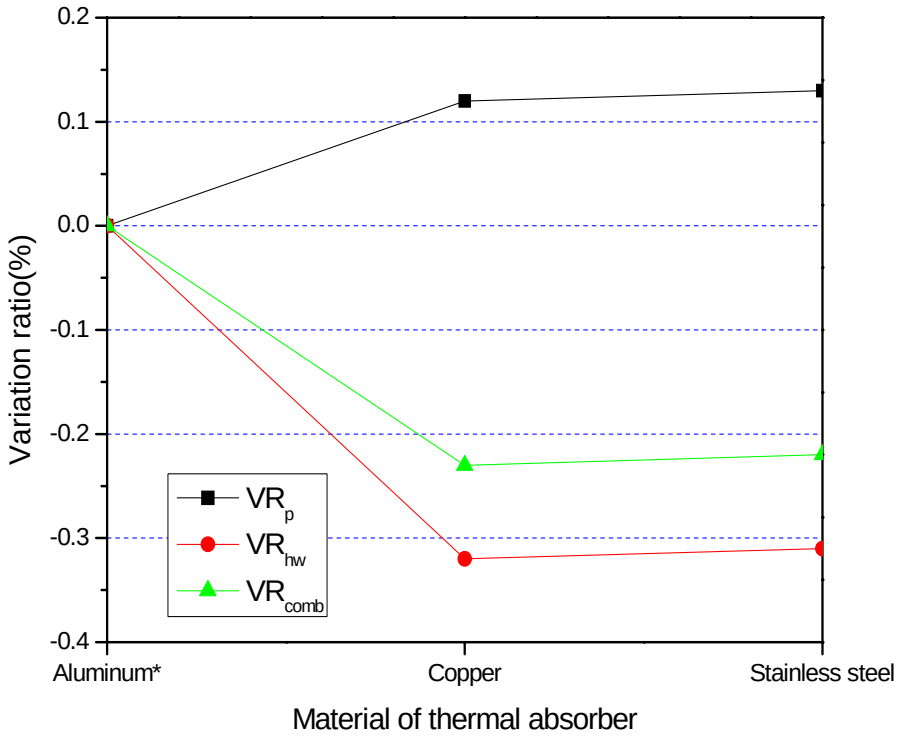

Figure 7.6 Variation ratios with respect to thermal absorber material

It is seen from Figure 7.6 that the smallest thickness is the optimum choice because of the best energy performance and lowest initial cost. On the other hand, the metal plate is easy to deform when it is thin and large. The deformation of the metal plate will affect the thermal contact between it and water tubes. Therefore, the thickness of 3mm is better when the thermal absorber is made of aluminum.

7.2.5 Internal diameter and spacing between water tubes (d_i & w)

The variation ratios of internal diameters and spacing between water tubes are shown in Figures 7.7 and 7.8. Comparing with Figures 7.7 and 7.8, it is obvious that the water tube spacing has more effects on the electrical power generation and water heat gain than the water tube internal diameter.

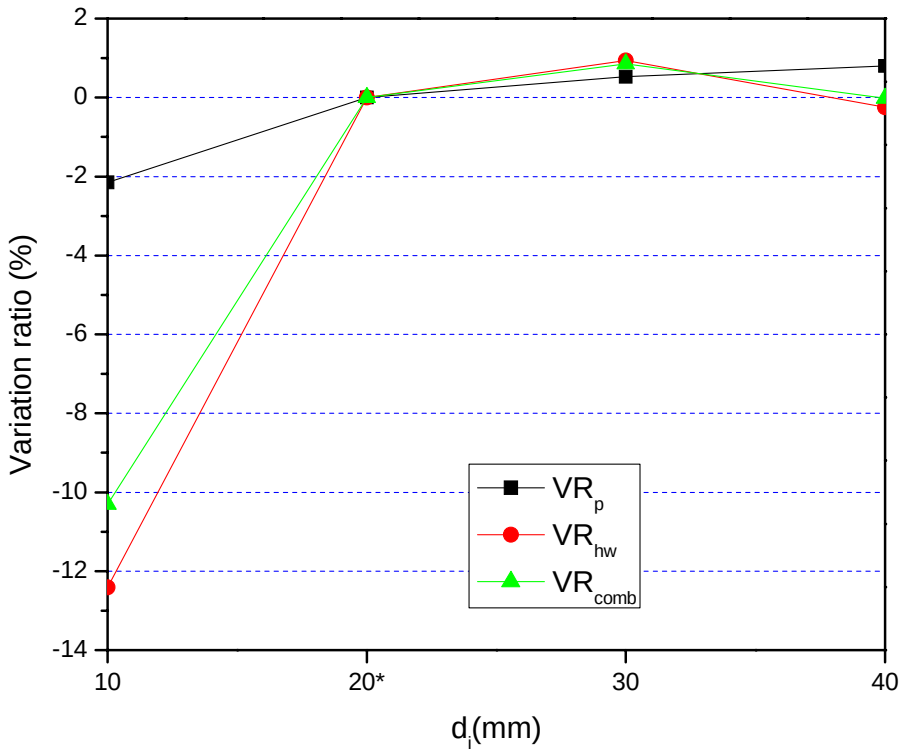

Figure 7.7 Variation ratios with respect to water tube internal diameter

Figure 7.7 shows that except the internal diameter of 10mm, the variation ratios of electrical power generation and water heat gain are lower than 2.0%. The electrical

power generation of the PVT module increases as the internal diameter increases. For the water heat gain and combined electrical energy, the water tube of 30mm can achieve their maximum values. When the internal diameter changes from 20mm to 30mm, the variation ratios for the combined electrical energy is as low as 1.0%. As the initial cost and the total weight of the PVT module are considered, 20mm is thought as a good choice of internal diameter.

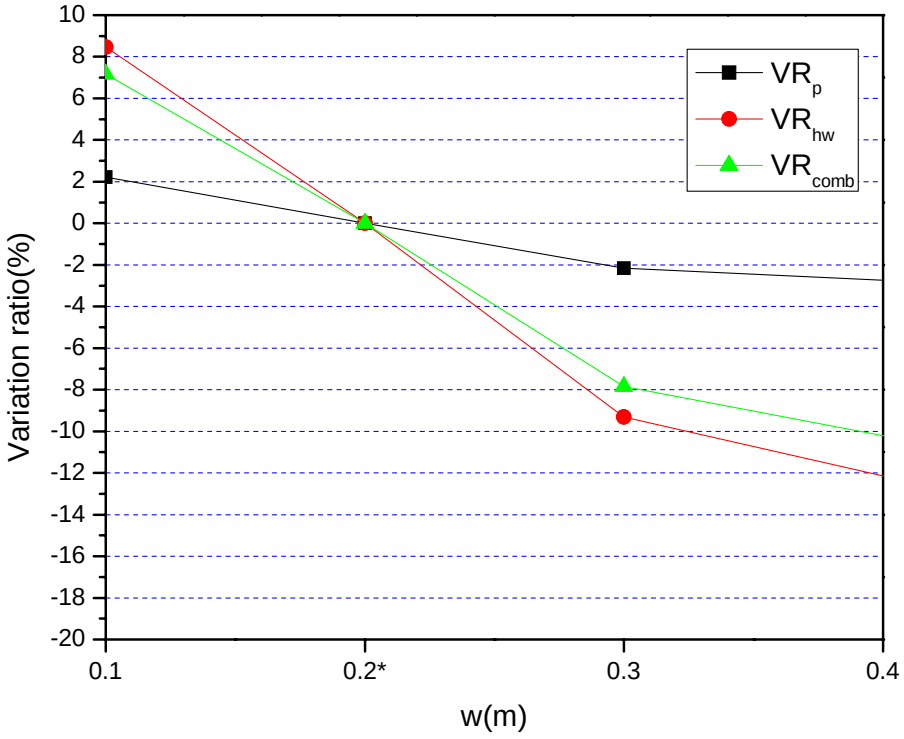

Figure 7.8 Variation ratios with respect to water tube spacing

It is clear from Figure 7.8 that when the spacing of water tubes increases from 0.1m to 0.4m both the electrical power generation and water heat gain decrease. The impact of the spacing between water tubes on the water heat gain is more significant than that of the electrical power generation. The variation ratios of the combined electrical energy are 7.18%, -7.84% and -14.94% respectively for the spacing of 0.1m, 0.3m and 0.4m. The numbers of water tubes are 12, 6, 4 and 3 when the spacing changes from 0.1m to 0.4m. Although the initial cost of the PVT module

with the water tube spacing of 0.2m is higher than that of 0.3m, smaller spacing is more cost-effective if the total energy benefits during the life time are considered.

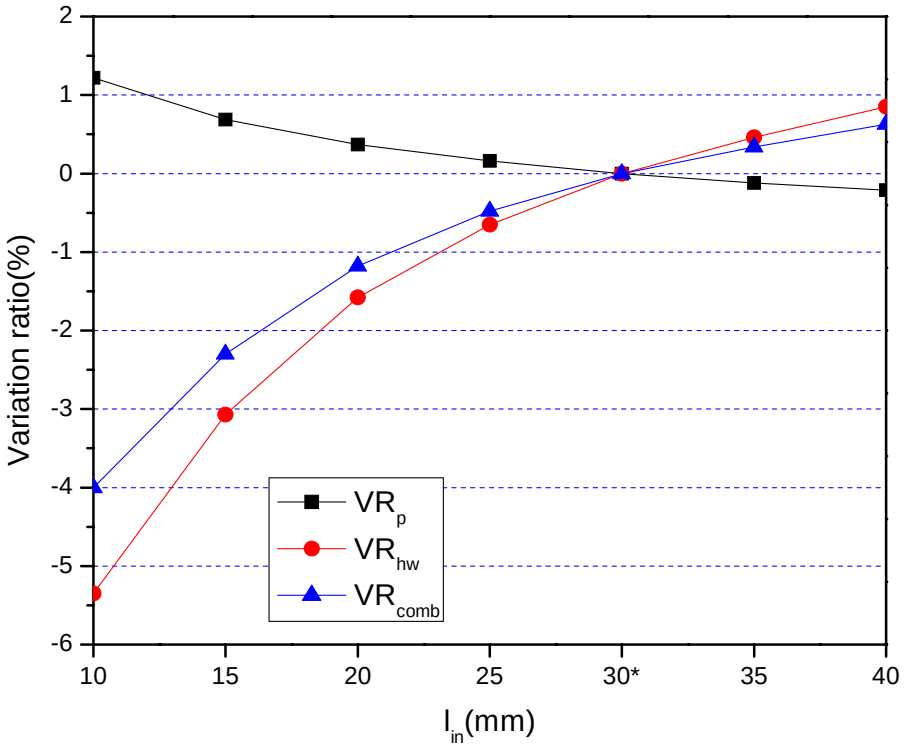

Figure 7.9 Variation ratios with respect to thermal insulation thickness

7.2.6 Thickness of thermal insulation material (l_{in})

Figure 7.9 shows variation ratios with respect to the thickness of thermal insulation material on the rear surface of the thermal absorber. As the thickness of thermal insulation material increases from 10mm to 40 mm, the water heat gain increases while the electrical power generation decreases. It is indicated that the insulation thickness has more significant impacts on the water heat gain than that of the electrical power generation. Therefore the thicker the thermal insulation layer is, the more combined electrical energy is. As the insulation thickness increases from 10mm to 40mm with 5mm increment (except 30mm), the variation ratios of combined electrical energy are -4.0%, -2.3%, -1.18, -0.48%, 0.34% and 0.63%,

respectively. Therefore, the thickness of the thermal insulation material of 20mm is thick enough for preventing heat loss from the rear surface of the thermal absorber.

7.2.7 Volume of thermal storage tank (V_w)

The volume of the thermal storage tank plays an important part in water temperature in the tank and then the temperature of the PV module. Therefore the tank volume has much more influences on the water heat gain than the electrical power generation. As shown in Figure 7.10, the thermal storage tank with larger volumes can obtain more electrical power generation and water heat gain. The variation ratios of combined electrical energy for the volumes of 0.64 m^3, 0.08m^3 and 0.96m^3 are respectively 5.95%, 9.75% and 12.6%. If the combined electrical energy is thought as the priority, the volume of 0.96m^3 is the best choice.

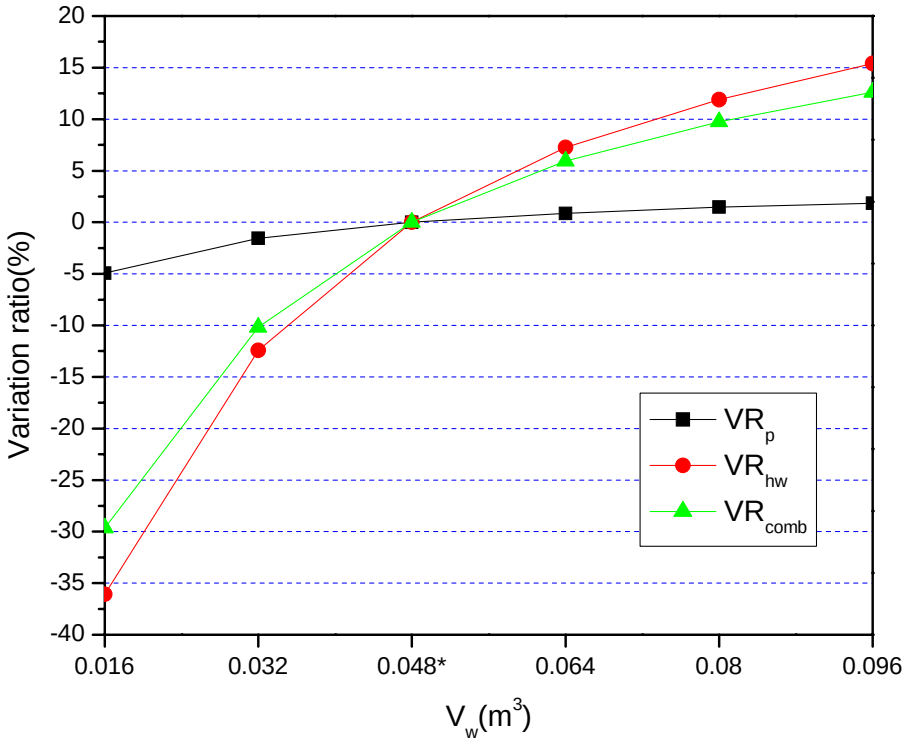

Figure 7.10 Variation ratios with respect to thermal storage tank volume

On the other hand, the temperature of water in the thermal storage tank is also a standard for estimating the energy performance of the BIPVT hot water system. As shown in Figure 7.11, the water temperature at the time of 20:00pm is 44.2℃, lower than the design temperature of hot water supply. So that the volume of the thermal storage tank is 0.08m^3 is better.

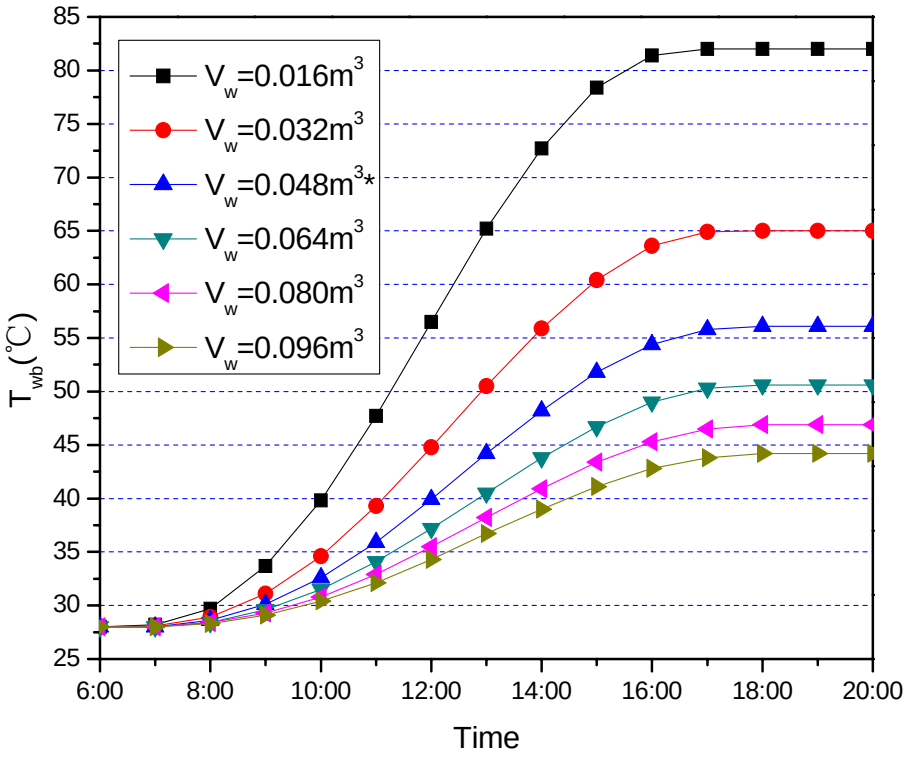

Figure 7.11 Hourly temperature of water in tank

7.2.8 Vertical distance of barycentres (ΔH)

In natural circulation, the flow rate depends on the vertical distance between the barycentres of the PVT module and the thermal storage tank, and then the thermal performance and electrical performance of the system. Figure 7.12 shows variation ratios for vertical distance of barycentres. It is seen that the vertical distance has more evident impacts on water heat gain than electrical power generation. As the vertical distances vary from 1.1m to 1.9m, the variation ratios are within the range of

-1.0%~1.0%. Thus the vertical distance of 1.1m is larger enough for natural circulation.

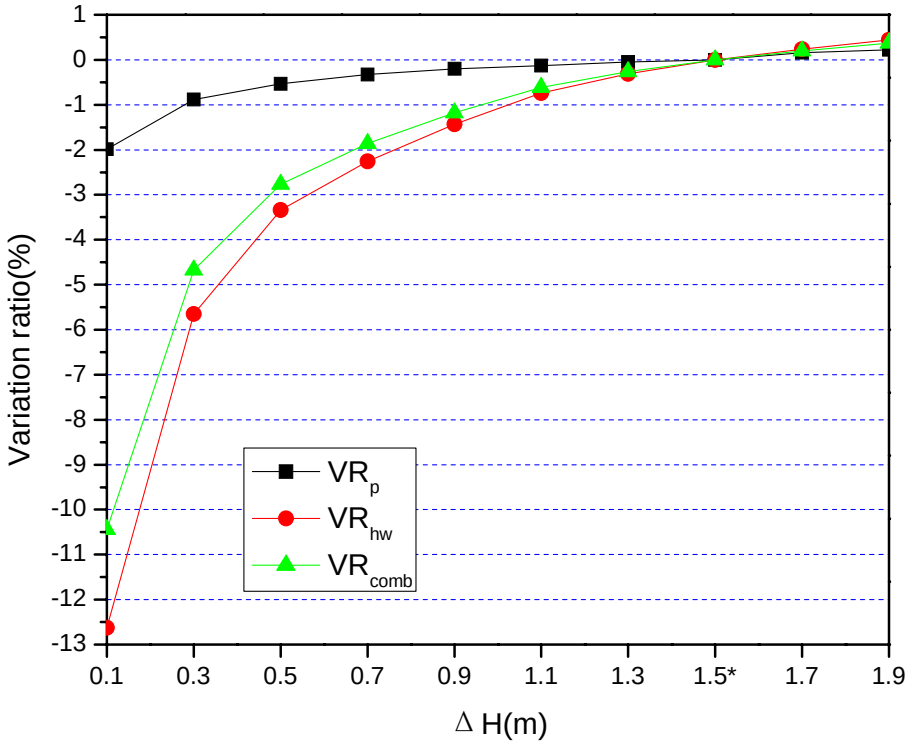

Figure 7.12 Variation ratios with respect to ΔH

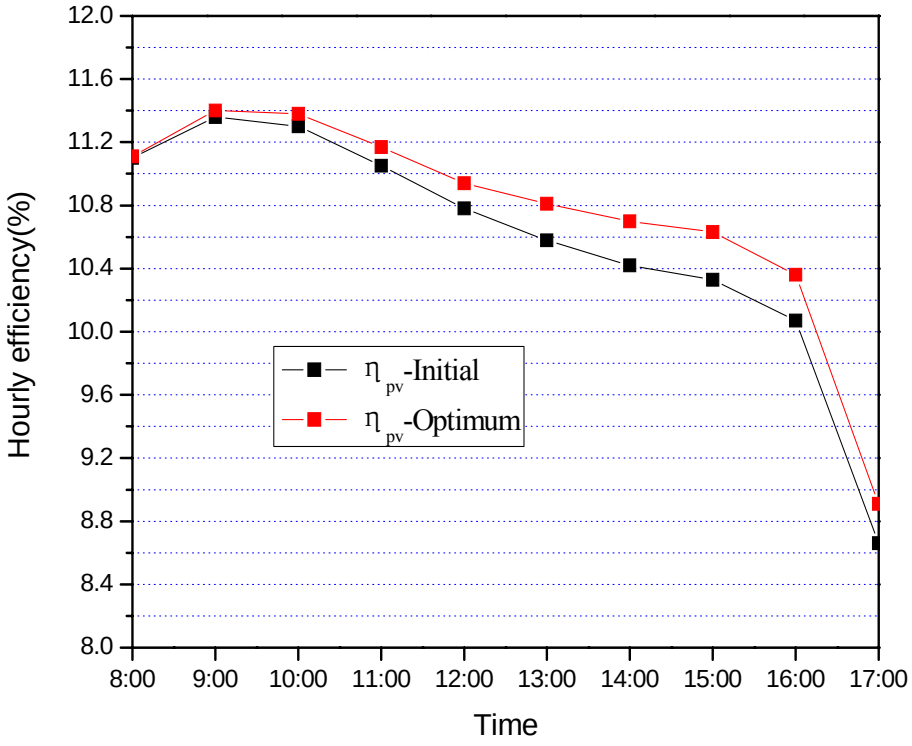

Figure 7.13 Hourly profile of electrical efficiency

7.3 Comparison of initial design and optimum design

The comparison of parameters mentioned above between the initial design and optimum design are listed in Table 7.1.

Table 7.1 Parameter comparison between initial design and optimum design

Parameters	Initial design	Optimum design
Thickness of cover glass	3mm	3mm
Thickness of air gap	15mm	15mm
Thickness of silicon gel	2mm	1mm
Thermal conductivity of silicon gel	3.0 W/(m·K)	1.85 W/(m·K)
Thickness of thermal absorber	3mm	3mm
Material of thermal absorber	Aluminum	Aluminum
Internal diameter of water tubes	20mm	20mm
Spacing between water tubes	0.2m	0.2m
Thickness of insulation material	30mm	20mm
Volume of thermal storage tank	$0.048m^3$	$0.08\ m^3$
Vertical distance of barycenters	1.9m	1.1m

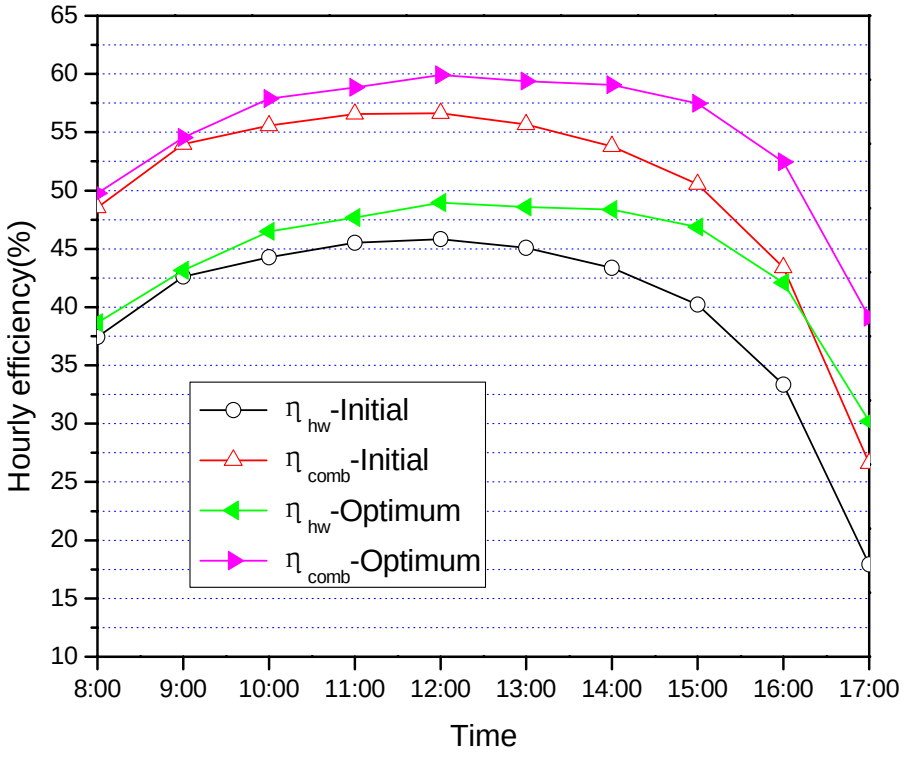

Figure 7.14 Hourly profiles of thermal efficiency and combined energy efficiency

Figures 7.13 and 7.14 show the hourly electrical efficiency, thermal efficiency and combined energy efficiency of the initial design and optimum design. It is obvious the energy performance of the BIPVT hot water system including electrical performance and thermal performance in the optimum design has been improved compared with that of the initial design. It also indicates that the impact of these parameters on the thermal performance is more significant than that of electrical performance. The average electrical efficiency, thermal efficiency and combined energy efficiency for the initial design are respectively 10.7%, 38.5% and 49.2%, increased by 1.5%, 11.1% and 9.0% compared with the initial design.

7.4 Summary

This chapter presents the effects of several main configuration parameters on the electrical generation and water heat gain of the PVT hot water system. The simulation results presented that except the covering glass thickness, most of the parameters have more obvious impacts on the water heat gain than those of the electrical power generation. The comparison of the initial design and the optimum design indicates that a little improvement of the configuration parameters of such a system can significantly increase the energy performance, especially the thermal efficiency.

CHAPTER 8: APPLICATION OF THE SHADING TYPE BIPVT HOT WATER SYSTEM IN RESIDENTIAL BUILDINGS

8.1 Introduction

The BIPV hot water system is very useful for electricity generation and domestic hot water supply in many areas around the world like Hong Kong. Application of the BIPVT hot water system in Hong Kong is worth detailed investigation. In Hong Kong, most of the buildings are high-rise buildings. Most people live in small to medium flats. There is not enough roof area for locating solar collectors for solar energy application on the roofs of the buildings. If the BIPVT panel can be used on vertical façades of such high-rise buildings, a problem of the less roof can be solved for solar energy applications. This chapter is to evaluate a BIPVT hot water system designed for a typical residential apartment of a high-rise building in Hong Kong.

In this chapter, a BIPVT hot water system is designed for a small flat of two residents in a high residential building. As shown in Figure 8.1, the system mainly consists of two PVT modules and a thermal storage tank. There are two types of BIPVT hot water systems according to different connection modes of the PVT modules. Each system is designed for natural circulation. Due to the small size of the system, natural circulation can provide enough impetus for circulating water. The dimension of each PVT module is 1.14m×0.52m. The volume of the thermal storage tank is 0.06m^3. The PVT modules are installed on a south external wall of typical residential buildings in Hong Kong (as shown in Figure 8.2). The thermal storage tank is placed in the bathroom. The barycentre of the thermal storage tank is higher

than the PVT module location. In addition, an electric backup system is provided in the water storage tank for use in evenings during cloudy and raining days.

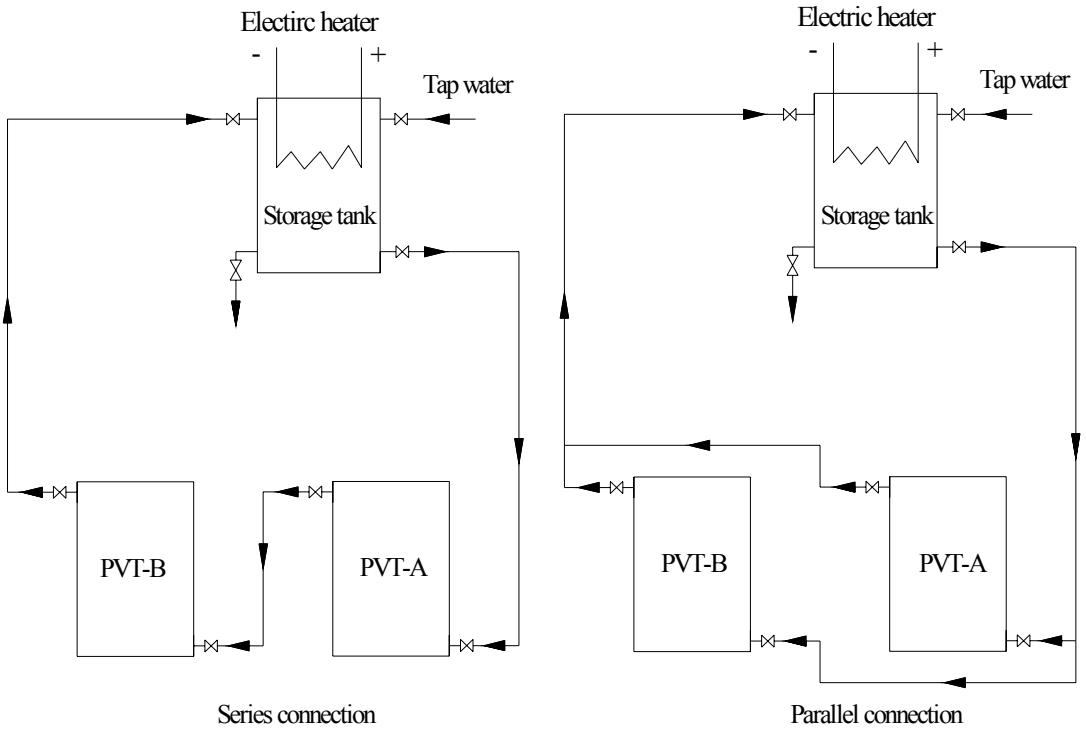

Figure 8.1 Schematic diagram of the BIPVT hot water system

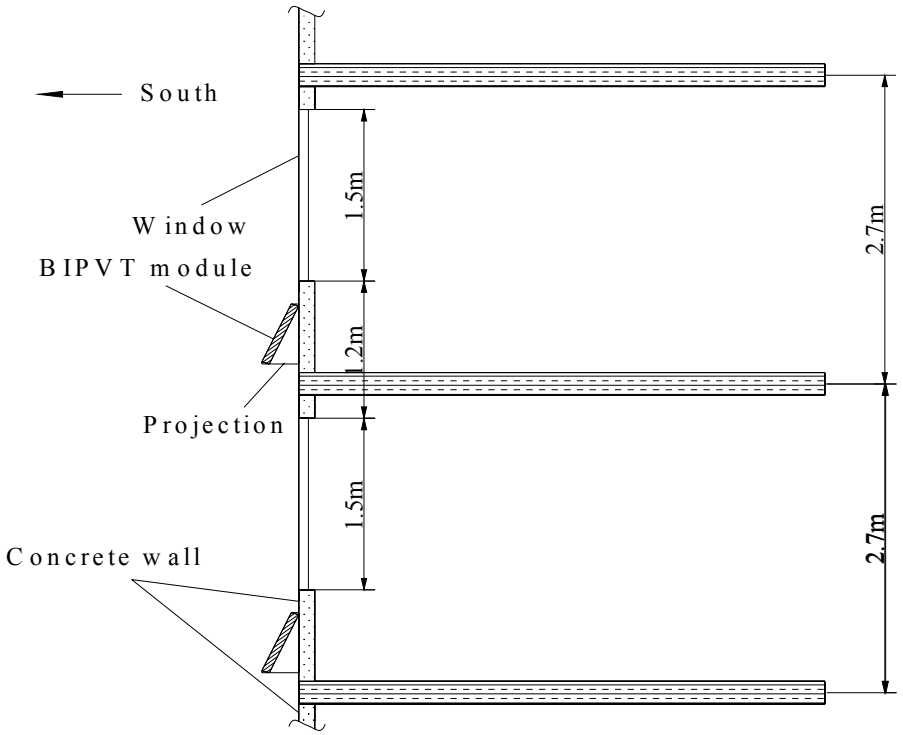

Figure 8.2 Arrangement of BIPVT modules

As shown in Figure 8.3, each PVT module is made of cover glass, PV module, silicon gel, thermal absorber, water tubes, insulation materials and metal frames. Ten water tubes are attached evenly along the length of the thermal absorber and placed in parallel.

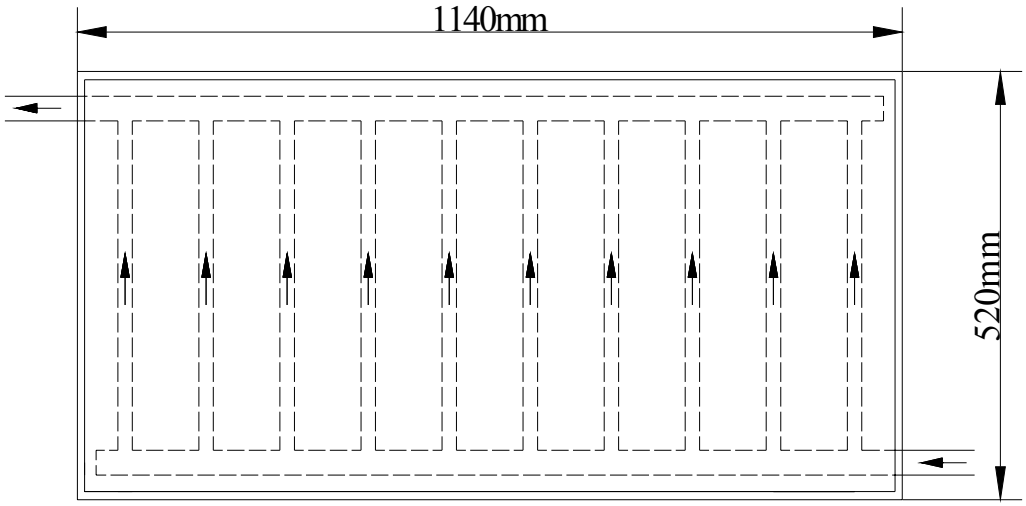

Figure 8.3 Front view of the BIPVT module

8.2 Simulation results and discussions

The annual energy performance of the proposed system is simulated on the base of the validated simulation models developed in this project and the hourly TMY weather data of Hong Kong (Lu et al, 2004). To simplify the simulation process, it is assumed that all the hot water in the thermal storage tank is consumed in the evening of a day and tap water is refilled into the thermal storage tank at 6:00am in the morning on each day. There is no water extracted out of the thermal storage tank during daytime. In early evening, if the water temperature in the thermal storage tank is lower than 45℃, the electric heater is used for heating water to its design temperature.

8.2.1 Yearly energy performance

Figures 8.4-8.6 show the annual power output of the PVT modules, thermal energy gain and total combined electrical energy of the PVT system with respect to tilt angles and connection modes. It can be seen that the optimum inclination of the PVT modules is 20° when the energy benefits brought by the PVT modules are concerned. The reason is that PVT modules can receive more solar energy at the tilt angle of 20° than that of other angles. As shown in Figure 8.1, compared with parallel connection, the temperatures of water and PVT modules are higher for the system in series connection so that the power output of the PVT modules is lower and the heat gain of water increases at the same time. Concerning the total combined electrical energy of the BIPVT hot water system, the PVT modules connected in series is a better choice. As the PVT modules are installed at the tilt angle of 20° and connected in series, the total annual combined electrical energy reaches up to 1981.5MJ, increased by 232.5% compared to the electrical power output of the PVT modules. The BIPVT hot water system can effectively increase the energy benefits related to the PV system. Comparing with Figures 8.4 and 8.5, the connection mode has more obvious impacts on the water heat gain than those on the power output of the PVT modules.

In addition, the length of the projection (as shown in Figure 8.2) also needs be considered when the PVT modules are installed. The reason is that it is difficult to install the PVT modules with long projection. Considering both the combined electrical energy and the length of the projection, the tile angle of 20° is not the optimum tilt angle. When the length of the PVT module is fixed, larger tilt angles can have shorter projections. However, when tilt angles are larger than 20°, the larger the tilt angles are, the smaller the combined electrical energy output is. Table 8.1

shows reduction ratios of both the combined electrical energy and the projection length as the tilt angle increase from 20° to 80°. It shows that as the tilt angle increases from 20° to 40°, the reduction ratio of the combined electrical energy is smaller than 2% while the projection length can decrease from 0.51m to 0.41m, shortened by 18.48%. It indicates that the tilt angle of 40° can achieve significant projection reduction and insignificant combined electrical energy reduction. Therefore, the tilt angle of 40° is chosen and utilized in the following simulation of this chapter.

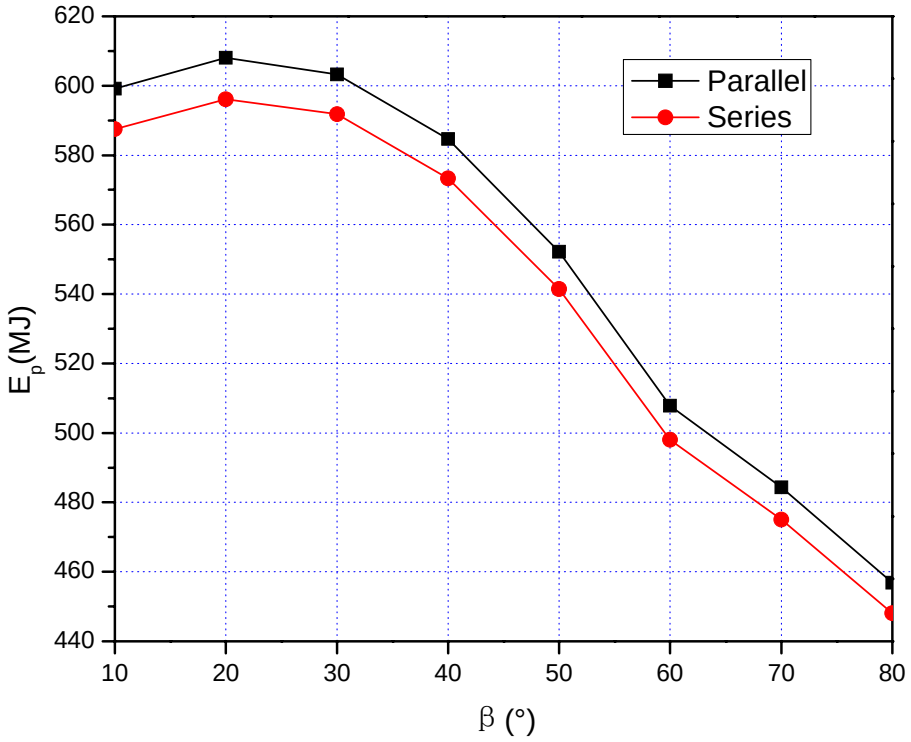

Figure 8.4 Annual power output of PVT modules

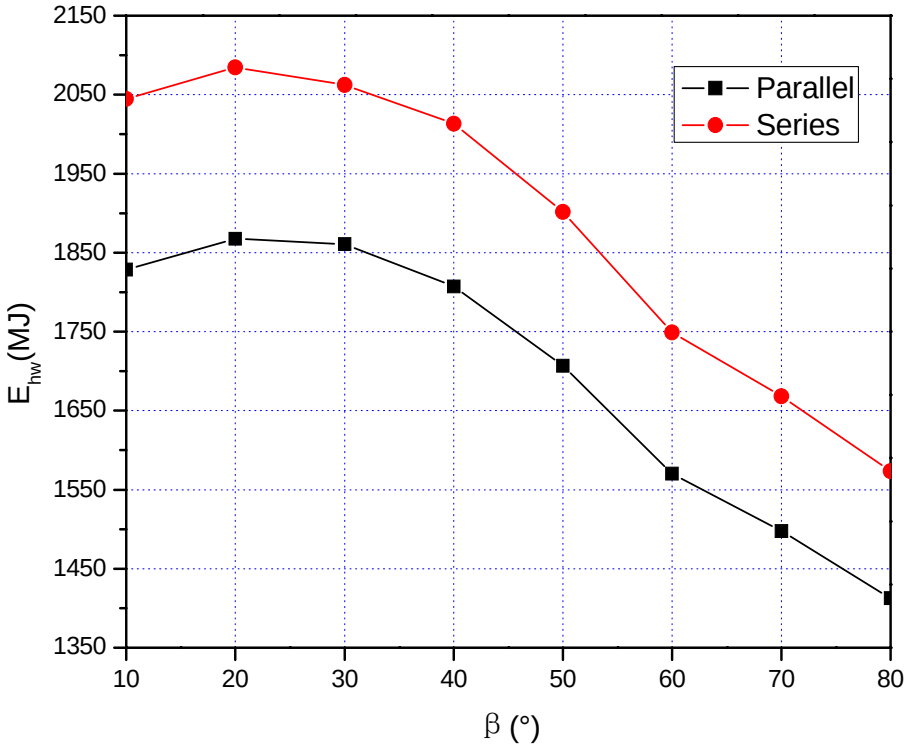

Figure 8.5 Annual heat gain of water

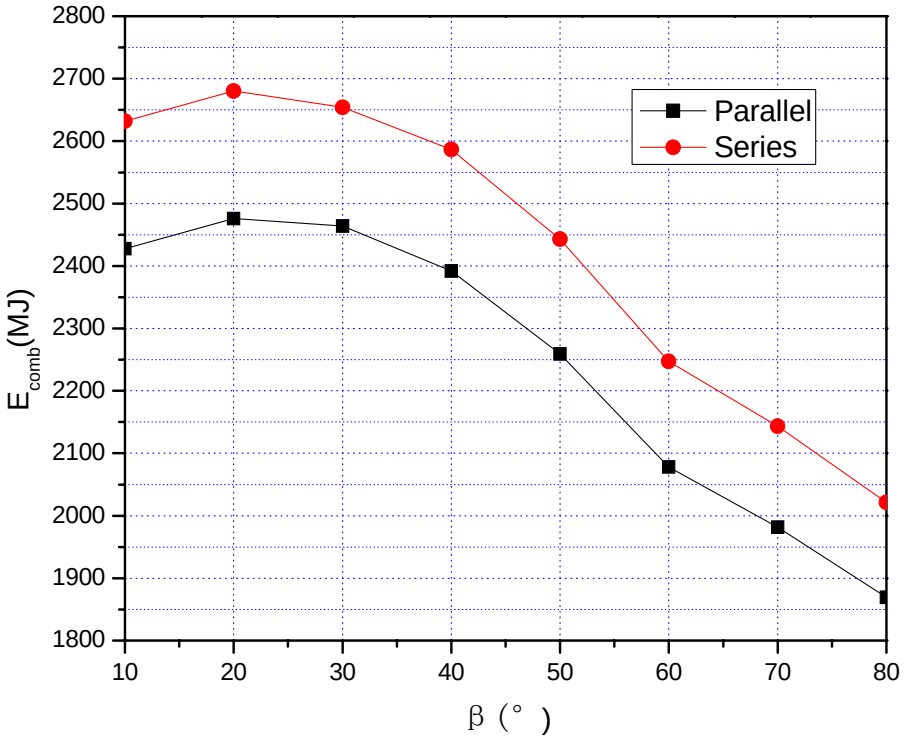

Figure 8.6 Annual combined electrical energy of the BIPV hot water system

Table 8.1 Reduction ratios of combined electrical energy and projection length

Tilt angle	Combined energy reduction ratio		Projection length reduction ratio	Projection length
	Parallel	Series		
20°	0	0	0	0.51m
30°	-0.47%	-0.99%	-7.84%	0.47m
40°	-3.38%	-3.50%	-18.48%	0.41m
50°	-8.75%	-8.86%	-31.60%	0.35m
60°	-16.07%	-16.17%	-46.79%	0.27m
70°	-19.95%	-20.05%	-63.60%	0.18m
80°	-24.49%	-24.58%	-81.52%	0.09m

8.2.2 Monthly energy performance

Figures 8.7-8.9 present the monthly energy performance of the BIPVT hot water system. As can be seen from Figures 8.7 and 8.8, in October the BIPVT hot water system can achieve the maximum power output of the PVT modules and heat gain of water both for parallel and series connections. The peak points of 190.0 J (parallel connection) and 191.4MJ (series connection) of the monthly combined electrical energy occur in November as in October less thermal energy is needed for shower so that more heat gain gathered from the PVT modules is wasted. In April, the BIPVT hot water system shows the worst energy performance during the whole year because of poorer solar radiation compared with other calendar months.

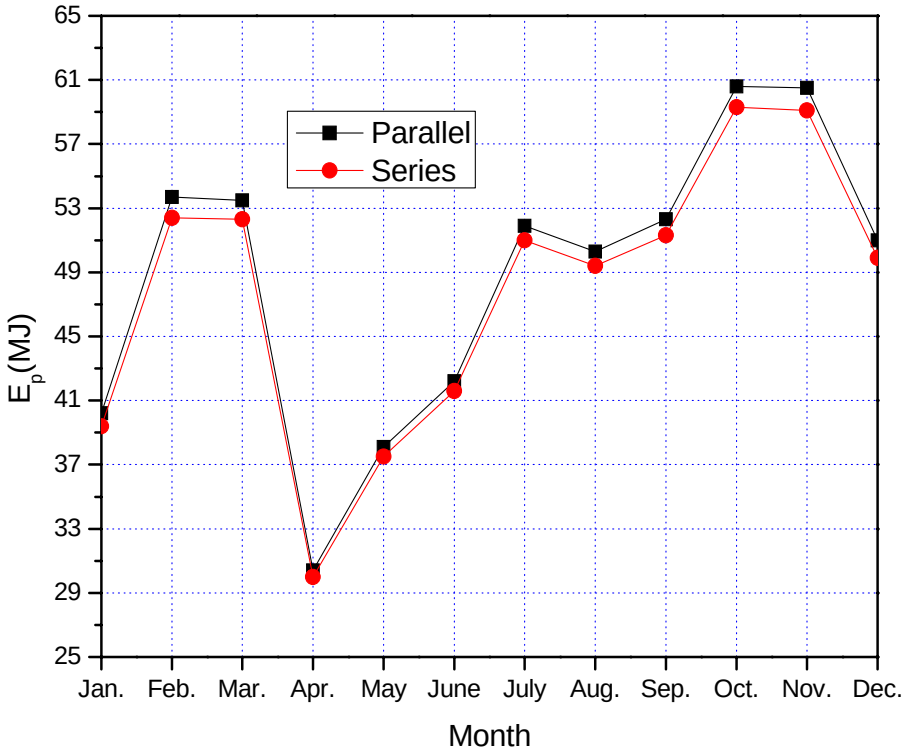

Figure 8.7 Monthly power output of PVT modules

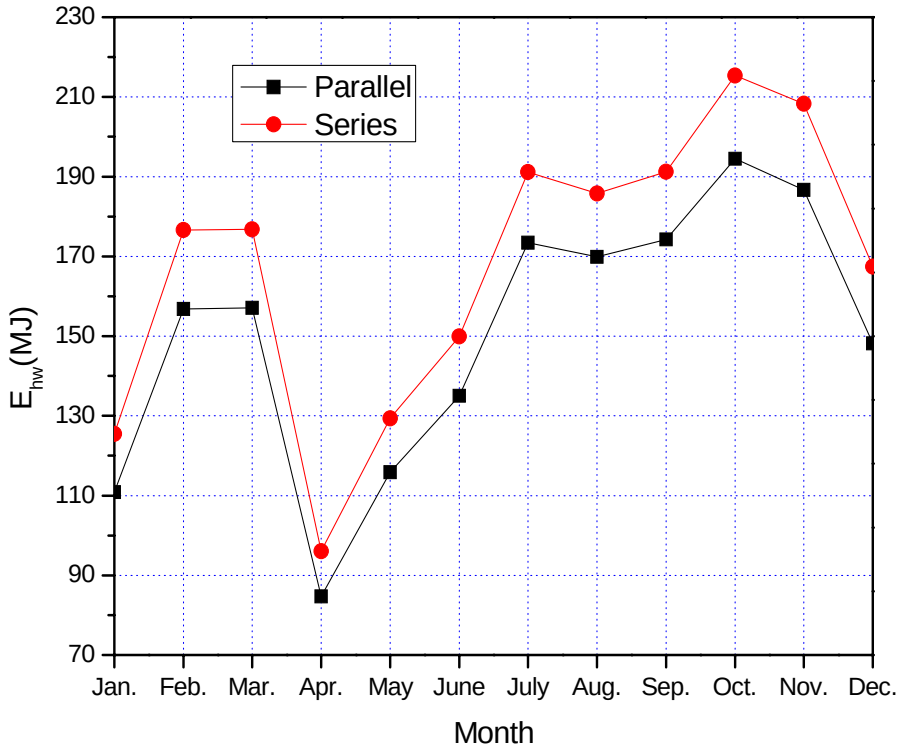

Figure 8.8 Monthly heat gain of water

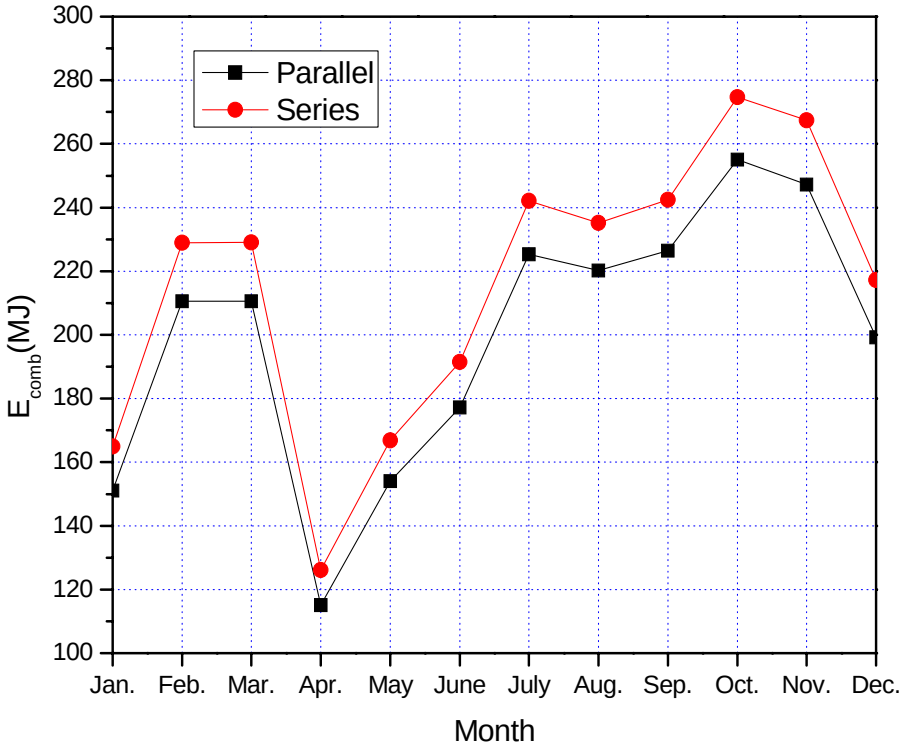

Figure 8.9 Monthly combined electrical energy of the BIPV hot water system

It can also be found from Figures 8.7 and 8.8 that the effects of the connection modes on the water heat gain are more significant than those on the power output of the PVT modules. Figure 8.9 shows that the combined electrical energy in series connection has distinct increase over the parallel mode.

Figures 8.10-8.12 illustrate the monthly energy efficiency of the BIPVT hot water system. Comparing Figure 8.10 with Figure 8.11, the impacts of the connection modes on the thermal energy efficiency are more significant relative to electrical efficiency. It is indicated in Figure 8.12 that there is no obvious difference between the combined electrical efficiencies of parallel connection and series connection during most of calendar months except January and April. In parallel connection, the monthly combined electrical efficiency can reach its maximum value of 39.7% in January, while 41.5% for series connection. It can also be concluded that the annual electrical efficiency, thermal efficiency and combined electrical efficiency of the

proposed system are respectively10.2%, 31.3% and 41.5% for the parallel connection and 10.0%, 34.9% and 44.9% for the series connection.

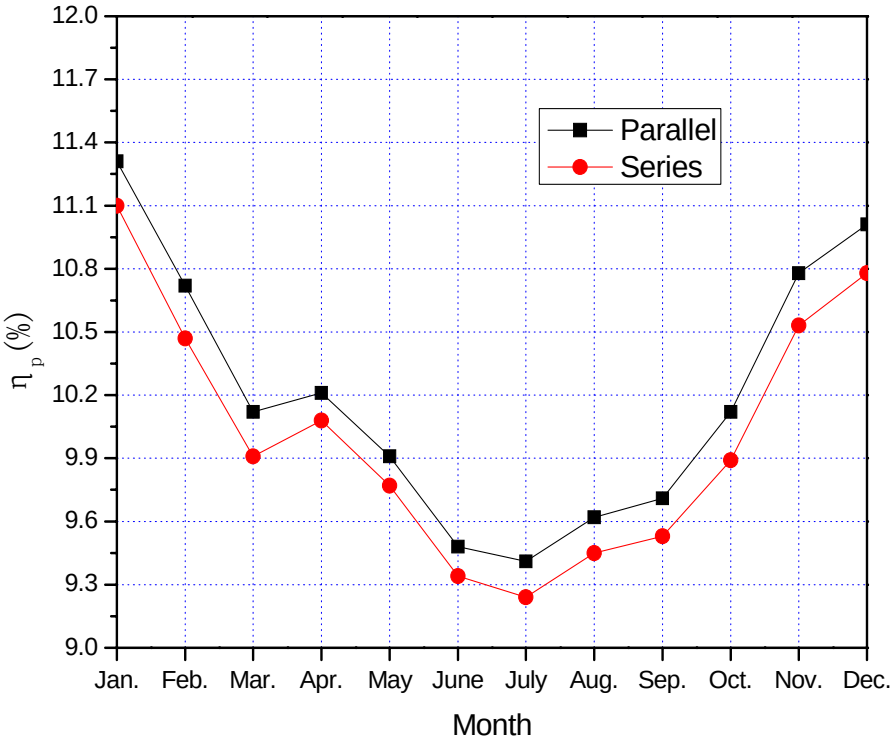

Figure 8.10 Monthly variations of electrical efficiency

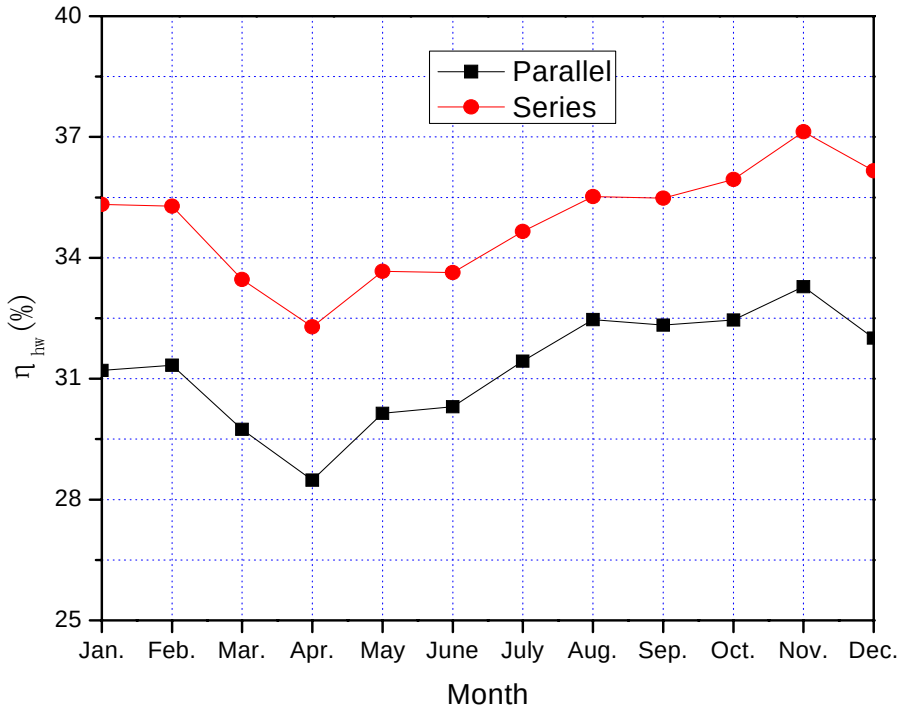

Figure 8.11 Monthly variations of thermal efficiency

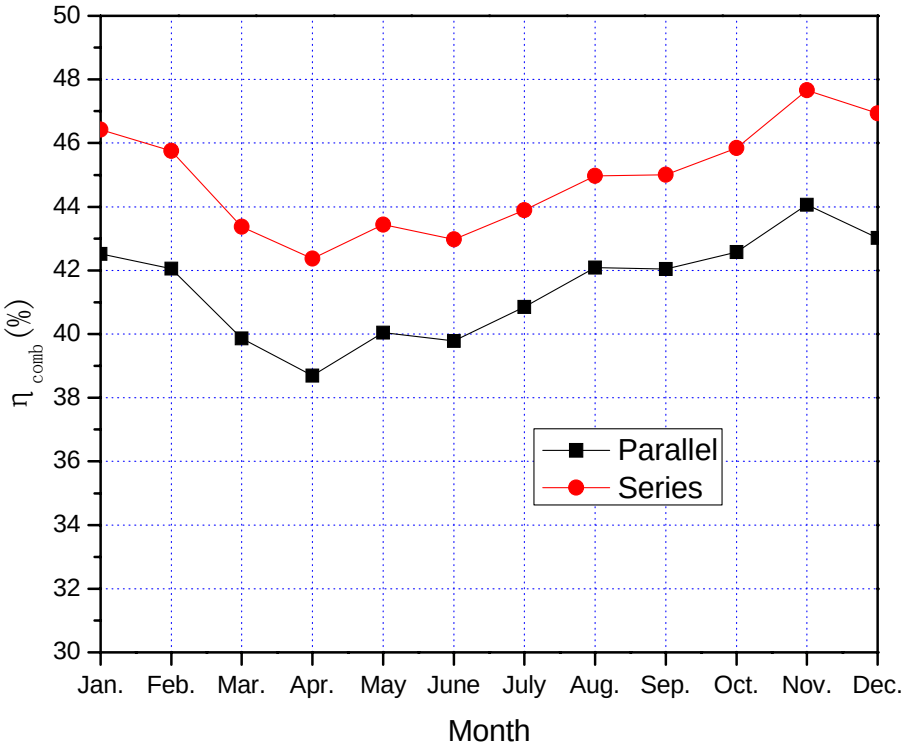

Figure 8.12 Monthly variations of combined electrical efficiency

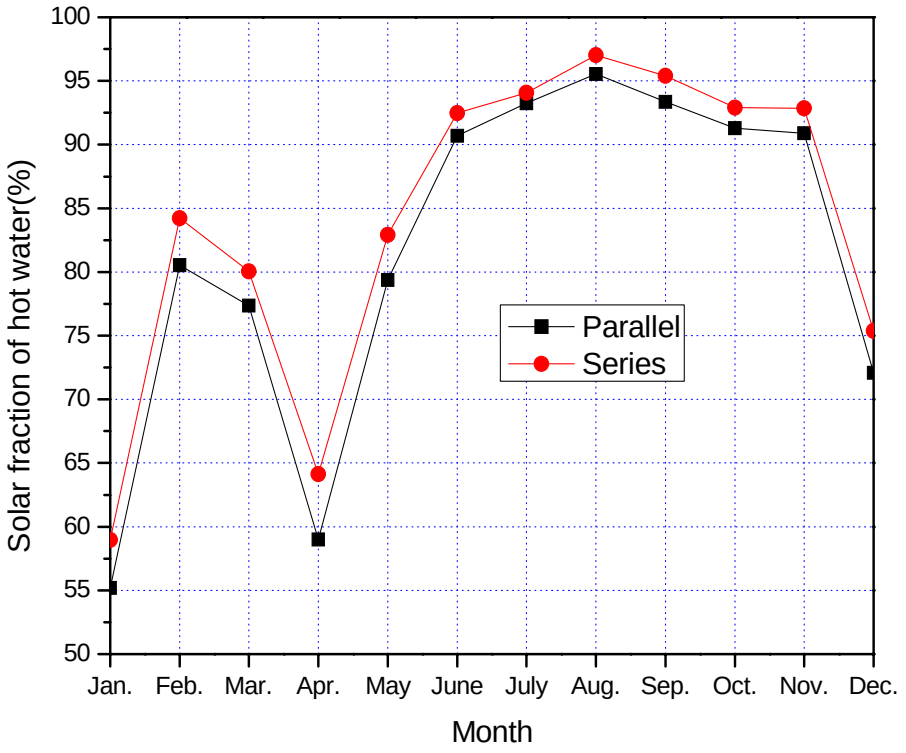

Figure 8.13 Monthly solar fraction of hot water supply

As shown in Figure 8.13, the BIPVT hot water system has high monthly solar fractions of hot water supply during the entire year. The monthly solar fractions of hot water supply in six months, from June to November, are all above 90%, while the lowest monthly solar fraction is also larger than 55%. The annual solar fractions are 79.5% and 82.3%, respectively, for the parallel connection and series connection.

It is found from Figure 8.14 that there are 188 days for the parallel connection and 208 days for the series connection that the water temperature in thermal storage tank can reach 45℃ or higher. The BIPVT hot water system can satisfy the hot water demand during most of the entire year, even without supplemental heating.

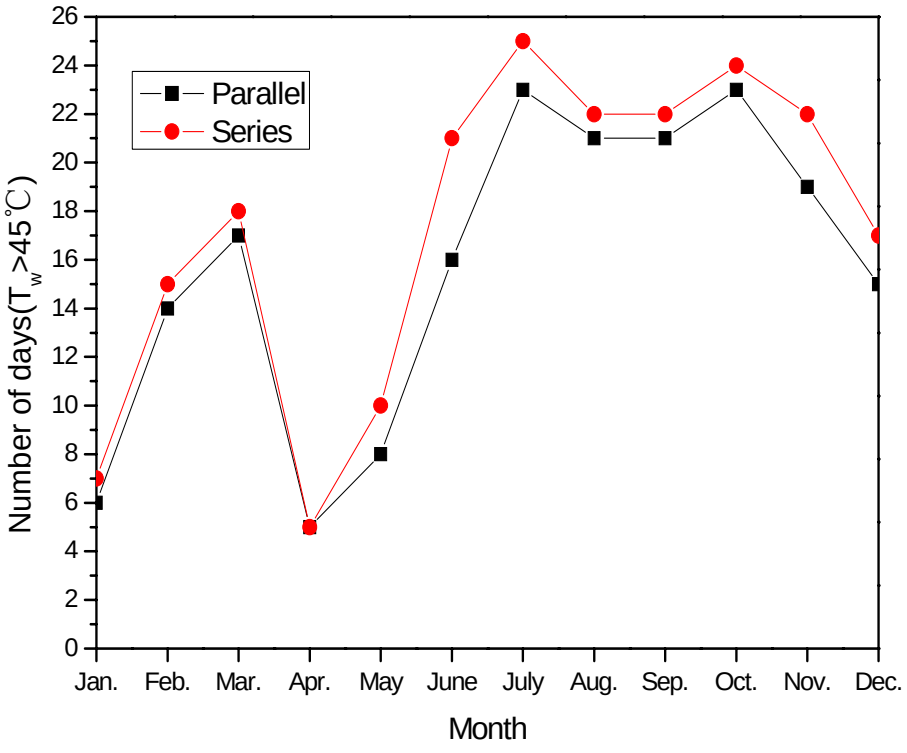

Figure 8.14 Number of days (T_w>45℃)

8.2.3 Hourly energy performance

From the annual simulation results, if no temperature control is implemented in the storage tank, it is found that on 26 September of the TMY, the temperature of hot water in the thermal storage tank reaches its peak point during the whole year. Figure 8.15 shows that on 26 September the hot water temperature is 62.6℃ for parallel connection and 66.2℃ for series connection. In series connection, the temperature of the PVT-B module is much higher than that of the PVT-A module. At the time of 14:00, the PVT-B module in series connection can achieve its highest temperature of 91.7℃, about 12.7℃ higher than that of the PVT-A module.

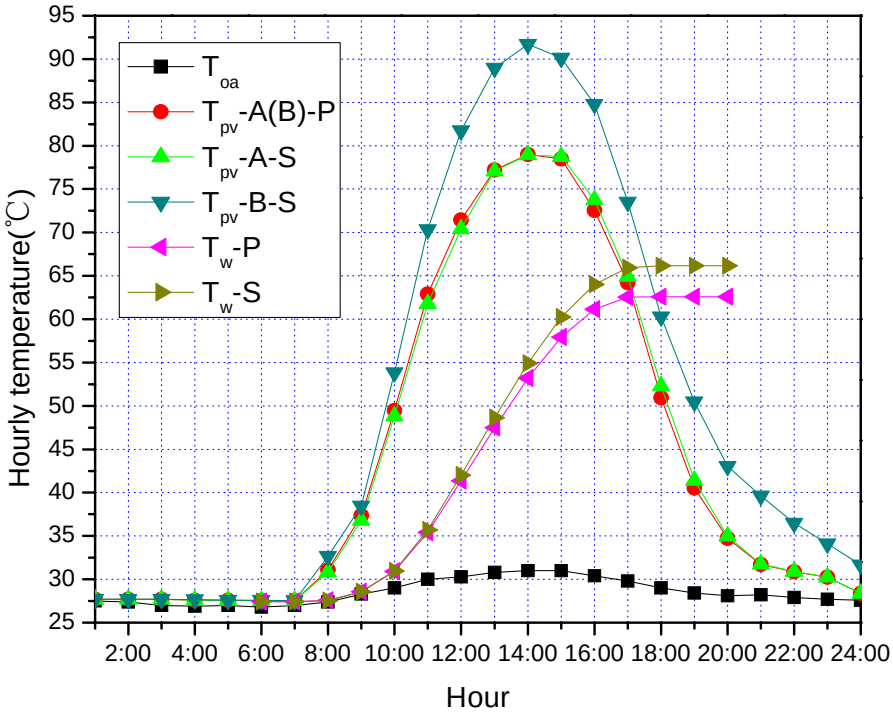

Figure 8.15 Hourly variation of temperature

Comparing with Figures 8.16 and 8.17, it is found that the hourly electrical efficiency of the parallel connection is larger than that of the series connection, contrary to the hourly thermal efficiency. The hourly electrical efficiency ranges from 8.01% to 11.19% for parallel connection and 7.83% to 10.70% for series connection. The range of hourly thermal efficiency of parallel connection is

8.12%~39.25% and the series connection is 16.0%~40.6%. The impacts of connection modes on the hourly thermal efficiency are more significant that those on the hourly electrical efficiency, especially at the time of 17:00pm.

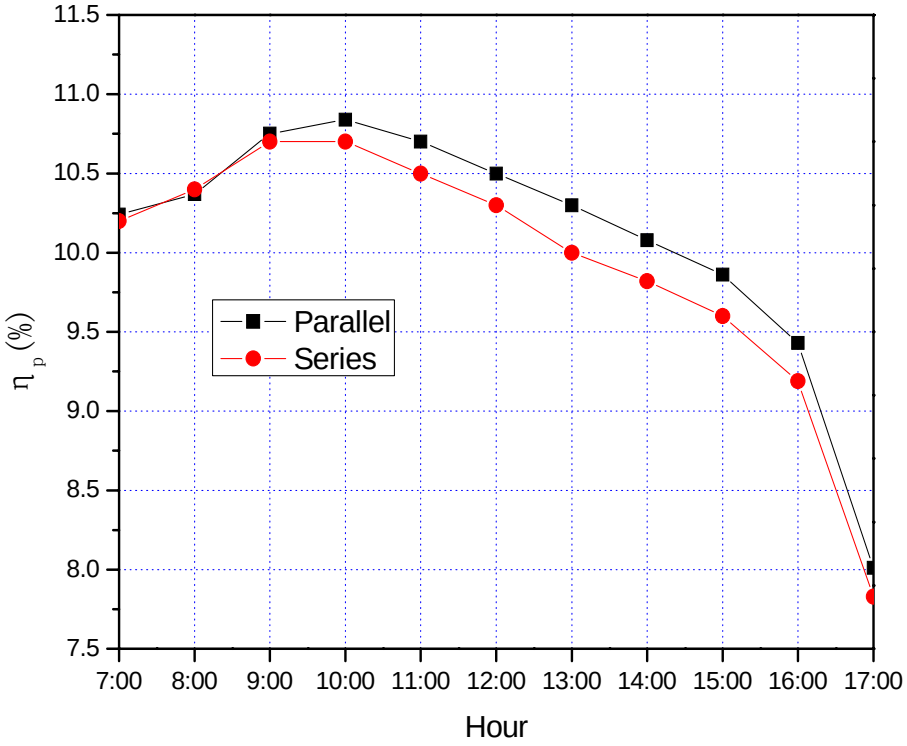

Figure 8.16 Hourly variation of electrical efficiency

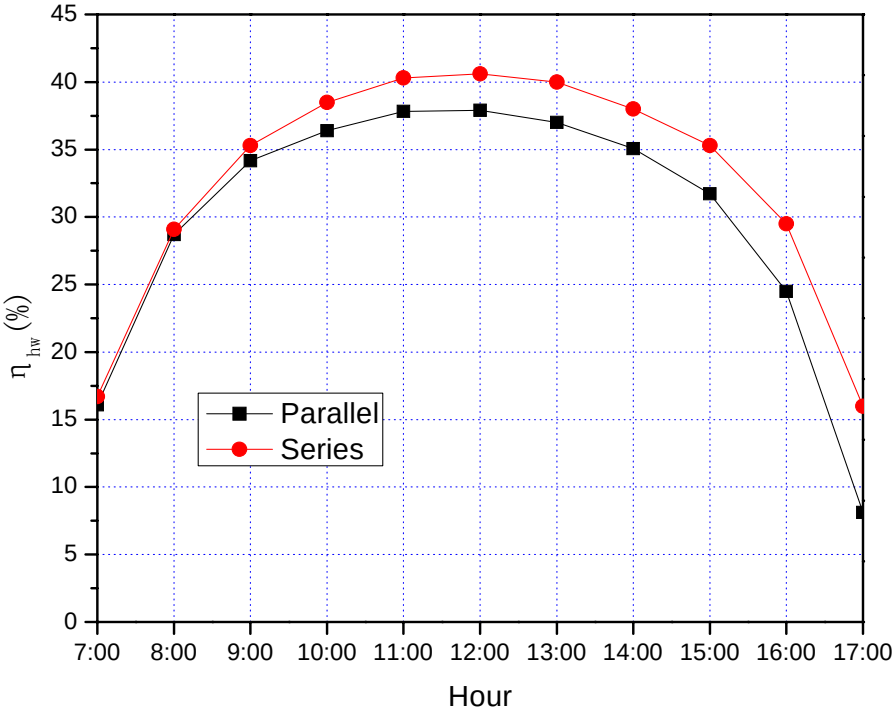

Figure 8.17 Hourly variation of thermal efficiency

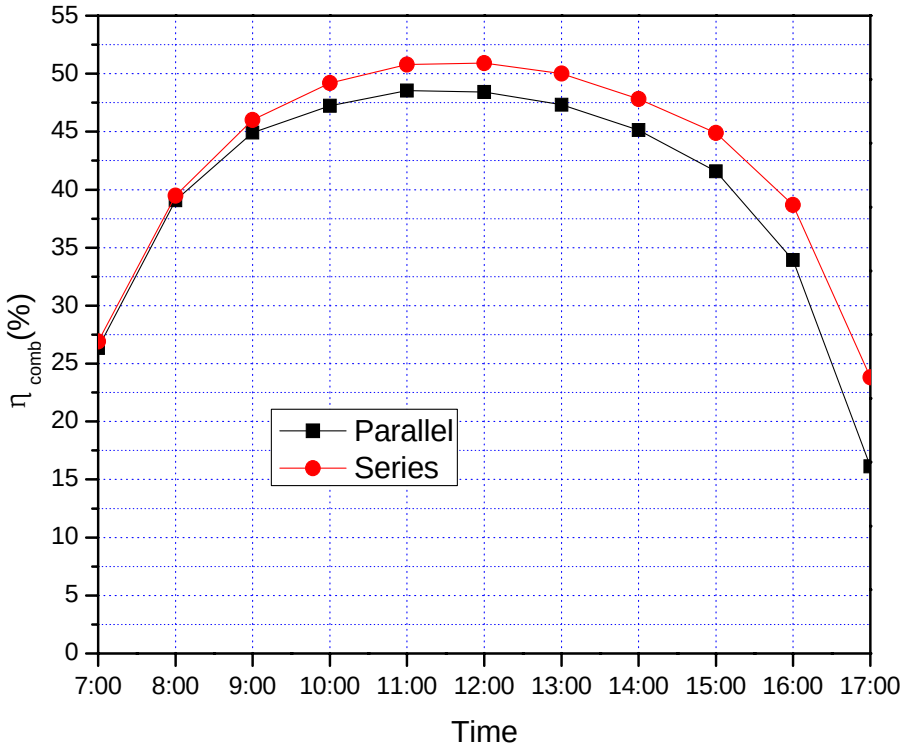

Figure 8.18 Hourly variation of combined electrical efficiency

8.3 Summary

In this chapter, a dynamic simulation model of a BIPVT hot water system designed for a small residential flat located in Hong Kong was developed to evaluate its energy performance. On the basis of the validated simulation model and the hourly TMY weather data of Hong Kong, the annual hourly simulation of the proposed system was performed and some specific findings from this case study are described as follows:

1) When the annual combined energy performance of the BIPVT hot water system is concerned, the optimum inclination of the PVT modules is 20 degree.

2) The BIPVT modules connected in series can produce more energy benefits than those in parallel connection. In addition, the connection modes have

more significant effects on the thermal efficiency in relative to the electrical efficiency.

3) When BIPVT modules are connected in series at the inclination of 40°, the annual electrical efficiency, thermal efficiency and combined electrical efficiency of the proposed system are, respectively, 10.0%, 34.9% and 34.5%. The BIPVT hot water system can support 82.3% of total hot water supply during the entire year. In addition, there are 208 days in a year when supplemental heating is not needed.

The investigations of the simulation results indicate that the BIPVT hot water system can significantly increase the total energy benefits compared with the BIPV system. It is thus a good choice to apply such a system in residential buildings where hot water is needed.

CHAPTER 9: CONCLUSIONS AND RECOMMENDATIONS FOR FUTURE WORK

9.1 Summary of research results

In this thesis, a dynamic simulation model is developed to estimate the energy benefits including the electrical power generation and the water heat gain of the shading BIPV and BIPVT claddings. On the basis of the model and the TMY weather data of Hong Kong, the impacts of building orientations, inclinations and wall utilization fractions on the energy performance of the shading-type BIPV and BIPVT claddings is evaluated.

The orientations of south and southwest are two better choices for PV module integrating into buildings in Hong Kong when the annual electricity generation is concerned. The maximum electricity generation is 76.8kWh/m^2 when the BIPV modules are installed on south façades at the tilt angle of 10°. The simulation results indicate that the shading-type BIPV claddings can significantly increase the total energy benefits relative to PV modules. The maximum combined electrical energy production of the shading-type BIPV claddings is 239.5kWh/m^2, which is twice more than the maximum electricity generation of the PV modules. In this case study, the optimum tilt angles for different designs vary from 30° to 50°. When installed with smaller wall utilization fractions, the shading-type BIPV claddings are more cost-effective than that with larger wall utilization fractions.

An experimental rig of the PVT hot water system was set up in the Solar Simulation Lab of the Hong Kong Polytechnic University. The experimental data were utilized to verify the simulation model of such a system, which was developed on the dynamic heat transfer analysis of the main components of the system. The simulation data shows good agreement with the experimental data. The simulation model has high accuracy and can be used for estimating the performance of the shading-type BIPVT hot water system.

Depending on the validated simulation model and the hourly TMY weather data of Hong Kong, the annual hourly simulation of the proposed system was performed. When the annual combined energy performance of the BIPVT hot water system is concerned, the optimum inclination of the PVT modules is 20°. However, the tilt angle of 20° is not applicable because the projection is too long to be installed. Thus, the tilt angle of 40° is used as the design inclination. The annual electrical efficiency, thermal efficiency and combined electrical efficiency of the proposed system are, respectively, 10.0%, 34.9% and 44.9%. The BIPVT hot water system can support 82.3% of the total hot water supply during the entire year. In addition, there are 208 days of a year when supplemental heating is not needed.

The effects of several main configuration parameters on the electrical generation and water heat gain of the PVT hot water system are investigated. The simulation results indicated that except for the covering glass thickness, most of the parameters have more obvious impacts on the water heat gain than those of the electrical power generation. The comparison of the initial design and the optimum design indicates that a little improvement of the configuration parameters of such a system can

significantly increase the energy performance, especially the thermal efficiency.

Finally, the indoor experimental data indicate that the electrical efficiency mainly depends on the temperature of the PV module. Both the solar radiation and the vertical distance of barycenters show nearly no significant influence on the electrical efficiency of the PVT module. For thermal performance of the PVT module and the PVT hot water system, the effect of the solar radiation is more significant than that of the vertical distance of barycenters.

9.2 Recommendations for future work

Due to time limitation, this study can not cover all aspects of the factors which need to be considered both in the numerical investigation and the experimental study. This may be the basis of further studies.

The current theoretical studies only consider the energy performance of both the shading-type BIPV system and the shading-type BIPVT hot water system. Future study could expand to use the Life Cycle Analysis Method to explore the energy benefits of the shading-type BIPV system and the shading-type BIPVT hot water system.

The current experimental studies only focus on indoor test of the PVT hot water system in the solar simulation lab. The outdoor test of such as system should be carried out in order to estimate its energy performance in the practical application.

REFERENCES

American Society of Heating, 2009. Refrigerating and Air Conditioning Engineers, ASHARE Handbook-Fundamentals, ASHARE Inc., Atlanta.

Arvind T. and Sodha M.S., 2006. Performance evaluation of solar PV/T system: an experimental validation. Solar Energy 80: 751-759.

Asl-Soleimani E., Farhangi, S. and Zabihi, M. S., 2001. The Effect of Tilt Angle, Air Pollution on Performance of Photovoltaic Systems in Tehran. Renewable Energy 24: 459-468.

Athienitis A. K. and Tzempelikos A., 2002. A methodology for simulation of daylight room illuminance distribution and light dimming for a room with a controlled shading device. Solar Energy 72(4): 271-281.

Bari S., 2000. Optimum slope angle and orientation of solar collectors for different periods of possible utilization. Energy Conversion & Management 41: 855-860.

Bergene, T., Lovvik, M., 1995. Model calculations on a flat-plate solar heat collector with integrated solar cells. Solar Energy 55, 453-462.

Burlon, R., Bivona, S. and Leone C., 1991. Instantaneous hourly and daily radiation on tilted surfaces. Solar Energy 47(2): 83-89.

Brinkworth B.J., 1997. Thermal regulation of photovoltaic cladding. Solar Energy 61(3): 169-178.

Brinkworth B.J., Marshall R.H. and Ibarahim, Z., 2000. A validated model of naturally ventilated PV cladding. Solar Energy 69(1): 67-81.

Chow T.T., 2003. Performance analysis of photovoltaic-thermal collector by explicit dynamic model. Solar Energy 75:143–52.

Chow T.T., He W. and Ji J. Hybrid photovoltaic-thermosyphon water heating system

for residential application. Sol Energy 80(3): 298-306.

Chow T.T., He W. and Ji J., 2007. An experimental study of facade-integrated photovoltaic/water heating system. Applied thermal engineering 27: 37-45.

Chow T.T., Chan A.L.S., Fong K.F., Lin Z. and Ji J., 2009. Annual performance of building-integrated photovoltaic water-heating system for warm climate application. Applied Energy 86: 689-696.

Chow T.T., 2010. A review on photovoltaic/thermal hybrid solar technology. Applied Energy 87: 365-379.

De Vries DW., 1998. Design of a photovoltaic/thermal combi-panel. PhD thesis, EUT.

Fraisse G., Me'ne'zo C. and Johannes K., 2007. Energy performance of water hybrid PV/T collectors applied to combisystems of direct solar floor type. Solar Energy 81:1426-1438.

Fung Y.Y, 2006. Energy performance of semi-transparent PV modules for application in Buildings. PhD thesis, The Hong Kong Polytechnic University.

Garg H.P. and Adhikari R.S., 1999. System performance studies on a photovoltaic/thermal (PV/T) air heating collector. Renewable Energy 16: 725-30.

He W., Chow T.T., Ji J., Lu J., Pie G. and Chan L., 2006. Hybrid photovoltaic and thermal solar collector designed for natural circulation of water. Applied Energy 83: 199–210.

Hong Kong Building Department, 2001. Joint Practice Note No. 1 – Incentives for Green Buildings, Hong Kong Special Administrative Region.

Hong Kong Electrical and Mechanical Services Department, 2010. Hong Kong Energy End-use Data 2010, Hong Kong Special Administrative Region.

Huang B.J., Lin T.H., Hung W.C. and Sun F.S., 2001. Performance evaluation of solar photovoltaic/thermal systems. Solar Energy 70(5):443–8.

James P.A.B., Jentsch M.F. and Bahaj A.S., 2009. Quantifying the added value of BiPV as a shading solution in atria. Solar Energy 83: 220-231.

Ji J., Chow T.T. and He W., 2003. Dynamic performance of hybrid photovoltaic/thermal collector wall in Hong Kong. Building and Environment 38: 1327-34.

Ji J., Lu J., Chow T.T., He W. and Pei G., 2007. A sensitivity study of a hybrid photovoltaic/thermal water-heating system with natural circulation. Applied Energy 84: 222-37.

Jones A.D. and Underwood C.P., 2001. A thermal model for photovoltaic systems, Solar Energy 70(4): 349-359.

Jones A.D. and Underwood C.P., 2002. A modeling method for building-integrated photovoltaic power supply. Building Services Engineering Research and Technology 23(3): 167-177.

Kalogirou S.A., 2001. Use of TRYNSYS for modeling and simulation of a hybrid PV thermal solar system for Cyprus. Renewable Energy 23: 247-60.

Loveday D.L. and Taki A.H., 1996. Convective heat transfer coefficients at a plane surface on a full-scale building façade. International Journal of Heat and Mass Transfer 39(8): 1729-1742.

Lu L. and Yang H.X., 2004. Study on Typical Meteorological Years and Their Effect on Building Energy and Renewable Energy Simulations. ASHARE Transaction 110(2): 424-431.

Mahmoud, M., and Nabhan, I., 1990. Determination of optimum tilt angle of single and multi rows of photovoltaic arrays for selected sites in Jordan. Solar & Wind

Technology 7(6): 739-745.

Moshfegh B. and Sandberg M., 1998. Flow and heat transfer in the air gap behind photovoltaic panels. Renewable and Sustainable Energy Reviews 2: 287-301.

Norton B., Eames P.C., Mallick T. K., Huang M.J., McCormack S.J., Mondol J.D. and Yohanis Y.G., 2010. Enhancing the performance of building integrated photovoltaics. Solar Energy, doi:10.1016/j.solener.2009.10.004.

Othman M.Y.H., Yatim B., Sopian K. and Bakar M.N.A., 2005. Performance analysis of a double-pass photovoltaic/thermal (PV/T) solar collector with CPC and fins. Renewable Energy 30: 2005-17.

Perez R., Stewart R., Arbogast C., Seals R. and Scott, J., 1986. An anisotropic hourly diffuse radiation model for sloping surfaces: description. performance validation, site dependency evaluation, Solar Energy 36(6): 481-497.

Perez R., Seals R., Ineichen P., Stewart R. and Menicucci D., 1987. A new simplified version of the Perez diffuse irradiance model for tilted surfaces. Solar Energy 39(3): 221-231.

Perez R., Ineichen P. and Seals, R., 1990. Modeling daylight availability and irradiance components from direct and global irradiance. Solar Energy 44(5): 271-289.

Powell G.L. and Yellott J.I., 1980. Solar Heat Gain Factors on Average Days. Proceeding of American Section of the International Solar Energy Society Annual Meeting: 826-830.

Radziemska E., 2003. Thermal performance of Si and GaAs based solar cells and modules:a review. Progress in Energy and Combustion Science 29: 407-24.

Reindl D.T., Beckman W.A. and Duffie, J.A., 1990. Evaluation of hourly tilted surface radiation models. Solar Energy 45(1): 9-17.

Robles-Ocampo B., 2007. Photovoltaic/thermal solar hybrid system with bifacial PV module and transparent plane collector. Solar Energy Materials & Solar Cells 91: 1966-1971.

Sandnes B, Rekstad J. A photovoltaic/thermal (PV/T) collector with a polymer absorber plate: Experimental study and analytic model. Solar Energy 2002; 72(1):63-73.

Sarhaddi F., Farahat S., Ajam H., Behzadmehr A. and Mahdavi Adeli, M., 2010. An improved thermal and electrical model for a solar photovoltaic thermal (PV/T) air collector. Applied Energy 87: 2328-2339.

Shariah A., Al-Akhras M. and Al-Omari I.A., 2002. Optimizing the tilt angle of solar collectors. Renewable Energy 26: 587-598.

Tiris M., and Tiris C., 1997. Optimum collector slope and model evaluation: case study for Gebze, Turkey. Energy Conversion and Management 39(3): 167-172.

Tiwari A. and Sodha M.S., 2006. Performance evaluation of solar PV/T system: an experimental validation. Solar Energy 80: 751-759.

Tripanagnostopoulos Y., Nousia T.H., Souliotis M. and Yianoulis P., 2002. Hybrid photovoltaic/thermal solar system. Solar Energy 72(3): 217–34.

Utzinger D.M. and Klein S.A., 1979. A Method of Estimating Monthly Average Solar Radiation on Shaded Receivers. Solar Energy 23: 369-378.

Vartiainen E., 2000. Daylight modeling and optimization of solar facades, Doctoral Thesis, Helsinki University of Technology, Helsinki University of Technology Publications in Energy Engineering Physics.

Wang Y.P., Tian W., Ren J.B., Zhu L. and Wang Q.Z., 2006. Influence of a building's integrated-photovoltaics on heating and cooling loads. Applied Energy 83(9): 989-1003.

Wolf M., 1976. Performance analysies of combined heating and photovoltaic power systems for residences. Energy Convers 16:79-90.

Yakup, M. and Malik A.Q., 2001. Optimum tilt angle and orientation for solar collector in Brunei Darussalam. Renewable Energy 24: 223-234.

Yang H.X., Burnett J. and Ji J., 2000. Simple approach to cooling load component calculation through PV walls. Energy and Buildings 31: 285-290.

Yik F.W.H., Burnett J. and Prescott I., 2001. Predicting Air-Conditioning Energy Consumption of A Group of Buildings Using Different Heat Rejection Methods. Energy and Buildings 33: 151-166.

Yoo S.H. and Lee E.T., 2002. Efficiency characteristic of building integrated photovoltaics as a shading device. Building and Environment 37: 615-623.

Yoo S.H. and Manz H., 2011. Available remodeling simulation for a BIPV as a shading device. Solar Energy and Materials & Solar Cells 95(1): 394-397.

Zakharchenko R., Licea-Jime'nez L., Pe'rez-Garci' a S.A., Vorobiev P., Dehesa-Carrasco U and Pe' rez-Robels J.F., 2004. Photovoltaic solar panel for a hybrid PV/ thermal system. Solar Energy Materials and Solar Cell 82(1-2): 253-61.

Zondag H.A., de Vries de D.W., Van Helden W.G.J., Van Zolengen R.J.C. and Van Steenhoven A.A., 2002. The thermal and electrical yield of a PV-thermal collector. Solar Energy 72(2): 113–28.

Zondag H.A., De Vries D.W., Van Helden W.G.J., Van Zolingen R.J.C. abd Van Steenhoven A.A., 2003. The yield of different combined PV-thermal collector designs. Sol Energy 74: 253-69.

Zogou O. and Stapountzis H., 2011. Energy analysis of an improved concept of integrated PV panels in an office building in central Greece. Applied Energy 88: 853-866.

Zondag H.A., 2008. Flat-plate PV-thermal collectors and systems: a review. Renewable and Sustainable Energy Reviews 12(4): 891-959.

Zuhairy, A.A. and Sayigh, A.A.M., 1995. Simulation and modeling of solar radiation in Saudi Arabia. Renewable Energy 6(2): 107-118.